TRAJECTORY ANALYSIS OF A FIN-STABILIZED ARTILLERY PROJECTILE

A Thesis Submitted
In Partial Fulfilment of the Requirements
for the Degree of
MASTER OF TECHNOLOGY

by

M. P. SINGH

to the

DEPARTMENT OF ELECTRICAL ENGINEERING
INDIAN INSTITUTE OF TECHNOLOGY, KANPUR
NOVEMBER 1984

14/11/84

CERTIFICATE

This is to certify that the thesis entitled 'TRAJECTORY ANALYSIS OF A FIN-STABILIZED ARTILLERY PROJECTILE' is a report of work carried out under our supervision by Major M.P. SINGH, and that it has not been submitted elsewhere for a degree.

(K.E. Holé)
Assistant Professor
Dept. of Elect. Engineering
IIT, Kanpur

(M. Krishnamurthy)
Assistant Professor
Dept. of Aeronautical Engineering
IIT, Kanpur.

EE-1984-M-SIN-TRA

ACKNOWLEDGEMENTS

I am indebted to many persons for the completion of this work. In particular, I am grateful to Dr. M. Krishnamurthy of Aeronautical Engineering department who imbued me with confidence to undertake this project and carry it to completion under his able guidance which was available at every stage of this work. I extend my gratitude to Dr. R.K.S. Rathore of Mathematics department, Dr. R. Sankar of Computer Science department and Dr. K.E. Hole of Electrical Engineering department for their critical and constructive review of the subject and valuable suggestions in solving the equations of motion. I extend my appreciation to Mr. Abhaya Kumar and Maj D.G. Wakankar for their assistance through discussions and suggestions. I am thankful to Mr. C.M. Abraham for typing the text and Mr. Qasim Hussain for preparing the figures.

CONTENTS

LIST OF SYMBOLS

A	any quantity, generally used to specify a vector quantity
a	speed of sound in air, m sec^{-1}
C	aerodynamic coefficients, $\frac{\text{Force}}{\frac{\rho}{2} V^2 S}$, $\frac{\text{Moment}}{\frac{\rho}{2} V^2 SL}$
$\bar{c}$	mean aerodynamic chord, m
C_D	drag coefficient
$(C_D)_B$	body drag coefficient
C_{DB}	base drag coefficient
C_{DF}	skin friction drag coefficient
C_{DP}	pressure drag coefficient
$(C_D)_W$	fin drag coefficient
C_{p1}	any normal pressure dependent coefficient at Mach number M_{a1}
C_{p2}	any normal pressure dependent coefficient at Mach number M_{a2}
D	operator, $D = \frac{d}{dt^+}$
d_B	base diameter of the projectile, m
d_{mid}	largest diameter of the projectile, m
F	constant in equation of motion, $\frac{gL}{V_o^2}$
F_G	gravitational force, Newton

F_R resultant external force acting on the body, Newton

F_T thrust force, Newton

g acceleration due to gravity, m sec^{-2}

H angular momentum of body, Kg m^2 sec^{-1}

I moment of inertia of the projectile, Kg m^2

I_{XY}, I_{XZ}, I_{YZ} product of inertia of the projectile Kg m^2

i unit vector along X direction

i_o unit vector along X_o direction

j unit vector in Y direction

j_o unit vector in Y_o direction

K_1 constant in equation of motion, $\frac{\rho SL^3}{4I_X}$

K_2 constant in equation of motion, $\frac{\rho SL^3}{4I_Y}$, $\frac{\rho SL^3}{4I_Z}$

k unit vector in Z direction

k_o unit vector in Z_o direction

L characteristic length of the body, m

$\bar{L}$ air foil thickness location parameter

M linear momentum of body, Kg m sec^{-1}

M_R resultant external moment acting on the body, Kg m

M_a, M_{a1}, M_{a2} Mach numbers

m mass of the projectile, Kg

p	X component of angular velocity $\bar{\omega}$, rad sec^{-1}
q	Y component of angular velocity $\bar{\omega}$, rad sec^{-1}
r	Z component of angular velocity $\bar{\omega}$, rad sec^{-1}
R	gas constant for air, m^2 sec^{-1} $^oK^{-1}$
Re	Reynolds number
R_{LS}	lifting surface correction factor
S	characteristic area = $\frac{\pi}{4} d^2$, m^2
S_L	portion of the wetted area over which the laminar flow exists, m^2
S_{ref}	reference area, m^2
S_{wet}	total wetted area, m^2
T	temperature of air, ^oK
T_o	temperature of air at mean sea level, ^oK
t	time, sec
t^+	non dimensional time
$\bar{t}$	thickness of the fin, m
U	non dimensional speed of the projectile
V	velocity of centre of gravity of the projectile, m sec^{-1}
V_o	initial velocity of projection, m sec^{-1}
V_R	velocity relative to the wind, m sec^{-1}
W	wind velocity, m sec^{-1}
X	body-fixed coordinate axis
X_o	space-fixed coordinate axis

X'_o	coordinate axis parallel to X_o and moving with wind velocity
x_o	non dimensional distance along X_o axis, m
Y	body-fixed coordinate axis
Y_o	space-fixed coordinate axis
y'_o	coordinate axis parallel to y_o and moving with wind velocity
y_o	non dimensional distance along Y_o axis, m
Z	body-fixed coordinate axis
Z_o	space-fixed coordinate axis
Z'_o	coordinate axis parallel to Z_o and moving with wind velocity
Z_o	non dimensional distance along Z_o axis, m
α	angle of attack, rad
β	angle of side slip, rad
γ	ratio of specific heats for air
δ	angle of graze, angle between X axis and the horizontal at the point of graze, rad.
θ	angle of pitch, rad
θ_L	angle between North and direction of fire, rad
θ_o	angle of projection, rad
θ_ω	angle between North and the wind vector $\overline{W}$
μ	constant in equation of motion, $\frac{m}{\rho S L}$
ν	kinematic viscosity of air
ρ	density of air, Kg m^{-3}
ρ_o	density of air at mean sea level, Kg m^{-3}
λ	time factor, $\frac{L}{V_o}$
ϕ	angle of roll, rad

Ψ	angle of yaw, rad
ω	angular velocity of the projectile with respect to $X_o Y_o Z_o$ axis system, rad sec^{-1}
$\measuredangle$	angle $\measuredangle$ XY = angle between X and Y, rad
(.)	operator, $\dot{A} = \frac{dA}{dt}$
(-)	vector quantity

Subscripts

The definition of all subscripts apply to their usage with all symbols except where the complete symbol with its subscripts is defined as a unit.

A	aerodynamic component
G	gravity component
l	component along X axis
m	component along Y axis
n	component along Z axis
p	operation, $A_p = \frac{\partial A}{\partial \frac{pL}{2V}}$
q	operation, $A_q = \frac{\partial A}{\partial \frac{qL}{2V}}$
r	operation, $A_r = \frac{\partial A}{\partial \frac{rL}{2V}}$
X	component along X axis
X_o	component along X_o axis
Y	component along Y axis
Y_o	component along Y_o axis
Z	component along Z axis
Z_o	component along Z_o axis

α operation, $A_\alpha = \frac{\partial A}{\partial \alpha}$

β operation, $A_\beta = \frac{\partial A}{\partial \beta}$

$\dot{\alpha}$ operation, $A_{\dot{\alpha}} = \frac{\partial A}{\partial \frac{\dot{\alpha} L}{2V}}$

$\dot{\beta}$ operation, $A_{\dot{\beta}} = \frac{\partial A}{\partial \frac{\dot{\beta} L}{2V}}$

o value of the coefficient with $\alpha = \beta = \dot{\alpha} = \dot{\beta} = p = q = r = 0$ and $V = V_o$

o value of the quantity at $t^+ = o$

* value after rotation by 90^o

LIST OF FIGURES

ABSTRACT

Equations of motion have been derived for a fin-stabilized projectile with time as independent variable. They have been simplified assuming that the rates of yaw, roll and pitch, and also angle of attack, sideslip angle and angle of roll to be small. The aerodynamic forces and moments are represented by the corresponding coefficients. These coefficients have been estimated for a 120 mm artillery projectile and the equations have been solved using a variable-order, variable-step Gear method. Corrections to the trajectory due to effects of atmospheric variations and wind have been incorporated. Parametric study consisting of variations in aerodynamic coefficients has been carried out to study their effect on the trajectory. The results have been compared with those in the range table.

CHAPTER 1

INTRODUCTION

1.1 GENERAL

Rapid advancement in technology since World War II has made the present day battle field environment highly complex. The modern armies are equipped with weapon systems which are both accurate and lethal and their increased mobility can greatly enhance the dimensions of the battle zone. Future conflicts will be short, fast and fluid. The lethal weapons which are the potential targets of artillery will be deployed swiftly and moved to a new location before they can be fired upon. Fleeting opportunities offered by the enemy will have to be seized to destroy the targets. Speed will be vital in this regard. Neutralization of targets by artillery will impose exacting demands on the accuracy of target acquisition devices, engagement procedures and weapon systems. This necessitates the employment of an efficient command, control, and communication system which can provide sufficient target intelligence, rapid target processing including assessment of priorities, optimum allocation of artillery resources, accurate computation of gun data, and reliable and secure communication, all with high speed of response. Only then it will be possible to use artillery in its vital battle winning and

challenging role.

The factors which greatly influence the accuracy of artillery fire are :

- The accuracy of the location of gun and target
- The accuracy, reliability and speed of communication of the firing data
- The accuracy of the meteorological report which includes information about the pressure, temperature, density and wind speed and direction in various layers of the atmosphere
- The accuracy of the weapon system
- The training standard of the crew.

1.2 MOTIVATION

With the help of survey techniques and target acquisition devices like radars, sound ranging, laser range finders and remotely piloted vehicles, the gun and target locations can be determined with high degree of precision. Meteorological radars equipped with radio-sonde and on-line computer to process the radio-sonde data will soon replace the balloon theodolites to provide accurate and timely information about the weather parameters. To achieve first salvo-effectiveness of artillery fire, it therefore becomes imperative to calculate the firing data for the guns quickly and accurately.

The present method of determining the firing data is slow and prone to human errors. Range table is used to compute the angle of projection for the guns to achieve the desired range. There is a range table supplied with each type of the artillery gun by the manufacturer. These range tables are compiled by actually observing the fall of shot at certain standard elevations. For intermediate elevations the data are interpolated. Corrections for the non-rigidity of the trajectory and other non-standard conditions are also included in the range table.

In a fluid battle situation where target information flows in continuously, paging through the range table to find the firing data for large number of targets may considerably slow down the response of artillery guns. A computer can greatly improve the accuracy and speed of response in this field. Range table contains large volume of data and since there is a range table for each type of projectile it is uneconomical to store the data of all the range tables in a computer memory and use it to calculate the firing data. Using a computer merely as a substitute for range tables will definitely improve the speed of response. But the disadvantages inherent in compilation of range tables and large requirement of memory space prohibit this approach. The most effective use of a computer lies in its ability to compute the firing data for all types of guns for different elevations and muzzle velocities. This can be achieved only when it is programmed to solve the equations of motion and determine the actual trajectory of the projectile through the atmosphere.

1.3 CURRENT APPROACH

In the present investigation a technique analogous to that used for the study of aircraft flight has been employed to derive the equations of motion of a projectile fired from artillery gun. The analysis is basically describing the motion of the projectile in terms of a set of differential equations written in an inertial frame of reference under the action of external forces and moments namely the aerodynamic and gravity. The aerodynamic forces and moments acting on the projectile are represented in terms of the corresponding aerodynamic coefficients. These equations are then suitably linearized and non-dimensionalized.

This method of computing the trajectory from the equations of motion is a more general approach and can be applied to any artillery projectile with known aerodynamic characteristics. It offers the following advantages :

- The firing data can be computed quickly and reliably
- Complete information about the trajectory of the projectile can be known. Any modifications like inclusion of thrust effect etc. can be easily taken care off.
- It is more economical than the present method of predicting the trajectory which entails maintaining establishments to compile the range table by actually observing the fall of shot. The process has to be repeated for every new

projectile which differs in shape and size. However, with the new method this expensive field study can be eliminated. Only aerodynamic coefficients need to be determined in a laboratory or estimated analytically.

- Parametric study can be carried out to arrive at the optimum combination of muzzle velocity and angle of projection for engaging a target.
- The parametric study may also help in arriving at the optimal projectile shape and inertial properties.

CHAPTER 2

BASIC CONCEPTS

In this chapter the geometry of fin-stabilized projectile and its orientation in space are introduced and the conditions of flight are postulated. The two axis systems, the earth-fixed axis system and the stability axis system, required for the development of equations of motion are discussed. The transformation matrix relating the two axis systems and the equations relating the components of angular velocity of projectile to the Eulerian angles of projectile in space have also been included.

2.1 GEOMETRY OF THE PROJECTILE

The projectiles fired from artillery mortars have stream-lined shape provided with fins at the tail end to provide stability during flight. These projectiles are considered to have a 90° roll symmetry. The geometry of a typical artillery projectile and its orientation in space are shown in Fig. 2.1. Consequence of this 90° roll symmetry is to reduce the number of aerodynamic coefficients in the equations of motion and thus reducing their complexity.

2.2 COORDINATE SYSTEM

In developing the equations of motion two right-handed orthogonal coordinate systems have been chosen. One of them is

stability axis system which is fixed to the projectile. The other set is fixed with respect to the earth and is known as earth-fixed axis system. If the rotation of earth is neglected the earth-fixed axis system forms an inertial system of reference frame. To derive the equations of motion Newton's laws are applied in this space fixed coordinate frame. The physical quantities such as linear and angular velocities and aerodynamic forces etc. are conveniently dealt with in a coordinate frame moving with the body and fixed to it. The equations of motion written with reference to space fixed coordinate system are subsequently transformed to stability axis system. Knowing the relative orientations of the two axis systems, the variables of interest in one coordinate system can be transformed to another coordinate system. The Fig. 2.1 shows the two axis systems and their relative orientations.

2.2.1 Space Fixed Axis System

It is designated by $X_oY_oZ_o$ and has its origin at the point of launch of the projectile. The directions of the individual axes are as follows :

X_o : aligned parallel to the longitudinal axis of the projectile and is positive in the forward direction.

Y_o : is horizontal at 90^o to X_o and is positive to the right of an observer facing forward.

Z_o : points downwards perpendicular to X_o and Y_o.

2.2.2 Stability Axis System

It is fixed to the projectile and is designated by XYZ. The origin of this axis system coincides with the centre of gravity of the projectile and the directions of the individual axes are as follows :

X : coincides with the longitudinal axis of the projectile and is positive in the forward direction.

Y : is at right angles to X and initially points in the same direction as Y_o.

Z : is at right angles to X and Y and initially points in the same direction as Z_o.

By virtue of the 90^o rotational symmetry of the projectile all the three axes of this axis system are the principal axes of inertia.

2.3 ORIENTATION OF THE PROJECTILE IN SPACE

The orientation of the projectile in space at any instant of time is defined by three angular coordinates Ψ, Θ and $\emptyset$ as shown in Fig. 2.1. These angles called Eulerian angles describe the orientation of stability axes, XYZ, with respect to space-fixed axes, $X_oY_oZ_o$. They are zero initially when the two coordinate systems coincide with each other and any subsequent orientation of the projectile can be obtained by giving three consecutive rotations of magnitudes Ψ, Θ and

in order. These rotations are non-commutative and must be carried out in an order always. The order generally followed is as given below :

- Starting from XYZ coincident with $X_oY_oZ_o$ rotate XYZ through an angle Ψ about the Z_o axis. This results in $X_1Y_1Z_1$.
- Rotate $X_1Y_1Z_1$ about Y_1 axis through an angle Θ. This gives $X_2Y_2Z_2$ in which X_2 is in its final position.
- The third rotation is about X_2 (X) axis by an angle ϕ. This brings the Y and Z axes to their final positions and the projectile to its actual orientation in space.

The Eulerian angles Ψ, Θ and ϕ can also be visualized as follows :

Ψ : angle between X_o axis and the line of intersection of the planes X_oY_o and XZ_o.

Θ : angle between the line of intersection of the planes X_oY_o and XZ_o and X axis.

ϕ : angle between the line of intersection of the planes YZ and X_oY_o and Y axis.

Figure 2.1 shows the direction of gravity vector which is vertical. Since Y_o axis is horizontal the X_oZ_o plane becomes the vertical plane and hence contains the gravity vector. The X_o axis is inclined to the horizontal plane at an angle Θ_o, the angle of projection of the projectile. The angle between Z_o

axis and the gravity vector is also equal to angle θ_o. This angle is considered positive when X_o axis is above the horizontal plane. In case of artillery projectiles angle θ_o will always be positive.

2.4 LINEAR AND ANGULAR VELOCITIES

The orientation of the velocity vector $\bar{V}$ with respect to stability axes X,Y,Z is given by the angle of attack α and the angle of side slip β as shown in Fig. 2.2. The angles α and β are defined by

$$\alpha = 90^\circ - \measuredangle\, \bar{V}\, Z,$$

$$\beta = 90^\circ - \measuredangle\, \bar{V}\, Y\ .$$

From these definitions of angles α and β it follows that the components of velocity $\bar{V}$ along X,Y and Z axes are

$$V_X = V\sqrt{1-\sin^2\alpha-\sin^2\beta}\ ,$$

$$V_Y = V \sin\beta, \qquad (2.1)$$

and

$$V_Z = V \sin\alpha\ .$$

The angular velocity components p,q,r of the projectile along X,Y,Z axes are related to the Eulerian angles Ψ, Θ and $\emptyset$, and their time derivatives $\dot{\Psi}$, $\dot{\Theta}$ and $\dot{\emptyset}$ by the following kinematic relations [1] :

$$p = \dot{\phi} - \dot{\psi}\sin\theta$$

$$q = \dot{\theta}\cos\phi + \dot{\psi}\cos\theta\sin\phi \qquad (2.2)$$

$$r = \dot{\psi}\cos\theta\cos\phi - \dot{\theta}\sin\phi$$

2.5 CONDITIONS OF FLIGHT

Following conditions are postulated for the geometry of the projectile and its flight :

- The projectile has 90° rotational symmetry about X axis
- The angles α, β and ϕ and also the time derivatives $\dot{\alpha}, \dot{\beta}, \dot{\psi}$, $\dot{\theta}$ and $\dot{\phi}$ are small.

It follows from the second assumption and from eqn. (2.2) that the components of angular velocity, p,q and r are also small.

2.6 RELATIONSHIP BETWEEN THE TWO AXIS SYSTEMS

The equations of motion are written in XYZ axis system. But in order to analyse the trajectory the distances travelled by the projectile must refer to $X_oY_oZ_o$ axis system. The transformation from one axis system to another can be made using the relationship between the unit vectors of the two axis systems. This relationship between i,j,k and i_o, j_o, k_o is given by [1]

$$\begin{bmatrix} i_o \\ j_o \\ k_o \end{bmatrix} = \begin{bmatrix} \cos\Theta\cos\Psi & \cos\Psi\sin\phi\sin\Theta - \sin\Psi\cos\phi & \cos\Psi\cos\phi\sin\Theta + \sin\Psi\sin\phi \\ \cos\Theta\sin\Psi & \sin\Psi\sin\phi\sin\Theta + \cos\Psi\cos\phi & \sin\Psi\cos\phi\sin\Theta - \cos\Psi\sin\phi \\ -\sin\Theta & \sin\phi\cos\Theta & \cos\Theta\cos\phi \end{bmatrix} \begin{bmatrix} i \\ j \\ k \end{bmatrix} \tag{2.3}$$

where i,j,k and i_o, j_o, k_o are unit vectors in XYZ and $X_oY_oZ_o$ axis systems respectively. If angle ϕ is small as postulated in Sec. 2.5, $\sin\phi$ can be approximated by ϕ and $\cos\phi$ by 1. With this eqn. (2.3) reduces to

$$\begin{bmatrix} i_o \\ j_o \\ k_o \end{bmatrix} = \begin{bmatrix} \cos\Theta\cos\Psi & \phi\cos\Psi\sin\Theta - \sin\Psi & \cos\Psi\sin\Theta + \phi\sin\Psi \\ \cos\Theta\sin\Psi & \phi\sin\Psi\sin\Theta + \cos\Psi & \sin\Psi\sin\Theta - \phi\cos\Psi \\ -\sin\Theta & \phi\cos\Theta & \cos\Theta \end{bmatrix} \begin{bmatrix} i \\ j \\ k \end{bmatrix} \tag{2.4}$$

CHAPTER 3

EQUATIONS OF MOTION

In this chapter the general equations of motion of a projectile are derived with time as independent variable. After suitable transformation, linearization and nondimensionalization these equations are rearranged in a form which is convenient for trajectory analysis.

3.1 THE VECTOR EQUATIONS

Newton's second law of motion expressing the conservation of linear and angular momenta provides the two basic vector equations which represent the motion of the projectile. They are

$$\frac{d}{dt}\bar{M} = \bar{F}_R \ , \tag{3.1}$$

and

$$\frac{d}{dt}\bar{H} = \bar{M}_R \ . \tag{3.2}$$

where $\bar{M}$ and $\bar{H}$ represent linear and angular momenta respectively, $\bar{F}_R$ the resultant external force acting on the projectile including the thurst and $\bar{M}_R$ the resultant external moment.

The components of linear momentum $\bar{M}$ along the X,Y and Z axes are mV_X, mV_Y and mV_Z respectively so that

$$\bar{M} = imV_X + jmV_Y + kmV_Z \ , \tag{3.3}$$

where m is the mass of the projectile and V_X, V_Y and V_Z are the velocity components given by eqn. (2.1).

Similarly the angular momentum vector $\bar{H}$ can be written in terms of its components H_X, H_Y and H_Z as

$$\bar{H} = iH_X + jH_Y + kH_Z \ , \tag{3.4}$$

where

$$\begin{aligned} H_X &= pI_X - rI_{XZ} - qI_{XY}, \\ H_Y &= qI_Y - pI_{XY} - rI_{YZ}, \\ \text{and} \\ H_Z &= rI_Z - qI_{YZ} - pI_{XZ} \ . \end{aligned} \tag{3.5}$$

In eqn. (3.5) I_X, I_Y, I_Z are the moments of inertia of the projectile about X,Y,Z axes and I_{XY}, I_{XZ} and I_{YZ} are the products of inertia. By virtue of the 90° rotational symmetry I_Y and I_Z will be equal and all the products of inertia will be zero. Thus the components of $\bar{H}$ given in eqn. (3.5) reduce to

$$\begin{aligned} H_X &= pI_X, \\ H_Y &= qI_Y, \\ \text{and} \\ H_Z &= rI_Z. \end{aligned} \tag{3.6}$$

And hence eqn. (3.4) reduces to

$$\bar{H} = iI_Xp + jI_Yq + kI_Zr, \tag{3.7}$$

where p,q and r, the components of angular velocity are given by eqn. (2.2).

The unit vectors in eqns. (3.3) and (3.7) are functions of time and hence the time derivatives in eqns. (3.1) and (3.2) have contributions arising from this which are accounted for by using the Poisson's formula

$$\frac{d\bar{A}}{dt} = \dot{\bar{A}} + \bar{\omega} \times \bar{A} \qquad (3.8)$$

where,

$\bar{A}$: any vector quantity with A_X, A_Y and A_Z as components along X,Y and Z axes respectively,

$\dot{\bar{A}}$: rate of change of $\bar{A}$ with respect to X Y Z, the rotating axis system,

$\frac{d\bar{A}}{dt}$: rate of change of $\bar{A}$ with respect to $X_o Y_o Z_o$, the fixed axis system,

and $\bar{\omega}$: angular velocity of the rotating axes X Y Z.

In the component form eqn. (3.8) can be expressed as

$$\frac{dA_X}{dt} = \dot{A}_X + qA_Z - rA_Y ,$$

$$\frac{dA_Y}{dt} = \dot{A}_Y + rA_X - pA_Z , \qquad (3.9)$$

and

$$\frac{dA_Z}{dt} = \dot{A}_Z + pA_Y - qA_X .$$

3.2 FORCES AND MOMENTS

The external force $\bar{F}_R$ in eqn. (3.1) comprises in general the aerodynamic force $\bar{F}_A$, gravitational force $\bar{F}_G$ and the thrust force $\bar{F}_T$ so that

$$\bar{F}_R = \bar{F}_A + \bar{F}_G + \bar{F}_T \ . \qquad (3.10)$$

The projectile under consideration has no thrust force acting on it and, therefore, $\bar{F}_T$ in eqn. (3.10) will be taken to be zero. The resultant external moment $\bar{M}_R$ in eqn. (3.2) is only aerodynamic moment.

3.2.1 Aerodynamic Forces and Moments

The aerodynamic forces and moments can be expressed in a general form as

$$F_{A_{X,Y,Z}} = C_{X,Y,Z} \frac{\rho}{2} V^2 S \ , \qquad (3.11)$$

where suffixes X,Y,Z refer to the components of the force $\bar{F}_A$ or the coefficient C in the X,Y,Z directions. Similarly the aerodynamic moments are expressed by

$$M_{X,Y,Z} = C_{l,m,n} \frac{\rho}{2} V^2 SL \qquad (3.12)$$

where l,m,n refer to the components about X,Y,Z axes respectively.

In eqns. (3.11) and (3.12) is the density of air and S and L denote the characteristic area and the characteristic length of the projectile respectively. Coefficients $C_{X,Y,Z}$ and $C_{l,m,n}$ are in general, functions of the variables $\alpha,\beta,\dot{\alpha},\dot{\beta},p,q$ and r and can be expanded in Taylor's series in these variables. A general expression for C_a can thus be written as

$$C_a = C_{a_o} + C_{a_\alpha}\alpha + C_{a_\beta}\beta + C_{a_{\dot{\alpha}}}\frac{\dot{\alpha}L}{2V} + C_{a_{\dot{\beta}}}\frac{\dot{\beta}L}{2V} + C_{a_p}\frac{pL}{2V} + C_{a_q}\frac{qL}{2V}$$

$$+ C_{a_r}\frac{rL}{2V} \quad [\text{higher order terms}] \qquad (3.13)$$

where 'a' stands for X,Y,Z,l,m,n . A quasi-linearity approximation is made so that the coefficients in the series are independent of the variables. These coefficients are called aerodynamic derivatives or stability derivatives and are in general, functions of the Reynolds number and Mach number. The stability derivatives are defined as follows :

$$C_{a_o} = C_a, \qquad \text{for} \quad \alpha,\beta,\dot{\alpha},\dot{\beta},p,q,r = 0$$

$$C_{a_\alpha} = \frac{\partial C_a}{\partial \alpha}\ ; \qquad C_{a_\beta} = \frac{\partial C_a}{\partial \beta}$$

$$C_{a_{\dot{\alpha}}} = \frac{\partial C_a}{\partial(\frac{\dot{\alpha}L}{2V})}\ ; \qquad C_{a_{\dot{\beta}}} = \frac{\partial C_a}{\partial(\frac{\dot{\beta}L}{2V})}$$

$$C_{a_p} = \frac{\partial C_a}{\partial(\frac{pL}{2V})}\ ; \qquad C_{a_q} = \frac{\partial C_a}{\partial(\frac{qL}{2V})}$$

$$C_{a_r} = \frac{\partial C_a}{\partial(\frac{rL}{2V})}$$

It can be seen from eqn. (3.13) that each force or moment coefficient requires 8 stability derivatives for representation. In order to describe all the force and moment coefficients completely,48 aerodynamic derivatives will be required. By virtue of 90° rotational symmetry of the projectile this number will reduce considerably and this simplification is discussed in the next paragraph.

3.2.2 Consequences of Mirror and 90° Rotational Symmetry

Consider two motions of the projectile so that one is the mirror image of the other about the plane of mirror symmetry-XZ. Then the aerodynamic force and moment due to the second motion must be the mirror images of those due to the first motion. To illustrate, consider the term $C_{l_p}(\frac{pL}{2V})$, the rolling moment due to rolling velocity, and $C_{m_p}(\frac{pL}{2V})$, the pitching moment due to rolling velocity. The mirror image of rolling velocity p is always - p. The mirror image of $C_{l_p}(\frac{pL}{2V})$ should be $-C_{l_p}(\frac{pL}{2V})$. This is indeed so since changing p to -p changes $C_{l_p}(\frac{pL}{2V})$ to $-C_{l_p}(\frac{pL}{2V})$. The stability derivative C_{l_p} is therefore allowable and can have a non-zero value. On the other hand the mirror image of the pitching moment M_y is M_y, hence the mirror image of $C_{m_p}(\frac{pL}{2V})$ should be $C_{m_p}(\frac{pL}{2V})$. It can be seen that this term actually reverses its sign when p is replaced by its mirror image -p.This clearly violates the requirement that due to mirror symmetry the mirror image of pitching moment M_y should be M_y itself. Therefore the aerodynamic derivative C_{m_p} is not

allowable and must be equal to zero. By applying the criterion of mirror symmetry similarly to all the stability derivatives the following derivatives are found to be equal to zero identically :

$$
\begin{aligned}
C_{X_\beta} &= C_{X_{\dot\beta}} = C_{X_p} = C_{X_r} = 0 \\
C_{Y_o} &= C_{Y_\alpha} = C_{Y_{\dot\alpha}} = C_{Y_q} = 0 \\
C_{Z_\beta} &= C_{Z_{\dot\beta}} = C_{Z_p} = C_{Z_r} = 0 \\
C_{l_o} &= C_{l_\alpha} = C_{l_{\dot\alpha}} = C_{l_q} = 0 \\
C_{m_\beta} &= C_{m_{\dot\beta}} = C_{m_p} = C_{m_r} = 0 \\
C_{n_o} &= C_{n_\alpha} = C_{n_{\dot\alpha}} = C_{n_q} = 0
\end{aligned}
\qquad (3.14)
$$

90° rotational symmetry implies that a rotation through 90° transforms the projectile into itself. It is obvious that the aerodynamic derivatives must have values such that a rotation of vector $\bar{V}$ and $\bar{\omega}$ by 90° about X axis will produce similar rotation of vector $\bar{F}_R$ and $\bar{M}_R$ by 90° about the same axis.

Let $\bar{A}$ be any vector and $\bar{A}_*$ be the vector obtained by rotating $\bar{A}$ by 90° about the X axis (ref. Fig. 3.1). If the direction of rotation is taken from Y to Z as shown in the figure, then the X component A_X does not rotate, the component

A_Y moves to Z direction and the component A_Z moves to -Y direction so that the new components A_{X_*}, A_{Y_*}, A_{Z_*} are related to A_X, A_Y, A_Z by

$$A_{X_*} = A_X \ ,$$

$$A_{Y_*} = -A_Z \ , \qquad (3.15)$$

and $$A_{Z_*} = A_Y \ .$$

The relationship between the components of the aerodynamic force and moment and also those of $\bar{V}$ and $\bar{\omega}$ after rotation of $\bar{V}$ and $\bar{\omega}$ can thus be obtained by applying eqn. (3.15) and they are

$$F_{X_*}(\bar{V}_*, \bar{\omega}_*) = F_X(\bar{V},\bar{\omega}) \ ,$$

$$F_{Y_*}(\bar{V}_*,\bar{\omega}_*) = -F_Z(\bar{V},\bar{\omega}) \ ,$$

$$F_{Z_*}(\bar{V}_*,\bar{\omega}_*) = F_Y(\bar{V},\bar{\omega}) \ , \qquad (3.16a)$$

$$M_{X_*}(\bar{V}_*,\bar{\omega}_*) = M_X(\bar{V},\bar{\omega}) \ ,$$

$$M_{Y_*}(\bar{V}_*,\bar{\omega}_*) = -M_Z(\bar{V},\bar{\omega}) \ ,$$

$$M_{Z_*}(\bar{V}_*,\bar{\omega}_*) = M_Y(\bar{V},\bar{\omega}) \ ,$$

and

$$
\begin{aligned}
V_{X_*} &= V_X \\
\alpha_* &= \beta \\
\beta_* &= -\alpha \\
p_* &= p \\
q_* &= -r \\
r_* &= q
\end{aligned}
\qquad (3.16b)
$$

It is noticed that the values of the force and moment components after rotation must be computed using the rotated values of velocities $\bar{V}_*$ and $\bar{\omega}_*$ as indicated by the functional notation of eqn. (3.16a). Equation (3.16a) must hold for all values of $\bar{V}$ and $\bar{\omega}$. Hence by computing the components of forces and moments from eqn. (3.16a), substituting for the components of $\bar{V}$ and $\bar{\omega}$ from eqn. (3.16b) and then using eqns. (3.11) - (3.13) the following relationships for the stability derivatives are obtained :

$$
\begin{aligned}
C_{Y_\beta} &= -C_{Z_\alpha} \\
C_{Y_{\dot{\beta}}} &= -C_{Z_{\dot{\alpha}}} \\
C_{Y_r} &= C_{Z_q} \\
C_{n_\beta} &= -C_{m_\alpha} \\
C_{n_{\dot{\beta}}} &= -C_{m_{\dot{\alpha}}} \\
C_{n_r} &= C_{m_q}
\end{aligned}
\qquad (3.17a)
$$

$$C_{X_\alpha} = C_{X_{\dot{\alpha}}} = C_{X_q} = C_{Y_p} = C_{Z_o} = C_{l_\beta} = C_{l_{\dot{\beta}}} = C_{l_r} = C_{m_o} = C_{n_p} = 0$$

(3.17b)

Thus the plane of symmetry assumption results in reducing all the coupling derivatives between the longitudinal and lateral modes to zero as given in eqn. (3.14). The 90° rotational symmetry further simplifies the problem by establishing equality between some of the longitudinal derivatives and lateral derivatives and also by reducing some of them to zero as given in eqn. (3.17).

Finally, the components of aerodynamic force and moment can be expressed as follows :

$$\begin{aligned}
F_{A_X} &= \frac{\rho}{2} V^2 S\, C_{X_o} \\
F_{A_Y} &= \frac{\rho}{2} V^2 S\left(C_{Y_\beta}\beta + C_{Y_{\dot{\beta}}} \frac{\dot{\beta}L}{2V} + C_{Y_r} \frac{rL}{2V}\right) \\
F_{A_Z} &= \frac{\rho}{2} V^2 S\left(C_{Z_\alpha}\alpha + C_{Z_{\dot{\alpha}}} \frac{\dot{\alpha}L}{2V} + C_{Z_q} \frac{qL}{2V}\right) \\
M_X &= \frac{\rho}{2} V^2 SL\, C_{l_p} \frac{pL}{2V} \\
M_Y &= \frac{\rho}{2} V^2 SL\left(C_{m_\alpha}\alpha + C_{m_{\dot{\alpha}}} \frac{\dot{\alpha}L}{2V} + C_{m_q} \frac{qL}{2V}\right) \\
M_Z &= \frac{\rho}{2} V^2 SL\left(C_{n_\beta}\beta + C_{n_{\dot{\beta}}} \frac{\dot{\beta}L}{2V} + C_{n_r} \frac{rL}{2V}\right)
\end{aligned} \qquad (3.18)$$

In view of eqn. (3.17a) there are only 8 independent aerodynamic derivatives in eqn. (3.18).

3.2.3 Gravitational Force

The components of gravitational force along X_o, Y_o and Z_o axes can readily be determined from Fig. 2.1. It can be seen that $\bar{F}_G$ lies in the X_oZ_o plane and that Y_o is horizontal. Therefore,

$$\bar{F}_G = i_o(-mg \sin\theta_o) + k_o(mg \cos\theta_o) \quad . \tag{3.19}$$

The components of $\bar{F}_G$ along X,Y and Z axes can now be found by using the rotation matrix of eqn. (2.4) and are given by

$$F_{G_X} = -mg(\sin\theta_o \cos\theta \cos\Psi + \cos\theta_o \sin\theta),$$

$$F_{G_Y} = mg[\phi\cos\theta_o \cos\theta - \sin\theta_o \sin\theta \cos\Psi) + \sin\theta_o \sin\Psi],$$

and

$$F_{G_Z} = mg[\cos\theta_o \cos\theta - \sin\theta_o(\cos\Psi \sin\theta + \phi\sin\Psi)] \tag{3.20}$$

3.3 THE DYNAMICAL EQUATIONS

The equations of motion are derived from the basic vector eqns. (3.1) and (3.2) by resolving the vector along the coordinate axes and using the equations for the external forces and moments. The final six scalar equations are obtained following the steps outlined below :

- Equations (3.1) and (3.2) are transformed using eqn.(3.9)
- Components of linear and angular momenta are introduced from eqns. (3.3) and (3.7)

- The linear and angular velocity components are substituted from eqns. (2.1) and (2.2) in terms of $V, \alpha, \beta, \Psi, \Theta, \Phi$ and $\dot{\Psi}, \dot{\Theta}, \dot{\Phi}$.
- The components of aerodynamic force and moment from eqn. (3.18) and those of gravitational force from eqn. (3.20) are finally substituted.

3.4 LINEARIZATION

It is assumed that the angles, Φ, α, β and the derivatives $\dot{\alpha}$, $\dot{\beta}$, $\dot{\Psi}$, $\dot{\Theta}$, and $\dot{\Phi}$ are small and hence only the first order terms in these variables are retained and the higher order terms are neglected. The procedure followed, therefore, is to group the first order and higher order terms separately in each equation and then neglect the higher order terms in comparison to the first order terms.

3.5 NON DIMENSIONALIZATION

The final step in the derivation is to non-dimensionalize the equations using the muzzle velocity and the characteristic dimensions of the projectile. The non-dimensional time t^+ is defined as $t^+ = \frac{t}{\tau}$, where τ is the characteristic time given by $\tau = \frac{L}{V_o}$, V_o being the initial velocity of projection of the projectile and L its characteristic length. τ indicates the time of flight for one characteristic length of the projectile. The non dimensional speed U is defined as $U = \frac{V}{V_o}$ and the non-dimensional time derivative operator D as $D = \frac{d^o}{dt^+}$.

The details of the derivation, linearization and non-dimensionalization of the equations are given in Appendix A and their final forms are as follows :

- X Force Equation

$$DU - \frac{1}{2\mu} C_{X_o} U^2 + F(\sin\theta_o \cos\theta \cos\Psi + \cos\theta_o \sin\theta) = 0 \quad (3.21)$$

- Y Force Equation

$$(1 - \frac{1}{4\mu} C_{Y_{\dot{\beta}}}) UD\beta + \cos\theta(1 - \frac{1}{4\mu} C_{Y_r}) UD\Psi + \frac{1}{2\mu} (C_{X_o} - C_{Y_\beta}) U^2\beta$$

$$- F(\sin\theta_o \cos\theta \cos\Psi + \cos\theta_o \sin\theta)\beta -$$

$$F[\phi(\cos\theta_o \cos\theta - \sin\theta_o \sin\theta \cos\Psi) + \sin\theta_o \sin\Psi] = 0 \quad (3.22)$$

- Z Force Equation

$$(1 - \frac{1}{4\mu} C_{Z_{\dot{\alpha}}}) UD\alpha - (1 + \frac{1}{4\mu} C_{Z_q}) UD\theta + \frac{1}{2\mu} (C_{X_o} - C_{Z_\alpha}) U^2\alpha$$

$$- F(\sin\theta_o \cos\theta \cos\Psi + \cos\theta_o \sin\theta)\alpha -$$

$$F[\cos\theta_o \cos\theta - \sin\theta_o(\cos\Psi \sin\theta + \phi \sin\Psi)] = 0 \quad (3.23)$$

- X Moment Equation

$$D^2\phi - \sin\theta D^2\Psi - K_1 C_{l_p} UD\phi + K_1 C_{l_p} \sin\theta UD\Psi = 0 \quad (3.24)$$

- Y Moment Equation

$$D^2\theta - K_2 C_{m_{\dot{\alpha}}} UD\alpha - K_2 C_{m_q} UD\theta - 2K_2 C_{m_\alpha} U^2\alpha = 0 \quad (3.25)$$

- Z Moment Equation

$$\cos\Theta\, D^2\Psi - K_2\, C_{n_\beta}\, UD\beta - K_2 C_{n_r}\, \cos\Theta\, UD\Psi - 2K_2 C_{n_\beta}\, U^2\beta = 0 \qquad (3.26)$$

where

$$F = \frac{gL}{V_o^2} ,$$

$$\mu = \frac{m}{\rho SL} ,$$

$$K_1 = \frac{\rho SL^3}{4I_X},$$

$$K_2 = \frac{\rho SL^3}{4I_Y} = \frac{\rho SL^3}{4I_Z} .$$

3.6 THE KINEMATIC RELATIONS

Equations (3.21) - (3.26) are six differential equations in six unknowns $U, \alpha, \beta, \Psi, \Theta$ and ϕ and a solution of these gives the velocity components along X,Y and Z axes. However, for the description of the trajectory of the projectile we need to transform these components along $X_oY_oZ_o$ system so that they can be integrated with time in the space-fixed $X_oY_oZ_o$ frame of reference to get the trajectory. Using transformation matrix of eqn. (2.4) the relationship between the velocity components in XYZ and $X_oY_oZ_o$ axis systems can be obtained as follows :

$$\begin{bmatrix} \dot{X}_o \\ \dot{Y}_o \\ \dot{Z}_o \end{bmatrix} = \begin{bmatrix} \cos\Theta\cos\Psi & \phi\cos\Psi\sin\Theta - \sin\Psi & \cos\Psi\sin\Theta + \phi\sin\Psi \\ \cos\Theta\sin\Psi & \phi\sin\Psi\sin\Theta + \cos\Psi & \sin\Psi\sin\Theta - \phi\cos\Psi \\ -\sin\Theta & \phi\cos\Theta & \cos\Theta \end{bmatrix} \begin{bmatrix} V_X \\ V_Y \\ V_Z \end{bmatrix} \tag{3.27}$$

where $\dot{X}_o$, $\dot{Y}_o$ and $\dot{Z}_o$ are the velocity components, along X_o, Y_o and Z_o axes respectively. Expanding eqn. (3.27) gives the following three first order nonlinear differential equations :

$$\dot{X}_o = V_X \cos\Theta\cos\Psi + V_Y(\phi\cos\Psi\sin\Theta - \sin\Psi) + V_Z(\cos\Psi\sin\Theta + \phi\sin\Psi) \tag{3.28}$$

$$\dot{Y}_o = V_X \cos\Theta\sin\Psi + V_Y(\phi\sin\Psi\sin\Theta + \cos\Psi) + V_Z(\sin\Psi\sin\Theta - \phi\cos\Psi) \tag{3.29}$$

$$\dot{Z}_o = -V_X \sin\Theta + V_Y \phi \cos\Theta + V_Z \cos\Theta \tag{3.30}$$

Equations (3.28) - (3.30) after linearization and non-dimensionalization reduce to

$$Dx_o = U\cos\Theta\cos\Psi - U\beta\sin\Psi + U\alpha\cos\Psi\sin\Theta , \tag{3.31}$$

$$Dy_o = U\cos\Theta\sin\Psi + U\beta\cos\Psi + U\alpha\sin\Psi\sin\Theta , \tag{3.32}$$

and

$$Dz_o = -U\sin\Theta + U\alpha\cos\Theta . \tag{3.33}$$

where $x_o = \frac{X_o}{L}$, $y_o = \frac{Y_o}{L}$ and $z_o = \frac{Z_o}{L}$.

3.7 SUMMARY

The trajectory is completely described with the help of nine differential equations (3.21) - (3.26) and (3.31) - (3.33). The six of these differential equations are of first order and the other three of second order. 12 initial conditions are required to solve these equations.

They are at $t^+ = 0$

$$U = 1 \ ,$$

$$\alpha = \beta = \Psi = \theta = \phi = \dot{\Psi} = \dot{\theta} = \dot{\phi} = 0 \ ,$$

and $$x_o = y_o = z_o = 0 \ .$$

The variation in atmospheric properties and wind which affect the trajectory significantly have not been considered so far. The corrections due to prevailing meteorological conditions are discussed in the next chapter.

CHAPTER 4

ATMOSPHERE AND ITS EFFECTS

4.1 ATMOSPHERIC STRUCTURE AND EFFECT OF COMPRESSIBILITY

The aerodynamic derivatives appearing in eqns. (3.21) - (3.26) which depend on the Mach number would change in the course of flight of the projectile due to change in speed and also due to variation in temperature of the atmosphere with height. Further, the parameters involving density also change with height. In order to obtain the actual trajectory these effects should be suitably incorporated by considering proper variations in density and temperature with altitude and accounting for the compressibility effect. Specifications of ICAO atmosphere are assumed in the present study and the corresponding variations in density, temperature and speed of sound for an altitude upto 11000 m are given by

$$\rho = \rho_o(1-0.22557695\times10^{-4}\ H)^{4.25587}\ , \qquad (4.1)$$

$$T = T_o - 0.0065\ H\ , \qquad (4.2)$$

$$a = \sqrt{\gamma RT}\ . \qquad (4.3)$$

where ρ is the density of air

ρ_o is the density of air at mean sea level = 1.225 kg/m^3

T is the temperature of air

T_o is the temperature of air at mean sea level

$= 288.15^{o}K$

H is the altitude in metres

a is the speed of sound in m/sec

γ is the ratio of specific heats for air = 1.4

R is the gas constant for air = 287.26 $m^2 sec^{-2} {}^{o}K^{-1}$

A similarity rule for axisymmetric bodies in the subsonic regime is used to account for the Mach number effect on the aerodynamic derivatives. According to similarity rule the pressure coefficient at any given point on the body, C_{p1} at a Mach number M_{a1}, is related to the pressure coefficient C_{p2} at another Mach number M_{a2} by [2]

$$C_{p1} = \frac{1 - M_{a2}^2}{1 - M_{a1}^2} C_{p2} \qquad (4.4)$$

The aerodynamic derivatives that arise from the normal pressure distribution can be corrected using this factor. However, the drag coefficient which is mainly due to the tangential pressure distribution can not be treated similarly. In a finned-projectile both the fins and the body contribute to drag coefficient. The total drag coefficient C_D is given by

$$C_D = (C_D)_B + (C_D)_W \ , \qquad (4.5)$$

where

$(C_D)_B$ is drag coefficient due to body, and $(C_D)_W$ is drag coefficient due to fins.

The body contribution to the drag coefficient is given by

$$(C_D)_B = C_{DP} + C_{DF} + C_{DB} \quad , \tag{4.6}$$

where

C_{DP} = pressure drag coefficient,

C_{DF} = skin friction drag coefficient,

and

C_{DB} = base drag coefficient.

The pressure drag coefficient C_{DP} is small compared to skin friction drag and base drag for the type of bodies under consideration and hence is neglected. The other two components are obtained from the following relationships [3] :

The skin friction drag coefficient C_{DF} is given by

$$C_{DF} = \left[\frac{4.96 \times 10^{-4}}{(1+0.03M_a^2)^{1/3}} \frac{SL}{S_{wet}} + \frac{0.032}{\sqrt{1+0.12M_a^2}} \left(\frac{1}{Re^{0.145}} - \frac{0.1\, S_L}{S_{wet}}\right)\right] \frac{S_{wet}}{S_{mid}} \tag{4.7}$$

where

S_L = porition of the wetted area over which laminar flow exists,

S_{wet} = total wetted area,

Re = Reynolds number = $\frac{V_L}{\nu}$, where ν is the kinematic viscosity of air and V and L are as already defined,

S_{mid} = largest cross-section area, and

M_a = flight Mach number.

In eqn. (4.7) the contributions to skin friction due to both the laminar and the turbulent flow have been included. The first part is due to laminar flow and the second part is due to turbulent flow. The base drag coefficient is expressed in terms of C_{DF} as

$$C_{DB} = \frac{0.029}{\sqrt{C_{DF}}} \left(\frac{d_B}{d_{mid}}\right)^3 , \qquad (4.8)$$

where

d_B = base diameter, and

d_{mid} = largest diameter.

The fin contribution to drag coefficient is given by [4]

$$(C_D)_W = C_f[1+ \bar{L}(\bar{t}/\bar{c})+100(\bar{t}/\bar{c})^4] \; R_{LS} \frac{S_{wet}}{S_{ref}} , \qquad (4.9)$$

where

C_f = turbulent flat-plate skin friction coefficient as a function of Mach number and Reynolds number,

$\bar{t}/\bar{c}$ = average stream wise thickness ratio of the fin,

$\bar{L}$ = airfoil thickness location parameter, $\bar{L}$ = 2.0 for $(\bar{t}/\bar{c})_{max}$ located at $x_t < 0.30_c$ (x_t is the chord-wise position of maximum thickness) (4.1.5.1) [4],

S_{wet} = wetted area of the fin,

S_{ref} = reference area, and

R_{LS} = lifting surface correction factor.

The lifting surface correction factor R_{LS} is a function of Mach number. For this type of projectiles an approximate relationship between R_{LS} and Mach number is given by

$$R_{LS} = 1.5\ Ma. \tag{4.10}$$

The aerodynamic coefficients except the drag coefficient have been estimated for a Mach number of 0.7 using DATCOM techniques and the details are presented in Appendix B. They have been subsequently corrected for actual Mach number using the similarity rule at every point on the trajectory during the computation. The drag coefficient on the other hand has been estimated at every point on the trajectory using the method discussed above for the actual Mach number.

4.3 EFFECT OF WIND

Wind has a considerable effect on the trajectory of the projectile. In order to analyse this effect on axis system $X_o'\ Y_o'\ Z_o'$ parallel to $X_o Y_o Z_o$ and moving with wind speed in the direction of wind is considered. The dynamical equations (3.21) - (3.26) and the kinematic equations (3.31) - (3.33) derived in Chapter 3 are now valid in $X_o'\ Y_o'\ Z_o'$ axis system. To obtain the trajectory in $X_o Y_o Z_o$ the effect of translation of $X_o'\ Y_o'\ Z_o'$ is accounted by including the wind velocity components along X_o, Y_o and Z_o axes. If $\bar{W}$, the wind vector has components W_{X_o}, W_{Y_o}, W_{Z_o} along X_o, Y_o, Z_o axes then the kinematic equations (3.31) - (3.33) accordingly get modified to

$$Dx_o = U\cos\Theta\cos\Psi - U\beta\sin\Psi + U\alpha\cos\Psi\sin\Theta + \frac{W_{X_o}}{V_o}, \qquad (4.11)$$

$$Dy_o = U\cos\Theta\sin\Psi + U\beta\cos\Psi + U\alpha\sin\Psi\sin\Theta + \frac{W_{Y_o}}{V_o}, \qquad (4.12)$$

and

$$Dz_o = -U\sin\Theta + U\alpha\cos\Theta + \frac{W_{Z_o}}{V_o}. \qquad (4.13)$$

If $\bar{W}$ has components W_X, W_Y, W_Z along X,Y,Z axes then the angle of attack, angle of side slip and the relative air speed V_R are given by the following modified expressions :

$$\sin\alpha = \frac{V_Z - W_Z}{V_R}, \qquad (4.14)$$

$$\sin\beta = \frac{V_Y - W_Y}{V_R}, \qquad (4.15)$$

$$V_R = \sqrt{V^2 + W^2} \qquad (4.16)$$

Since angles α and β are small eqns. (4.14) and (4.15) can be approximated by

$$\alpha = \frac{V_Z - W_Z}{V_R}, \qquad (4.17)$$

and

$$\beta = \frac{V_Y - W_Y}{V_R}. \qquad (4.18)$$

It can be seen from eqns. (4.17) and (4.18) that even though $V_Y = V_Z = 0$ at $t^+ = 0$, angles α and β are not zero. This calls for a modification in the initial conditions which arise from wind. The initial values of these two angles are therefore,

$$\alpha_o = - \frac{W_{Zo}}{\sqrt{V_o^2 + W^2}} , \tag{4.19}$$

$$\beta_o = - \frac{W_{Yo}}{\sqrt{V_o^2 + W^2}} , \tag{4.20}$$

and

$$U_o = \frac{V_o}{\sqrt{V_o^2 + W^2}} . \tag{4.21}$$

In Fig. 4.1 the relative orientations of $X_oY_cZ_o$ axis system and $\overline{W}$ in horizontal plane are shown. The wind direction and line of fire are always referred to North which is also shown in this figure. If θ_ω and θ_L are the angles between North and wind direction and North and line of fire respectively then W_{Xo}, W_{Yo}, W_{Zo} are given by

$$W_{X_o} = \frac{W}{V_R} \cos(\theta_w - \theta_L) \cos\theta_o , \tag{4.22}$$

$$W_{Y_o} = \frac{W}{V_R} \sin(\theta_w - \theta_L) , \tag{4.23}$$

and

$$W_{Z_o} = \frac{W}{V_R} \cos(\theta_w - \theta_L) \sin\theta . \tag{4.24}$$

CHAPTER 5

SOLUTION OF EQUATIONS

5.1 GENERAL

The eqns. (3.21) - (3.26) and (4.11) - (4.13) have been solved numerically on Dec-10 computer using the library routines written by the 'Numerical Algorithms Group' (NAG) [5]. Three methods, namely the Runge Kutta Merson method, the Adams method and the Gear method were tried and the Gear method was chosen based on time consideration. This routine integrates a system of first order, ordinary nonlinear differential equations with suitable initial conditions using a variable-order, variable-step Gear method and returns the solutions at points specified by the user [5]. The accuracy of integration and interpolation are controlled by the parameters TOL and IRELAB which are discussed in the subsequent paragraph. The stiffness of equations, if any, is also accounted by this routine.

4.2 ERROR CONTROLLING PARAMETERS

The parameter TOL specifies the accuracy tolerance. The step size is automatically adjusted by the routine to meet the tolerance requirements. Values of TOL between 10^{-5} and 10^{-7} were tried and it was noticed that the results were uneffected upto the 5th significant digit. A value of 10^{-5} was chosen to keep the execution time small.

The other parameter which controls the error is IRELAB. It controls the error based on the value specified for TOL. At each step in the numerical solution an estimate of the local error, EST is made, For the current step to be accepted the following conditions must be satisfied :

IRELAB = 0 $\quad$ EST $\leq$ TOL x max$[1.0, \frac{1}{N} \sum_{I=1}^{N} Y(I)^2]$;

IRELAB = 1 $\quad$ EST $\leq$ TOL ;

IRELAB = 2 $\quad$ EST $\leq$ TOL x max $[esp, \frac{1}{N} \sum_{I=1}^{N} Y(I)^2]$.

where eps is a small machine dependent number, Y is the matrix that contains all the variables of the set of differential equations being solved.

The program requires on an average about 5-6 seconds of CPU time to compute a complete trajectory and write all the variables at steps of 500 non dimensional time. The time required for writing the results at all intermediate points which is about 30-40% of the total time can be eliminated if only the results at the end point are required. The program in its present form requires 70 blocks on the disc.

4.3 PHYSICAL PARAMETERS OF THE TRAJECTORY

Besides the variables appearing in the equations of motion, the parameters of interest along the trajectory are the range, height and the angle of graze at the end point,

all referred to the horizontal plane passing through the point of launch.

Expressions for range and height are obtained referring to Fig. 4.1 and are given by

$$\text{Range} = L(x_o^2 \cos^2\theta_o + y_o^2 + z_o^2 \sin^2\theta_o + x_o z_o \sin 2\theta_o)^{1/2}, \qquad (5.1)$$

$$\text{Height} = L(x_o \sin\theta_o - z_o \cos\theta_o). \qquad (5.2)$$

The angle of graze δ is given by

$$\delta = \frac{\pi}{2} - \cos^{-1}(-\cos\theta \cos\Psi \sin\theta_o - \sin\theta \cos\theta_o) \qquad (5.3)$$

In the present study the equations have been solved for a 120 mm artillery projectile and the results are presented in the next chapter.

CHAPTER 6

RESULTS AND DISCUSSION

6.1 GENERAL

Time histories of angle of attack, angle of side slip, angle of roll, angle of pitch, angle of yaw and the lateral deviation and also the variations of range, height and lateral deviation for different angles of projection, muzzle velocities and wind conditions have been studied. The angle of graze at the terminal point of the projectile has also been determined for different angles of projection. Due to uncertainties in the estimated value of the aerodynamic coefficients, a parametric study has been carried out to ascertain the sensitivity of the trajectory to variations in these coefficients. The results are presented in Figs. 6.1 - 6.29 and discussed in the subsequent paragraphs.

6.2 RANGE AND HEIGHT

Figures 6.1 and 6.2 show the trajectories for several muzzle velocities and angles of projection. The range table values of the range and height are plotted for comparison. For 60^{o} projection angle the trajectory of an equivalent point mass is also presented. Percentage deviations in the overall trajectory parameters compared to the range table data are presented in Table 6.1.

It is seen clearly from Fig. 6.1 and Table 6.1 that the finite size of the projectile and its associated aerodynamics has a significant contribution for the trajectory. It can also be seen that the computed results are very close to the range table results. Range and height increase with increase in muzzle velocity where as with increase of angle of projection the range decreases and height increases.

In Fig. 6.3 variations of range and height versus muzzle velocity are presented. They are also compared with the range table data. The plots show very close agreement of both range and height with the present computed results for all muzzle velocities. It is further noted that while the estimated range is lower than the range table data for all muzzle velocities, the estimated height is lower than the range table for muzzle velocities below 205 m/sec and higher than the range table data for muzzle velocities above this.

In Fig. 6.4 variations of range and height with angle of projection are shown. For comparison the range table data are also plotted and it can be observed that the computed results for both range and height are very close to the range table results.

6.3 SPEED, ANGLE OF PITCH AND ANGLE OF ATTACK

In Figs. 6.5, 6.6 and 6.7 the time histories of non-dimensional speed, angle of pitch and angle of attack are

Table 6.1 Comparison of computed results with range Table Data

	V_o = 248.1 m/sec				θ_o = 60 deg.		
θ_o (deg)	Actual Trajectory		Point Mass Trajectory		V_o (m/sec)	% difference in range	% differer in height
	% difference in range	% difference in height	% difference in range	% difference in height			
45	-.4	1.5	24.6	14.0	153.0	-2.8	-2.8
60	-.44	.65	25.0	16.1	217.4	- .2	2.1
75	-.1	1.0	24.4	17.0	277.4	- .5	1.3

presented. The range table value of the terminal velocity at the point of graze is also shown. It is observed that the terminal velocity from computation agrees very closely with the range table value. The minimum speed of the projectile along the trajectory occurs at the vertex, i.e., the point where height is maximum. From Fig. 6.6 it can be seen that the angle of pitch remains negative through out the trajectory, of the projectile. It builds up slowly in the initial part upto about $\frac{1}{5}$th of the trajectory and thereafter its rate of build up increases till towards the end of the trajectory where once again the build up rate becomes small. Angle of attack variation in Fig. 6.7 shows that it is oscillatory and the oscillations get damped out in about $\frac{1}{5}$th of the trajectory, after which it practically remains at zero. Since θ variation presented in Fig. 6.6 does not indicate this type of oscillatory nature, these transient oscillations in α are due to the heaving motion of the projectile.

6.4 EFFECT OF WIND

6.4.1 Effect of Range Wind

6.4.1.1 Range

Effect of range wind on range is shown in Fig. 6.8 and the results are compared with range table data. It is noticed that while a tail wind increases the range a head wind results in a decrease of it. In either case the variation in range is

linear with wind speed. Comparison with the range table results shows that the present method slightly underestimates the range for head wind and the difference reduces as the wind speed increases. As for the effect of tail wind, the present study gives an underestimate of the range for wind speeds upto about 10 m/sec and for speeds above this it gives an overestimate of the range.

6.4.1.2 Angle of Attack

Figure 6.9 brings out the effect of range wind on angle of attack. It is seen that the angle of attack variation is characterised by high frequency transient oscillations. The peak amplitude of these oscillations is highest for head wind and lowest for zero wind as can be seen from Figs. 6.7 and 6.9. It is also noticed from these figures that these transient oscillations subside earlier for tail wind than for the head wind.

6.4.2 Effect of Cross Wind

Throughout the study a right cross wind is considered. For a left cross wind the results will be mirror images of those for right cross wind.

6.4.2.1 Lateral Deviation

In Figs. 6.10 and 6.11 the lateral deviation Y_o is plotted as a function of non dimensional time and the

variation of the terminal value of Y_o with cross wind velocity is presented in Fig. 6.12. It can be seen from Figs. 6.10 and 6.11 that build up in Y_o is quite slow and gradual initially. For lower wind velocities the trend continues to be gradual whereas for higher wind velocities the build up in the later part of the trajectory becomes quite rapid. It even seems to reach a maximum value after which it starts decreasing as can be noticed from the curve for V_o = 248.1 m/sec and $\theta_o = 70^\circ$ in Fig. 6.11. In order to understand this type of behaviour of lateral deviation, the two major contribution for Y_o have also been plotted for $\theta_o = 70^\circ$ on the same figure. The wind contribution increases linearly and is positive for right cross wind throughout the trajectory whereas the contribution due to yaw is negative and increases linearly only in the first half of the trajectory. In the second half of the trajectory this term decreases rapidly and starts increasing again after some time. Because of this behaviour of the contribution due to yaw, Y_o increases slowly and almost linearly in the first half and rapidly in the later part. This suggests that the variation of terminal Y_o with wind velocity may not be monotonic for higher wind velocities and large angles of projection and Fig. 6.12 indeed, confirms this. In this figure the range table results are also plotted. For angles of projection upto 60°, Y_o variation is almost linear with wind speed upto about 10 m/sec

whereas for $\theta_o > 60^o$ this monotonic variation breaks down. This is because of the yaw angle component as discussed earlier. In range table the wind effect has been compiled based on the concept of equivalent constant wind. This implies a linear dependence of Y_o on wind velocity and does not take into consideration the contribution of yaw to lateral deviation. Since this second contribution is quite significant at large angles of projection and wind speeds as has been noted, the lateral deviation as compiled in range table for these conditions can be highly unreliable.

6.4.2.2 Angle of Sideslip

Figure 6.13 shows the time history of angle of sideslip β with cross wind. The angle of sideslip is nonzero initially due to cross wind and it damps out quite rapidly to zero steady state value after going through transient oscillations as seen from the figure. This indicates that the projectile aligns itself to the resultant wind direction quickly after going through lateral oscillations initially.

6.4.2.3 Angle of Roll and Angle of Yaw

Time histories of angle of roll and angle of yaw are presented in Figs. 6.14 and 6.15 for different angles of projection and muzzle velocities. From Fig. 6.14 it is seen that for $\theta_o = 45^o$ and $V_o = 153.0$ m/sec, both ϕ and Ψ show oscillatory behaviour initially. The oscillation die out in

about $\frac{1}{5}$th of the trajectory after which they start slowly increasing. The magnitude of ϕ is small compared to that of Ψ (ϕ is very close to zero) initially. Towards the end of the trajectory both of them build up rapidly and reach maximum values. Beyond this they start reducing equally rapidly and seem to cross the time axis if the trajectory had continued. This change of sign of ϕ and Ψ is realised for higher muzzle velocities and angles of projection as can be seen from Fig. 6.15. In this figure also, initially the magnitude of Ψ is much larger than that of ϕ. This fast build up in the magnitude of Ψ initially is because of yawing of the projectile in response to nonzero side slip by virtue of its directional stability C_{n_β}. The projectile undergoes rapid yaw oscillations till it aligns to zero sideslip. The corresponding initial oscillations in β have been shown in Fig. 6.13 and have already been discussed. It is also noticed that over almost the entire trajectory ϕ and Ψ maintain opposite signs.

6.4.2.4 Angular Velocity Components

Figure 6.16 presents the time histories of the angular velocities p,q and r. The roll rate p shows a build up in oscillations initially which subsequently die out. Variation of q is negative and non oscillatory and reflects the variation of Θ in Fig. 6.6. The yaw rate r however, shows oscillations of much larger frequency than p and dies out much more rapidly

to zero than p. This is due to rapid oscillatory variations in Ψ discussed earlier. In order to study the correspondence between the angular velocities and the time rate derivatives of the Eulerian angles their time histories are plotted together in Figs. 6.17 and 6.18. It can be seen from Fig. 6.17 that p and $\dot{\phi}$ variations are different except between 1500 and 6000 non-dimensional time. This can be understood clearly from the expression for p in eqn. (2.2). In the initial part of the trajectory which is characterised with the presence of transients, the magnitudes of both the contributions for p namely, $\dot{\Psi}\sin\theta$ and $\dot{\phi}$ are comparable and hence p and $\dot{\phi}$ vary differently. After about $t^+ \simeq 1500$ while θ is still small $\dot{\Psi}$ also becomes very small and the contribution to p due to $\Psi \sin\theta$ becomes relatively insignificant. Therefore, p and $\dot{\phi}$ show almost identical variations in this part of the trajectory. Subsequently for t^+ greater than about 6000, θ also builds up and results in different variations of p and ϕ. The variations of r and $\dot{\Psi}$ in Fig. 6.18 are identical initially after which r becomes almost zero while $\dot{\Psi}$ continues with a small value and eventually becomes zero.

6.5 ANGLE OF GRAZE

In order to study the orientation of the projectile with respect to the horizontal plane at the point of graze, the variation of angle of graze δ with angle of projection is

plotted in Fig. 6.19. The angle of graze variation with θ_o is linear throughout. If the angle of yaw is small at the terminal point, the magnitude of δ is equal to $|\theta| - \theta_o$. Since δ is found to vary linearly with θ_o it can be concluded that $|\theta|$ at the point of graze also varies linearly with θ_o. The effect of wind on angle of graze is also shown in this figure. Increase in wind velocities above 4.0 m/sec did not show any noticeable change in the angle of graze.

6.6 PARAMETRIC STUDY

The variations in the trajectory parameters range, height, lateral deviation, angle of attack and angle of side slip due to variation in the aerodynamic coefficients are presented in Figs. 6.20 - 6.29.

6.6.1 Effect of Drag Coefficient

Figure 6.20 shows the sensitivity of range, height and lateral deviation to drag coefficient C_{X_o}. It is noticed that both the range and height increase with decrease of drag coefficient and decrease with increase of it. The effect of drag coefficient on lateral deviation is seen to be insignificant. Drag coefficient is the most significant parameter in determining the range.

The effects of other aerodynamic coefficients namely, C_{Z_α}, $C_{Z_{\dot{\alpha}}}$, C_{Z_q}, C_{m_α}, $C_{m_{\dot{\alpha}}}$, C_{m_q} and C_{l_p} on the range, height and

lateral deviation are shown in Figs. 6.21 - 6.27. It is seen that the variations of these coefficients have no significant effect on the range and height. However, the effect on lateral deviation is noticeable in some cases. Y_o decreases continuously with increase of C_{Z_α}, C_{Z_q} and C_{m_q}. As for the effect of $C_{Z_{\dot{\alpha}}}$, the lateral deviation is minimum at the base value of $C_{Z_{\dot{\alpha}}}$ and increases on either side of the base value as shown in Fig. 6.22. A similar variation of Y_o is seen in case of C_{l_p} also (Fig.6.27). With C_{m_α}, Y_o has its maximum at the base value and decreases for other values of C_{m_α} on either side of it. The effect of $C_{m_{\dot{\alpha}}}$ is seen to be practically insigificant. However, at lower values of $C_{m_{\dot{\alpha}}}$ the lateral deviation obtained is slightly more than that obtained at the base value.

6.6.2 Effect of C_{m_α} on Angle of Attack

Figure 6.28 shows the time histories of angle of attack for different values of C_{m_α}. The amplitude and frequency of the transient short period oscillations increase with increase of C_{m_α}. The increase in frequency is due to increase in stiffness (in pitching motion) arising from C_{m_α}. It is also noticed that for lower values of C_{m_α} the short period oscillations are followed by oscillations of relatively larger period which continue over a large part of the trajectory and this behaviour is almost not there for higher C_{m_α}.

6.6.3 Effect of C_{n_β} on Angle of Side Slip

In Fig. 6.29 time histories of angle of side slip for different values of C_{n_β} are plotted. It can be seen that the frequency of oscillations increases due to increase of C_{n_β} from -0.792 to -2.286. However, the curve for $C_{n_\beta} = -1.585$ shows very few oscillations and is better damped. This is likely to be due to the fact that a variation in C_{n_β} changes the damping ratio and $C_{n_\beta} = -1.585$ may be closer to critical damping than the other two.

CHAPTER 7

CONCLUSIONS

Obtaining the trajectory by solving equations of motion is a generalized approach and the method can easily be applied and extended to obtain the trajectory of any projectile with similar or modified configurations. The results of the present computations have shown that the angle of attack α, angle of side slip β, angle of roll ϕ and the time derivatives $\dot{\psi}$, $\dot{\theta}$ and $\dot{\phi}$ are very small and this justifies the assumptions made in simplifying the equations of motion.

The results of the present study show a good agreement with the range table results for range and height. But the lateral deviations in the two cases differ considerably. The differences in the computed results and the range table data can be attributed to the following :

- Uncertainties in the compilation of range table data which can be due to variations in the gun performance, limitations of measuring instruments and the errors in interpolation.
- The scheme used in the preparation of range tables to reduce the fired-data to the standard meteorological conditions itself is unsatisfactory and may introduce errors in the range table results.

- The range table assumes a linear dependence of the lateral drift on cross wind and neglects the contribution arising from the yaw angle term. The second contribution is quite significant and cannot be ignored.
- Uncertainties in the estimation of the stability derivatives of the projectile in the present study.
- Use of similarity rule to account for the compressibility effects is not exact and hence might introduce errors in the aerodynamic derivatives.

The parametric study carried out by varying the aerodynamic coefficients shows that the trajectory is significantly affected by only a few of these derivatives. It is found that the drag coefficient has the most dominant effect and the rest of the derivatives have negligible effect on the overall trajectory. It is therefore, imperative to determine the drag coefficient to a high degree of accuracy.

In this study the ICAO standard atmosphere has been used but the method is applicable in any atmosphere whose structural properties are known.

The speed and accuracy of computation of the present method strongly recommend its application in the modern environment of battle field. The program to solve the equations is small in size and occupies only 70 blocks on the disc in the present

form. Since the NAG routines used to solve the differential equations are also available on small computers, it would be possible to implement this model on a microprocessor. A ruggedised model of such a microprocessor will further advance its suitability for application in the battle field.

CHAPTER 8

SCOPE FOR FURTHER WORK

The present method can be successfully applied to study many other aspects of the motion of a projectile which could not be carried out due to time restriction and non availability of sufficient aerodynamic data. It has a wide scope and a few suggestions in this regard are as follows :

- The present model is restricted to subsonic speeds. The technique can be extended to transonic and supersonic speeds by choosing proper aerodynamic coefficients obtained either analytically or from wind tunnel tests.
- The equations of motion can be applied for rocket-assisted projectiles by including the thrust effect.
- The effect of rotation and curvature of earth can be incorporated which are significant only for long range projectiles.
- Probabilistic study on the point of fall can be carried out based on some given distribution of muzzle velocity, angle of projection etc.
- The present model can be optimized, an error analysis made for smaller machines and finally implemented on a microprocessor.

APPENDIX A

DERIVATION OF EQUATIONS OF MOTION

The equations of motion presented in Chapter 3 are derived step by step here. Linearization and non dimensionalization of these equations are also discussed in detail.

X COMPONENT OF FORCE

Equation (3.1) is resolved along X axis and transformed using eqn. (3.9) to get

$$\dot{M}_X + qM_Z - rM_Y = F_{AX} + F_{GX} ,$$

or

$$\frac{d}{dt}(m V_x) + qmV_Z - rmV_Y = F_{AX} + F_{GX} .$$

Substituting for V_X, V_Y, V_Z from eqn. (2.1), for q,r from eqn. (2.2) and for F_{AX} and F_{GX} from eqns. (3.18) and (3.20) respectively it follows that

$$m\left[\sqrt{1-\sin^2\alpha-\sin^2\beta}\,\frac{dV}{dt} - \frac{V(\sin 2\alpha\,\frac{d\alpha}{dt} + \sin 2\beta\,\frac{d\beta}{dt})}{2\sqrt{1-\sin^2\alpha-\sin^2\beta}}\right]$$

$$+ m(\dot{\theta}\cos\phi + \dot{\Psi}\sin\phi\cos\theta)\,V\sin\alpha - m(\dot{\Psi}\cos\theta\cos\phi - \dot{\theta}\sin\phi)V\sin\beta$$

$$= \frac{\rho}{2}V^2 S\,C_{X_o} - mg(\sin\theta_o\cos\theta\cos\Psi + \cos\theta_o\sin\theta),$$

or

$$m\sqrt{1-\sin^2\alpha-\sin^2\beta}\,\frac{dV}{dt} - \frac{\rho}{2}V^2S\,C_{X_o} + mg(\sin\theta_o\cos\theta\cos\Psi + \cos\theta_o\sin\theta)$$

$$= \frac{mV(\sin2\alpha\,\frac{d\alpha}{dt} + \sin2\beta\,\frac{d\beta}{dt})}{2\sqrt{1-\sin^2\alpha-\sin^2\beta}} - m(\dot\theta\cos\phi + \dot\Psi\sin\phi\cos\theta)\,V\sin\alpha$$

$$+ m(\dot\Psi\cos\theta\cos\phi - \dot\theta\sin\phi)V\sin\beta \quad . \qquad (A1)$$

Y COMPONENT OF FORCE

Equation (3.1) is resolved along Y axis and transformed using eqn. (3.9). This gives

$$\dot M_Y + rM_X - pM_Z = F_{AY} + F_{GY} \ ,$$

or

$$\frac{d}{dt}(mV_Y) + rmV_X - pmV_Z = F_{AY} + F_{GY} \ .$$

Substituting for V_X, V_Y, V_Z from eqn. (2.1), for p,r from eqn. (2.2) and for F_{AY} and F_{GY} from eqns. (3.18) and (3.20) respectively it follows that

$$m\sin\beta\,\frac{dV}{dt} + mV\cos\beta\,\frac{d\beta}{dt} + m(\dot\Psi\cos\theta\cos\phi - \dot\theta\sin\phi)\,V\sqrt{1-\sin^2\alpha-\sin^2\beta}$$

$$-m(\dot\phi - \dot\Psi\sin\theta)\,V\sin\alpha = \frac{\rho}{2}V^2S(C_{Y_\beta}\beta + C_{Y_{\dot\beta}}\frac{\dot\beta L}{2V} + C_{Y_r}\frac{rL}{2V})$$

$$+ mg[\phi(\cos\theta_o\cos\theta - \sin\theta_o\sin\theta\cos\Psi) + \sin\theta_o\sin\Psi],$$

or

$$m\sin\beta\,\frac{dV}{dt} + mV\cos\beta\,\frac{d\beta}{dt} + mV\sqrt{1-\sin^2\alpha-\sin^2\beta}\,(\dot\Psi\cos\theta\cos\phi)$$

$$- \frac{\rho}{2}V^2S(C_{Y_\beta}\beta + C_{Y_{\dot\beta}}\frac{\dot\beta L}{2V} + C_{Y_r}\frac{L}{2V}\dot\Psi\cos\theta\cos\phi) - mg[\phi(\cos\theta_o\cos\theta -$$

$$\sin\theta_o\sin\theta\cos\Psi) + \sin\theta_o\sin\Psi] = mV\sin\alpha(\dot\phi - \dot\Psi\sin\theta)$$

$$+ mV\sqrt{1-\sin^2\alpha-\sin^2\beta}(\dot\theta\sin\phi) - \frac{\rho}{2}V^2S\,C_{Y_r}\frac{L}{2V}\dot\theta\sin\phi \qquad (A2)$$

Z COMPONENT OF FORCE

Equation (3.1) is resolved along Z axis and transformed using eqn. (3.9) to obtain

$$\dot{M}_Z + pM_Y - qM_X = F_{AZ} + F_{GZ} ,$$

or

$$\frac{d}{dt}(mV_Z) + pmV_Y - qmV_X = F_{AZ} + F_{GZ} .$$

Substituting for V_X, V_Y, V_Z from eqn. (2.1), for p,q from eqn. (2.2) and for F_{AZ} and F_{GZ} from eqns. (3.18) and (3.20) respectively results in

$$m\sin\alpha \frac{dV}{dt} + mV\cos\alpha \frac{d\alpha}{dt} + mV\sin\beta(\dot{\phi} - \dot{\Psi}\sin\theta)$$

$$-m(\dot{\theta}\cos\phi + \dot{\Psi}\sin\phi\cos\theta)\, V\sqrt{1-\sin^2\alpha-\sin^2\beta} = \frac{\rho}{2} V^2 S[C_{Z_\alpha}\alpha +$$

$$C_{Z_{\dot{\alpha}}} \frac{\dot{\alpha}L}{2V} + C_{Z_q} \frac{L}{2V}(\dot{\theta}\cos\phi + \dot{\Psi}\sin\phi\cos\theta)] + mg[\cos\theta_o\cos\theta -$$

$$\sin\theta_o(\cos\Psi\sin\theta + \phi\sin\Psi)],$$

or

$$m\sin\alpha \frac{dV}{dt} + mV\cos\alpha \frac{d\alpha}{dt} - mV\sqrt{1-\sin^2\alpha-\sin^2\beta}(\dot{\theta}\cos\phi)$$

$$- \frac{\rho}{2} V^2 S(C_{Z_\alpha}\alpha + C_{Z_{\dot{\alpha}}} \frac{\dot{\alpha}L}{2V} + C_{Z_q} \frac{L}{2V}\dot{\theta}\cos\phi) - mg[\cos\theta_o\cos\theta -$$

$$\sin\theta_o(\cos\Psi\sin\theta + \phi\sin\Psi)] = -mV\sin\beta(\dot{\phi} - \dot{\Psi}\sin\theta) +$$

$$mV\sqrt{1-\sin^2\alpha-\sin^2\beta}(\dot{\Psi}\sin\phi\cos\theta) + \frac{\rho}{2} V^2 S\, C_{Z_q} \frac{L}{2V} \dot{\Psi}\sin\phi\cos\theta \qquad (A3)$$

X COMPONENT OF MOMENT

Equation (3.2) is resolved along X axis and transformed using eqn. (3.9) to get

$$\dot{H}_X + qH_Z - rH_Y = M_X \ .$$

Substituting for H_X, H_Y and H_Z from eqn. (3.7) gives

$$\frac{d}{dt}(I_X p) + qr(I_Z - I_Y) = M_X \ .$$

Substituting $I_Z = I_Y$ and for p and M_X from eqns. (2.2) and (3.18) respectively it follows that

$$I_X \frac{d}{dt}(\dot{\phi} - \dot{\Psi}\sin\theta) = \frac{\rho}{2} V^2 SLC_{l_p} \frac{L}{2V}(\dot{\phi} - \dot{\Psi}\sin\theta),$$

or

$$I_X \frac{d^2\phi}{dt^2} - I_X \sin\theta \frac{d^2\Psi}{dt^2} - \frac{\rho}{2} V^2 SL\, C_{l_p} \frac{L}{2V}\left(\frac{d\phi}{dt} - \sin\theta \frac{d\Psi}{dt}\right)$$

$$= I_X \cos\theta \frac{d\Psi}{dt}\frac{d\theta}{dt} \ . \qquad \text{(A4)}$$

Y COMPONENT OF MOMENT

Equation (3.2) is resolved along Y axis and transformed using eqn. (3.9). This gives

$$\dot{H}_Y + rH_X - pH_Z = M_Y \ .$$

Substituting for H_X, H_Y, H_Z from eqn. (3.7), for p,q,r from eqn. (2.2) and for M_Y from eqn. (3.18) results in

$$I_Y \frac{d}{dt}(\dot{\theta}\cos\phi + \dot{\psi}\cos\theta\sin\phi) + (\dot{\phi} - \dot{\psi}\sin\theta)(\dot{\psi}\cos\theta\cos\phi - \dot{\theta}\sin\phi)(I_X - I_Z)$$

$$= \frac{\rho}{2} V^2 SL\left[C_{m_\alpha}\alpha + C_{m_{\dot{\alpha}}}\frac{\dot{\alpha}L}{2V} + C_{m_q}\frac{L}{2V}(\dot{\theta}\cos\phi + \dot{\psi}\cos\theta\sin\phi)\right],$$

or

$$I_Y \cos\phi \frac{d^2\theta}{dt^2} - \frac{\rho}{2} V^2 SL\left(C_{m_\alpha}\alpha + C_{m_{\dot{\alpha}}}\frac{\dot{\alpha}L}{2V} + C_{m_q}\frac{L}{2V}\dot{\theta}\cos\phi\right)$$

$$= I_Y \sin\phi \frac{d\theta}{dt}\frac{d\phi}{dt} - I_Y \sin\phi\cos\theta \frac{d^2\psi}{dt^2} - I_Y \frac{d\psi}{dt}\left(\cos\theta\cos\phi\frac{d\phi}{dt}\right.$$

$$\left. - \sin\phi\sin\theta\frac{d\theta}{dt}\right) + \frac{\rho}{2} V^2 SLC_{m_q}\frac{L}{2V}\dot{\psi}\sin\phi\cos\theta -$$

$$(\dot{\phi} - \dot{\psi}\sin\theta)(\dot{\psi}\cos\theta\cos\phi - \dot{\theta}\sin\phi)(I_X - I_Z) \qquad \text{(A5)}$$

Z COMPONENT OF MOMENT

Equation (3.2) is resolved along Z axis and transformed using eqn. (3.9) to get

$$\dot{H}_Z + pH_Y - qH_X = M_Z$$

Substituting for H_X, H_Y, H_Z from eqn. (3.7), for p,q,r from eqn. (2.2) and for M_Z from eqn. (3.18) it follows that

$$I_Z \frac{d}{dt}(\dot{\psi}\cos\theta\cos\phi - \dot{\theta}\sin\phi) + (\dot{\phi} - \dot{\psi}\sin\theta)(\dot{\theta}\cos\phi + \dot{\psi}\cos\theta\sin\phi)(I_Y - I_X)$$

$$= \frac{\rho}{2} V^2 SL\left[C_{n_\beta}\beta + C_{n_{\dot{\beta}}}\frac{\dot{\beta}L}{2V} + C_{n_r}\frac{L}{2V}(\dot{\psi}\cos\theta\cos\phi - \dot{\theta}\sin\phi)\right],$$

or

$$I_Z \cos\Theta \cos\phi \frac{d^2\Psi}{dt^2} - \frac{\rho}{2} V^2 SL\left(C_{n_\beta}\beta + C_{n_{\dot\beta}} \frac{\dot\beta L}{2V} + C_{n_r} \frac{L}{2V} \dot\Psi \cos\Theta \cos\phi\right)$$

$$= -(\dot\phi - \dot\Psi \sin\Theta)(\dot\Theta\cos\phi + \dot\Psi \cos\Theta \sin\phi)(I_Y - I_X) + I_Z \sin\phi \frac{d^2\Theta}{dt^2}$$

$$+ I_Z \cos\phi \frac{d\phi}{dt}\frac{d\Theta}{dt} + I_Z \frac{d\Psi}{dt}\left(\cos\Theta \sin\phi \frac{d\phi}{dt} + \cos\phi \sin\Theta \frac{d\Theta}{dt}\right)$$

$$- \frac{\rho}{2} V^2 SL\, C_{n_r} \frac{L}{2V} \dot\Theta \sin\phi \qquad \text{(A6)}$$

LINEARIZATION

Equations (A1) - (A6) represent six scalar equations of motion of the projectile and are arranged in such a way that most of the higher order terms appear on the right hand side of the equations. All the first order terms have been written on the left hand side. Since the magnitude of the second and higher order aerodynamic terms is insignificant relative to the first order aerodynamic terms, all the second and higher order terms on the right hand side of eqns. (A1) - (A6) are neglected. The equations are further linearized by making the following simplifications :

$$\sin\phi = \phi \quad ; \quad \cos\phi = 1 - \frac{\phi^2}{2}$$

$$\sin\alpha = \alpha \quad ; \quad \cos\alpha = 1 - \frac{\alpha^2}{2}$$

$$\sin\beta = \beta \quad ; \quad \cos\beta = 1 - \frac{\beta^2}{2}$$

$$\sqrt{1-\sin^2\alpha-\sin^2\beta} = 1 - \left(\frac{\alpha^2+\beta^2}{2}\right) .$$

After making these substitutions the second order terms in angles ϕ, α and β are also neglected. Thus eqns. (A1) - (A6) can be simplified to get

$$m\frac{dV}{dt} - \frac{\rho}{2}V^2 S\, C_{X_o} + mg(\sin\theta_o \cos\theta \cos\psi + \cos\theta_o \sin\theta) = 0, \quad (A7)$$

$$m\beta\frac{dV}{dt} + mV\frac{d\beta}{dt} + mV\cos\theta\frac{d\psi}{dt} - \frac{\rho}{2}V^2 S(C_{Y_\beta}\beta + C_{Y_{\dot\beta}}\frac{d\beta}{dt}\frac{L}{2V} + C_{Y_r}\frac{L}{2V}\cos\theta\frac{d\psi}{dt}) - mg[\phi(\cos\theta_o\cos\theta - \sin\theta_o\sin\theta\cos\psi) + \sin\theta_o\sin\psi] = 0 \quad (A8)$$

$$m\alpha\frac{dV}{dt} + mV\frac{d\alpha}{dt} - mV\frac{d\theta}{dt} - \frac{\rho}{2}V^2 S(C_{Z_\alpha}\alpha + C_{Z_{\dot\alpha}}\frac{L}{2V}\frac{d\alpha}{dt} + C_{Z_q}\frac{L}{2V}\frac{d\theta}{dt}) - mg[\cos\theta_o\cos\theta - \sin\theta_o(\cos\psi\sin\theta + \phi\sin\psi)] = 0, \quad (A9)$$

$$I_X\frac{d^2\phi}{dt^2} - I_X\sin\theta\frac{d^2\psi}{dt^2} - \frac{\rho}{2}V^2 S\, LC_{l_p}\frac{L}{2V}(\frac{d\phi}{dt} - \sin\theta\frac{d\psi}{dt}) = 0, \quad (A10)$$

$$I_Y\frac{d^2\theta}{dt^2} - \frac{\rho}{2}V^2 S_L(C_{m_\alpha}\alpha + C_{m_{\dot\alpha}}\frac{L}{2V}\frac{d\alpha}{dt} + C_{m_q}\frac{L}{2V}\frac{d\theta}{dt}) = 0, \quad (A11)$$

$$I_Z\cos\theta\frac{d^2\psi}{dt^2} - \frac{\rho}{2}V^2 SL(C_{n_\beta}\beta + C_{n_{\dot\beta}}\frac{L}{2V}\frac{d\beta}{dt} + C_{n_r}\frac{L}{2V}\cos\theta\frac{d}{dt}) = 0 \quad (A12)$$

NON-DIMENSIONALIZATION

To non-dimensionalize eqns. (A7) - (A12), a projectile time factor is defined as

$$\tau = \frac{L}{V_o} \quad (A13)$$

where,

τ : projectile time factor

L : characteristic length

V_o : initial velocity of projection .

The non dimensional time t^+ is given by

$$t^+ = \frac{t}{\tau} ,$$

or

$$t^+ = \frac{V_o}{L} t \quad . \tag{A14}$$

Differentiating eqn. (A14) with respect to t gives

$$\frac{dt^+}{dt} = \frac{V_o}{L} \tag{A16}$$

The time derivatives in eqns. (A7) - (A12) are now replaced by the derivatives with respect to non dimensional time t^+. Using concise notations for the coefficients of the variables, the eqns. (A7) - (A12) with non dimensional time as independent variable are finally expressed as follows :

$$DU - \frac{1}{2\mu} C_{X_o} U^2 + F(\sin\theta_o \cos\theta \cos\Psi + \cos\theta_o \sin\theta) = 0, \tag{A17}$$

$$(1 - \frac{1}{4\mu} C_{Y_\beta})UD\beta + \cos\theta(1 - \frac{1}{4\mu} C_{Y_r})UD\Psi + \frac{1}{2\mu} (C_{X_o} - C_{Y_\beta}) U^2\beta$$

$$-F(\sin\theta_o \cos\theta \cos\Psi + \cos\theta_o \sin\theta)\beta - F[\phi(\cos\theta_o \cos\theta -$$

$$\sin\theta_o \sin\theta \cos\Psi) + \sin\theta_o \sin\Psi] = 0 , \tag{A18}$$

$$(1 - \frac{1}{4\mu} C_{Z_{\dot{\alpha}}})UD\alpha-(1+ \frac{1}{4\mu} C_{Z_q})UD\theta + \frac{1}{2\mu} (C_{X_o} - C_{Z_\alpha})U^2\alpha$$

$$- F(\sin\theta_o \cos\theta \cos\Psi + \cos\theta_o \sin\theta)\alpha - F[\cos\theta_o \cos\theta -$$

$$\sin\theta_o(\cos\Psi \sin\theta + \phi\sin\Psi)] = 0 , \qquad (A19)$$

$$D^2\phi-\sin\theta\, D^2\Psi -K_1 C_{l_p} UD\phi + K_1 C_{l_p} \sin\theta\, UD\Psi = 0 \qquad (A20)$$

$$D^2\theta-K_2 C_{m_{\dot{\alpha}}} UD\alpha-K_2 C_{m_q} UD\theta - 2K_2 C_{m_\alpha} U^2\alpha = 0 \qquad (A21)$$

$$\cos\theta\, D^2\Psi -K_2 C_{n_{\dot{\beta}}} UD\beta - K_2 C_{n_r} \cos\theta\, UD\Psi - 2K_2 C_{n_\beta} U^2\beta = 0 \qquad (A22)$$

where,

$$D = \frac{d}{dt^+} ,$$

$$U = \frac{V}{V_o} ,$$

$$\mu = \frac{m}{\rho SL} ,$$

$$F = \frac{gL}{V_o^2} ,$$

$$K_1 = \frac{\rho SL^3}{4I_X} ,$$

$$K_2 = \frac{\rho SL^3}{4I_Y} = \frac{\rho SL^3}{4I_Z} .$$

APPENDIX B

PROJECTILE BODY PARAMETERS AND ESTIMATED AERODYNAMIC COEFFICIENTS

BODY PARAMETERS

The results have been computed in the present study for a 120 mm projectile which has the following body parameters :

Total length : 0.6746 m

Location of centre of gravity from base : 0.4037 m

Maximum diameter : 0.1196 m

Base diameter : 0.0455 m

Length of the fin : 0.0615 m

Width of the fin : 0.042 m

Number of fins : 12

Weight of the projectile : 13.216 Kg

Moments of Inertia

I_X : 0.02580 Kg m^2

$I_Y = I_Z$: 0.24610 Kg m^2

AERODYNAMIC COEFFICIENTS

The aerodynamic coefficients have been estimated for the following conditions :

Characteristic length : 0.675 m

Characteristic area : 0.011122 m^2

Speed : 236.4 m/sec

The estimated values of the aerodynamic coefficients are as follows :

C_{X_o} = -0.151 [3], (4.1.5.1) [4]

C_{Z_α} = -8.44 (4.3.1.2) [4]

$C_{Z_{\dot{\alpha}}}$ = -0.723 (7.3.4.1) [4]

C_{Z_q} = -9.12 (7.3.1.1) [4]

C_{l_p} = -0.6 (7.3.2.2) [4]

C_{m_α} = -1.585 (4.2.2.1) [4]

$C_{m_{\dot{\alpha}}}$ = 0.047 (7.2.2.2) [4]

C_{m_q} = -2.754 (7.3.1.2) [4]

REFERENCES

1. Charters, A.C., 'The linearized equations of motion underlying the dynamic stability of aircraft, spinning projectiles and symmetrical missiles', NACA TN 3350,1955.

2. Liepmann, H.W., Roshko, A., 'Elements of Gas dynamics', John Wiley and Sons, Inc, 1957.

3. Krasnov, N.E., 'Aerodynamics of bodies of revolution', American Elsevier Publishing Co.Inc., New York, 1970.

4. US Air Force Stability and Control DATCOM (Data Compendium), A Wright Patterson Air Force Base, Ohio, 1968.

5. Numerical Algorithms Group Fortran Library Manual, Mark 8, Vol. I, 1978.

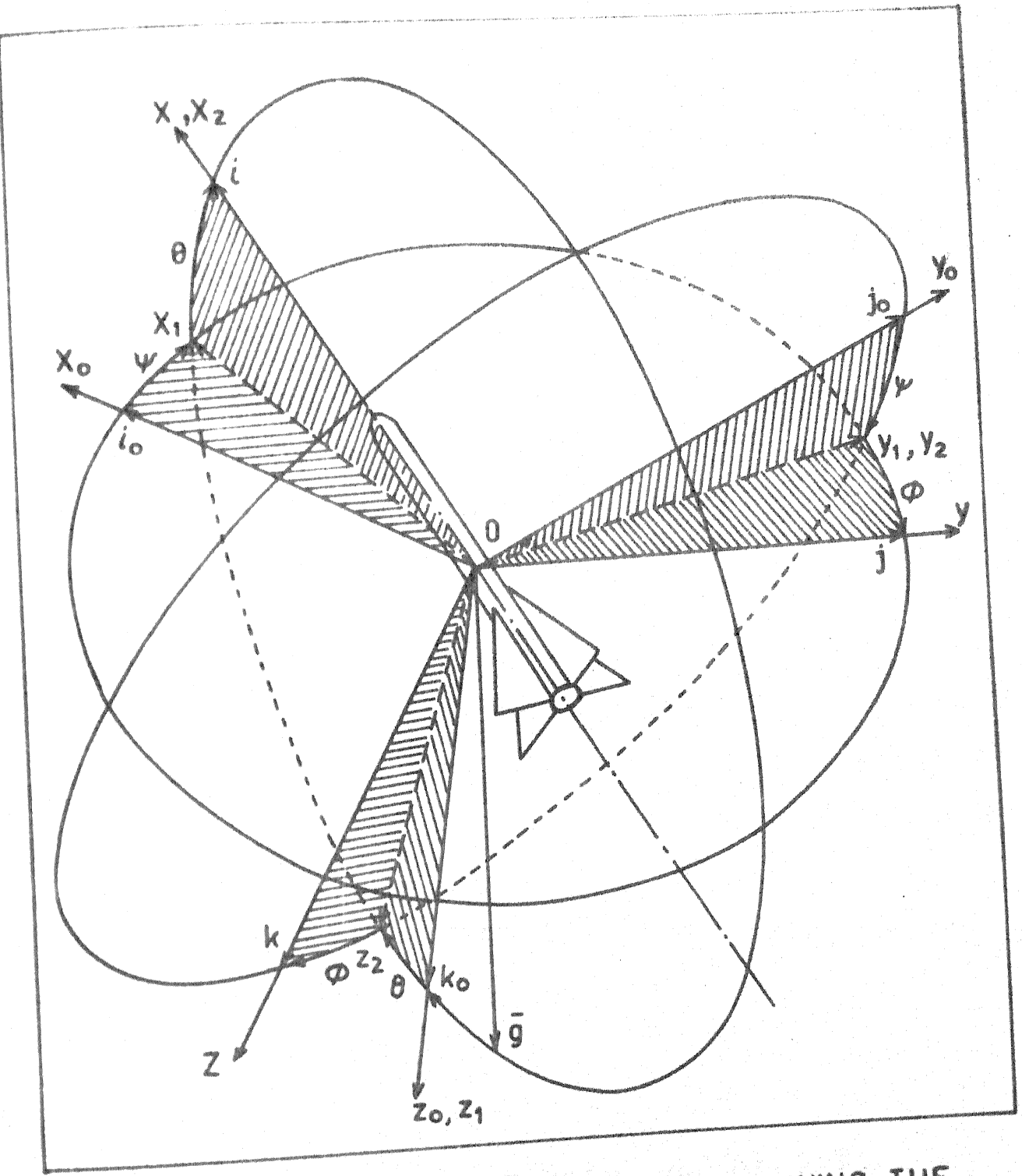

FIG.2.1 SPACE GEOMETRY OF PROJECTILE SHOWING THE ORIENTATIONS OF STABILITY AXES, EARTH-FIXED AXES, AND GRAVITY VECTOR.

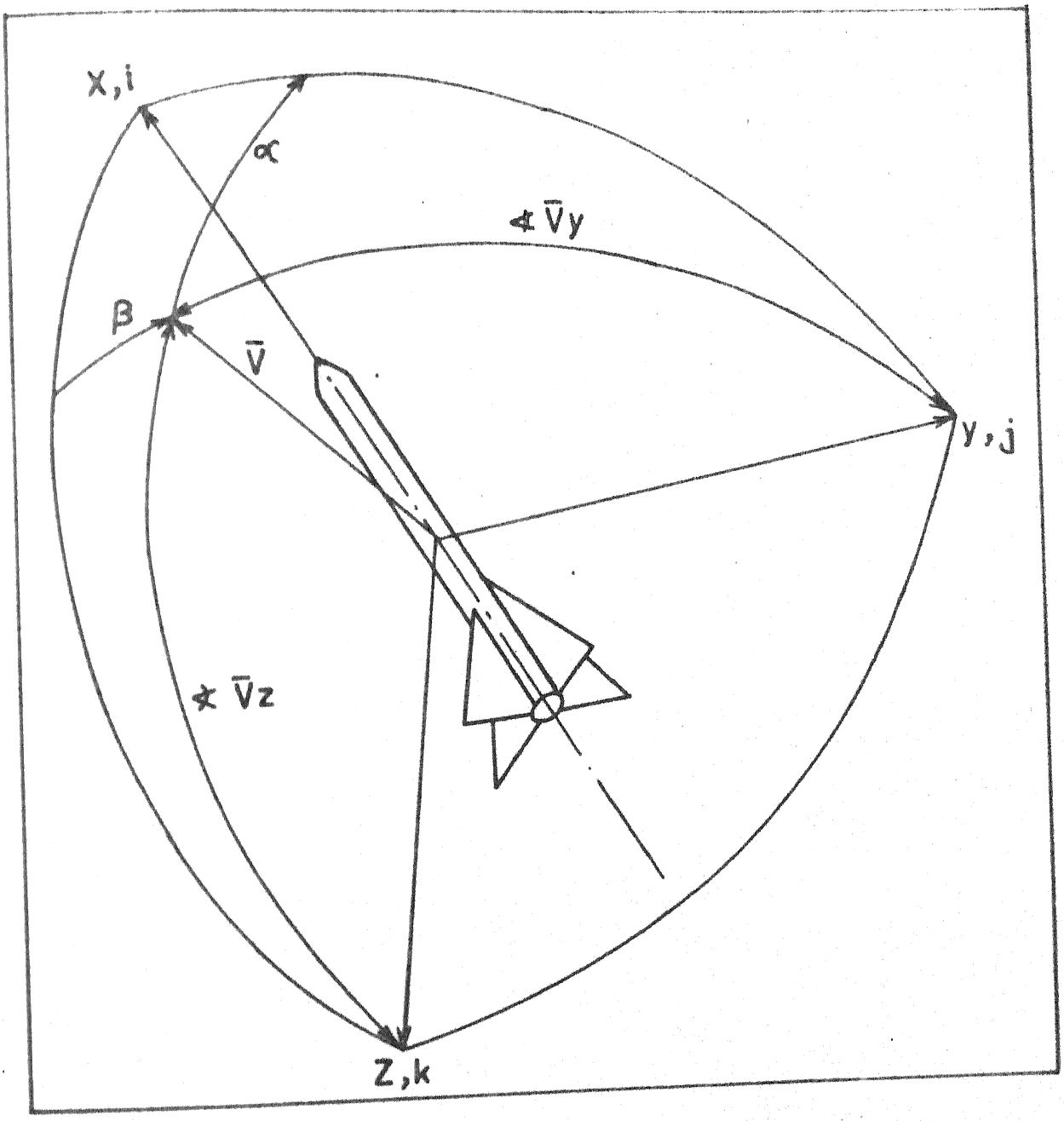

FIG.2.2 ORIENTATION OF VELOCITY VECTOR WITH RESPECT TO STABILITY AXES.

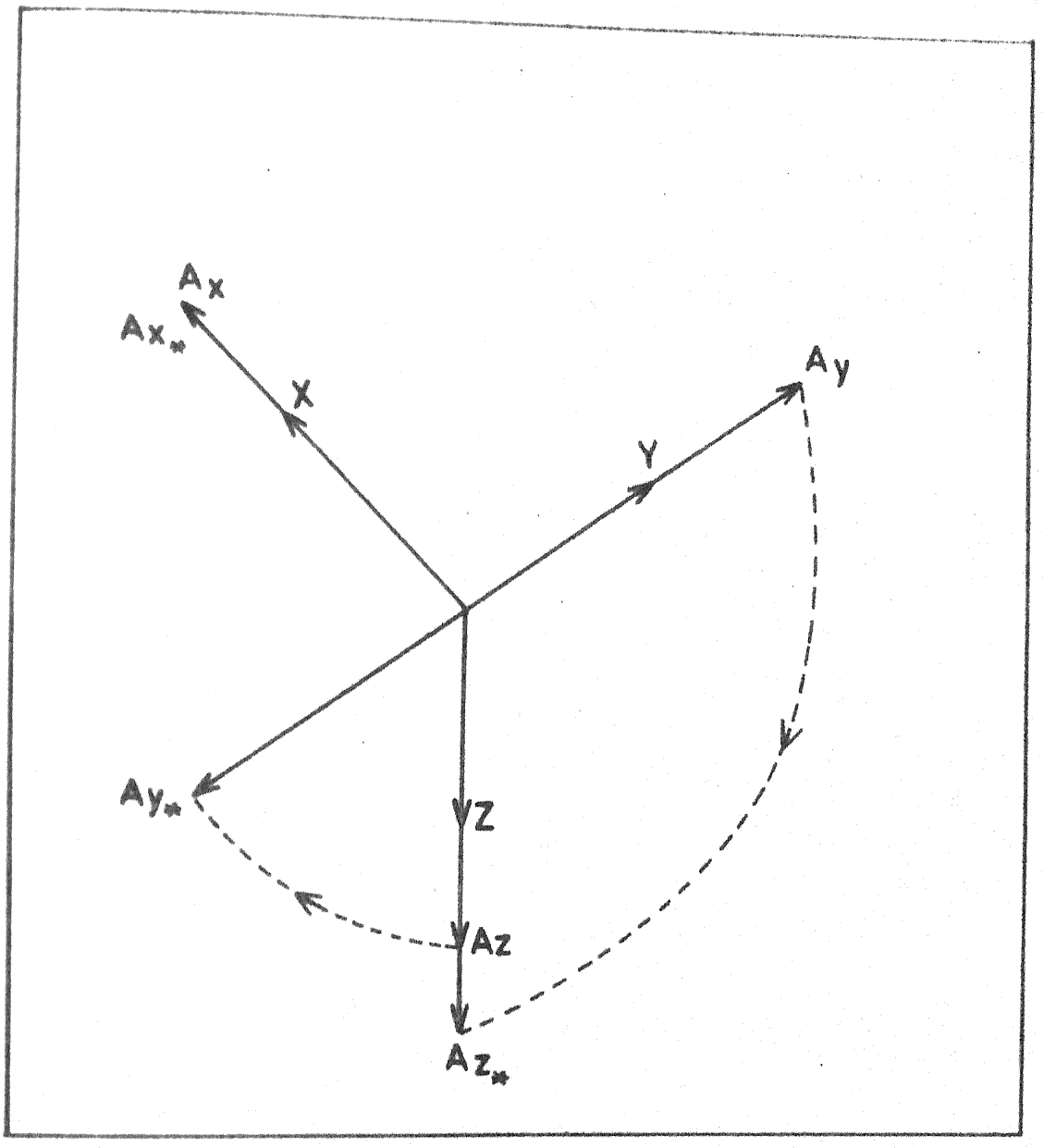

FIG.3.1 ROTATION OF A VECTOR BY 90° ABOUT X AXIS.

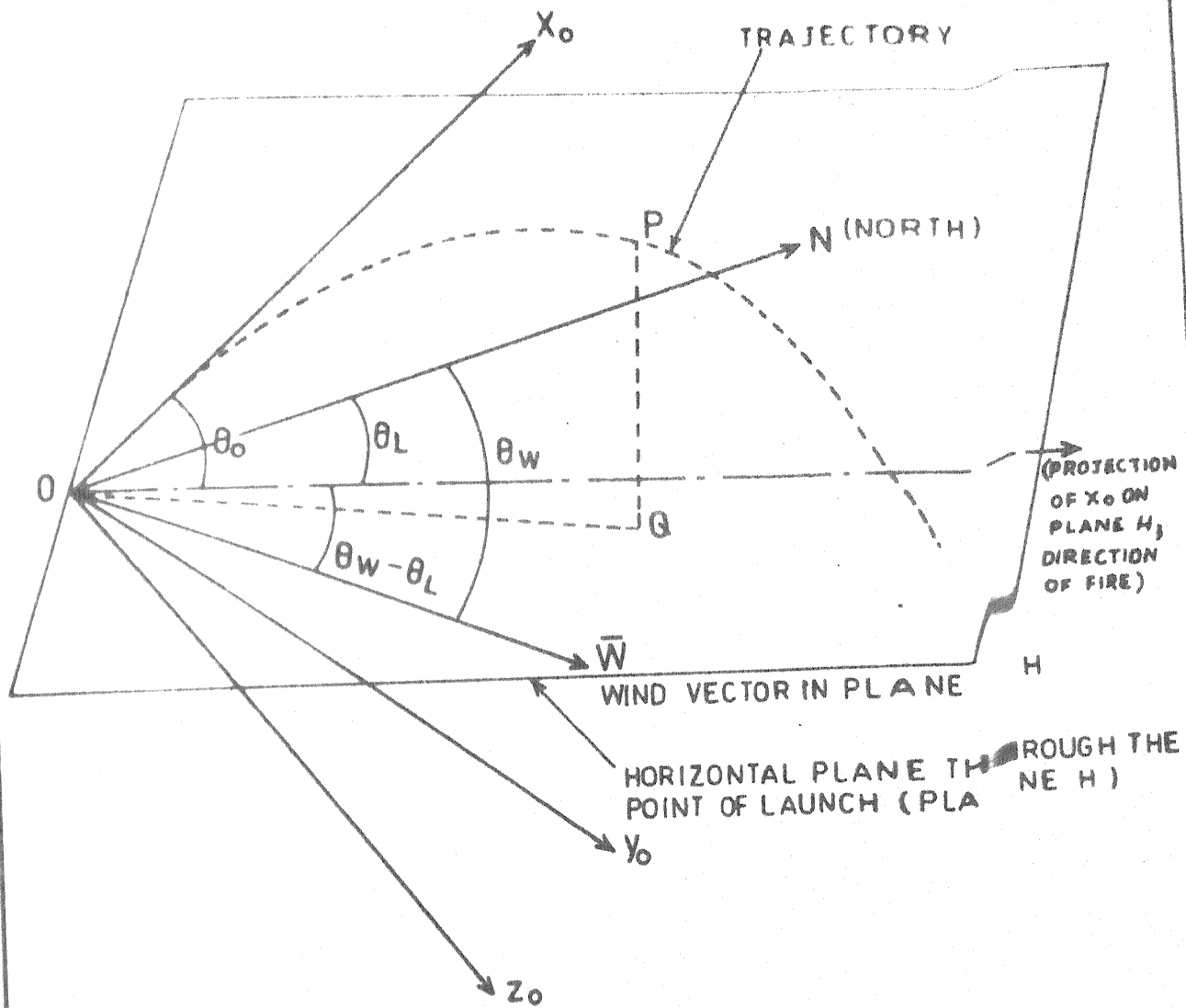

P : A point on the trajectory (x_o, y_o, z_o)

OQ : Range of point P in the plane H.

PQ : Vertical height of point P above plane H.

FIG.4.1 SCHEMATIC DIAGRAM OF TRAJECTORY WITH WIND

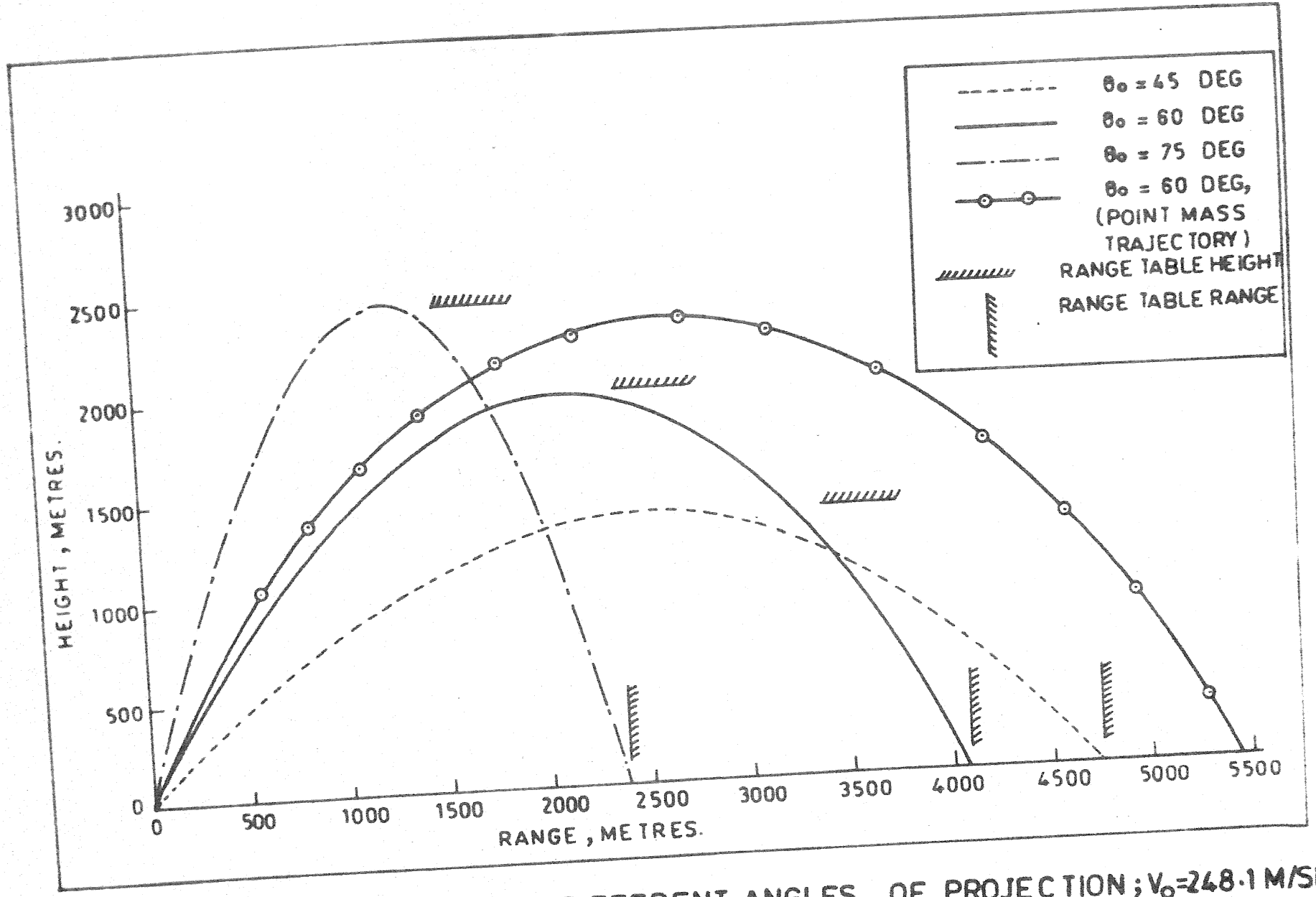

FIG.6.1 RANGE VS HEIGHT FOR DIFFERENT ANGLES OF PROJECTION; V_o=248.1 M/SEC.

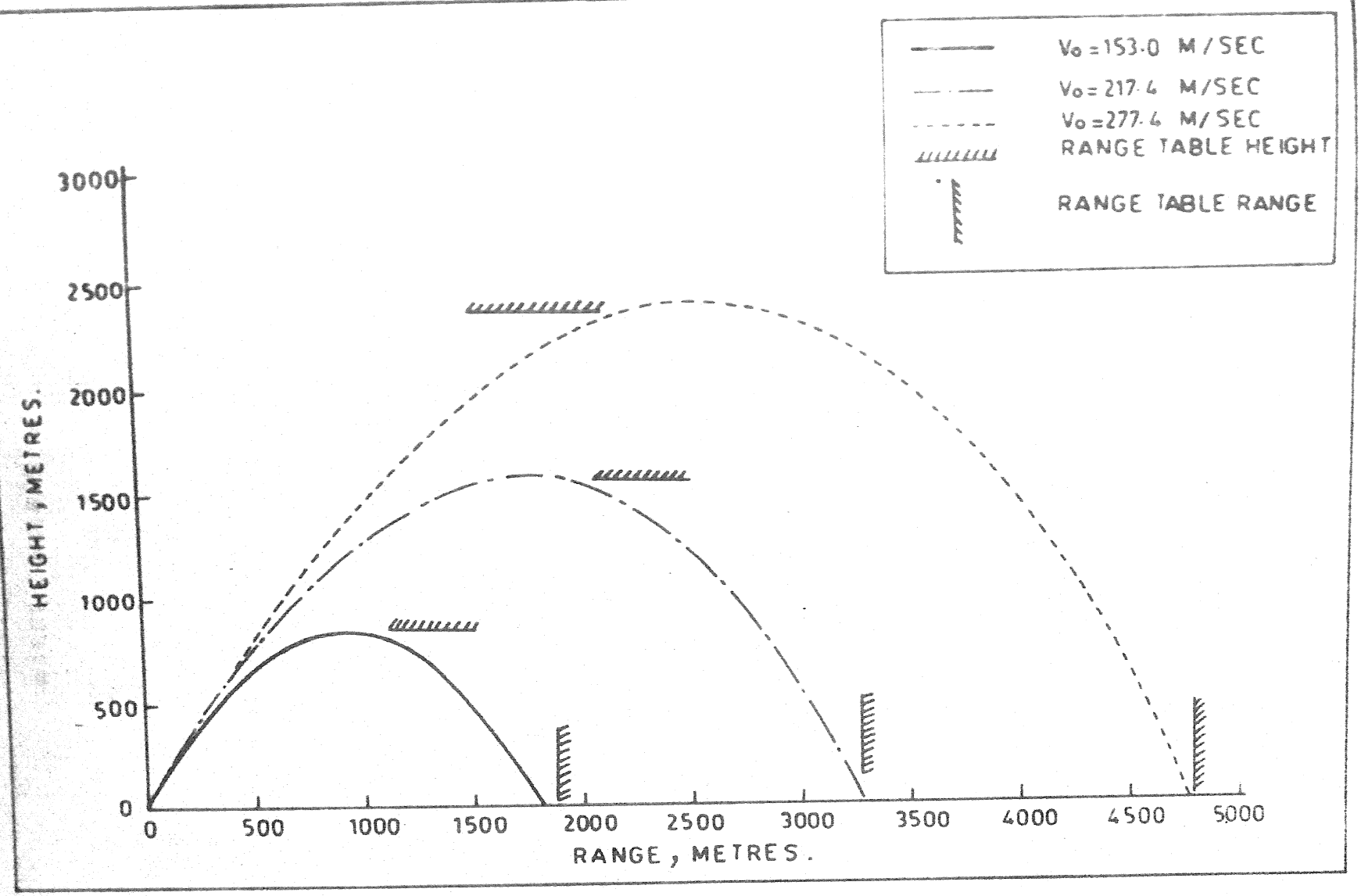

FIG.6.2 RANGE VS HEIGHT FOR DIFFERENT MUZZLE VELOCITIES; θ_o=60 DEG.

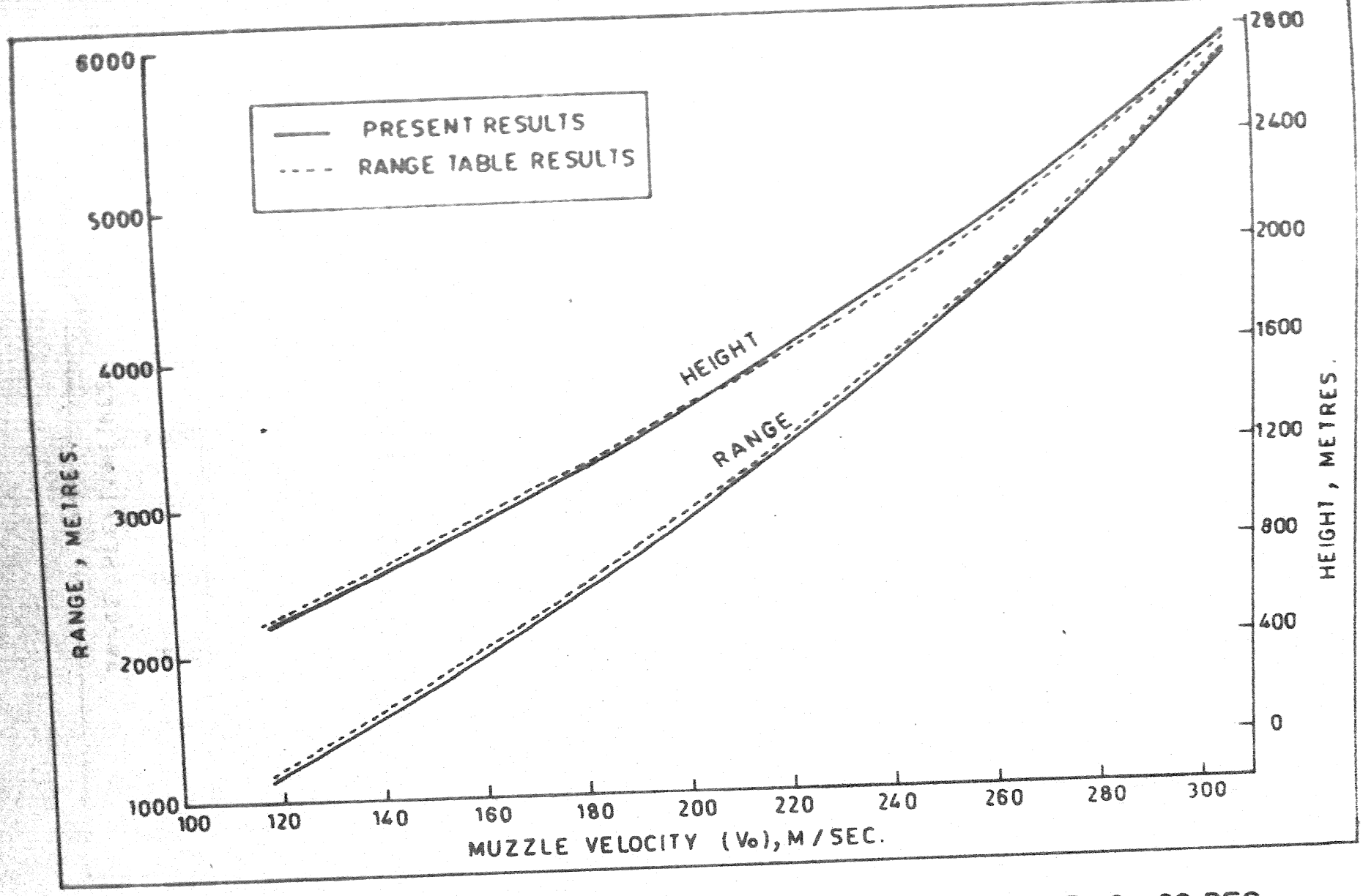

FIG.6.3 EFFECT OF MUZZLE VELOCITY ON RANGE AND HEIGHT; θ_0=60 DEG.

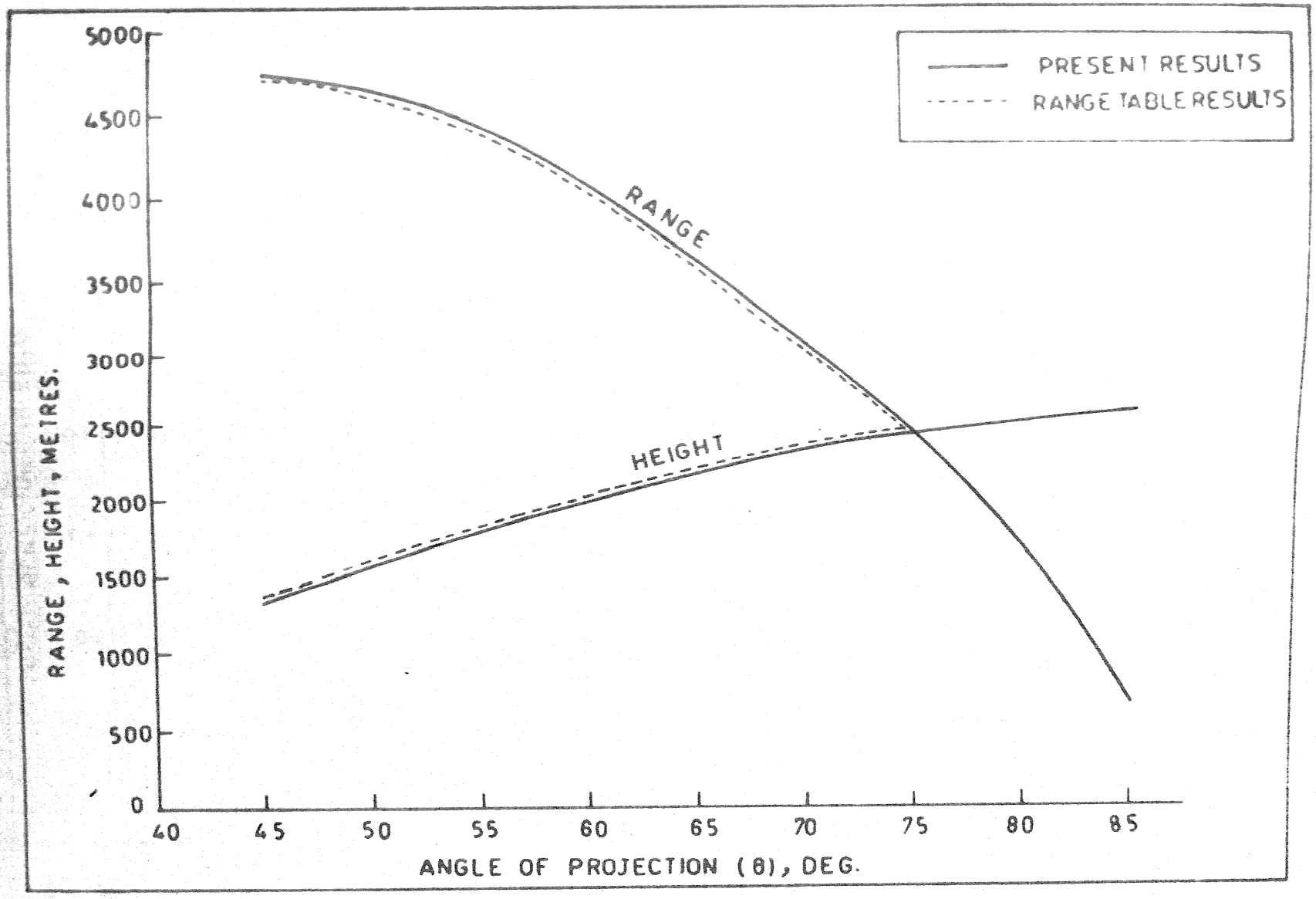

FIG.6.4 EFFECT OF ANGLE OF PROJECTION ON RANGE AND HEIGHT; V_0 = 248·1 M/SEC.

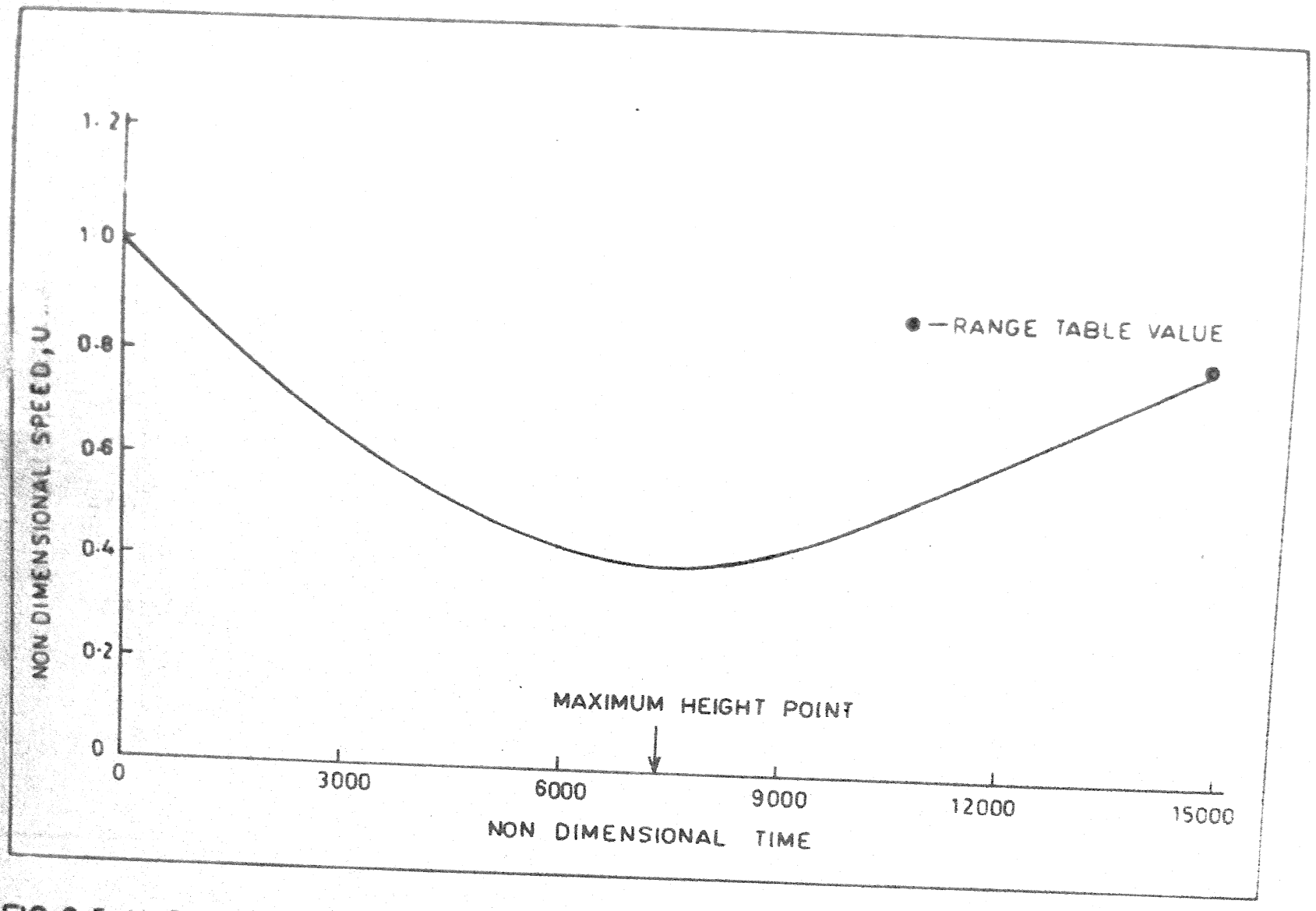

FIG.6.5 VARIATION OF SPEED WITH NON DIMENSIONAL TIME; θ_o=60 DEG, V_o = 248·1 M/SEC.

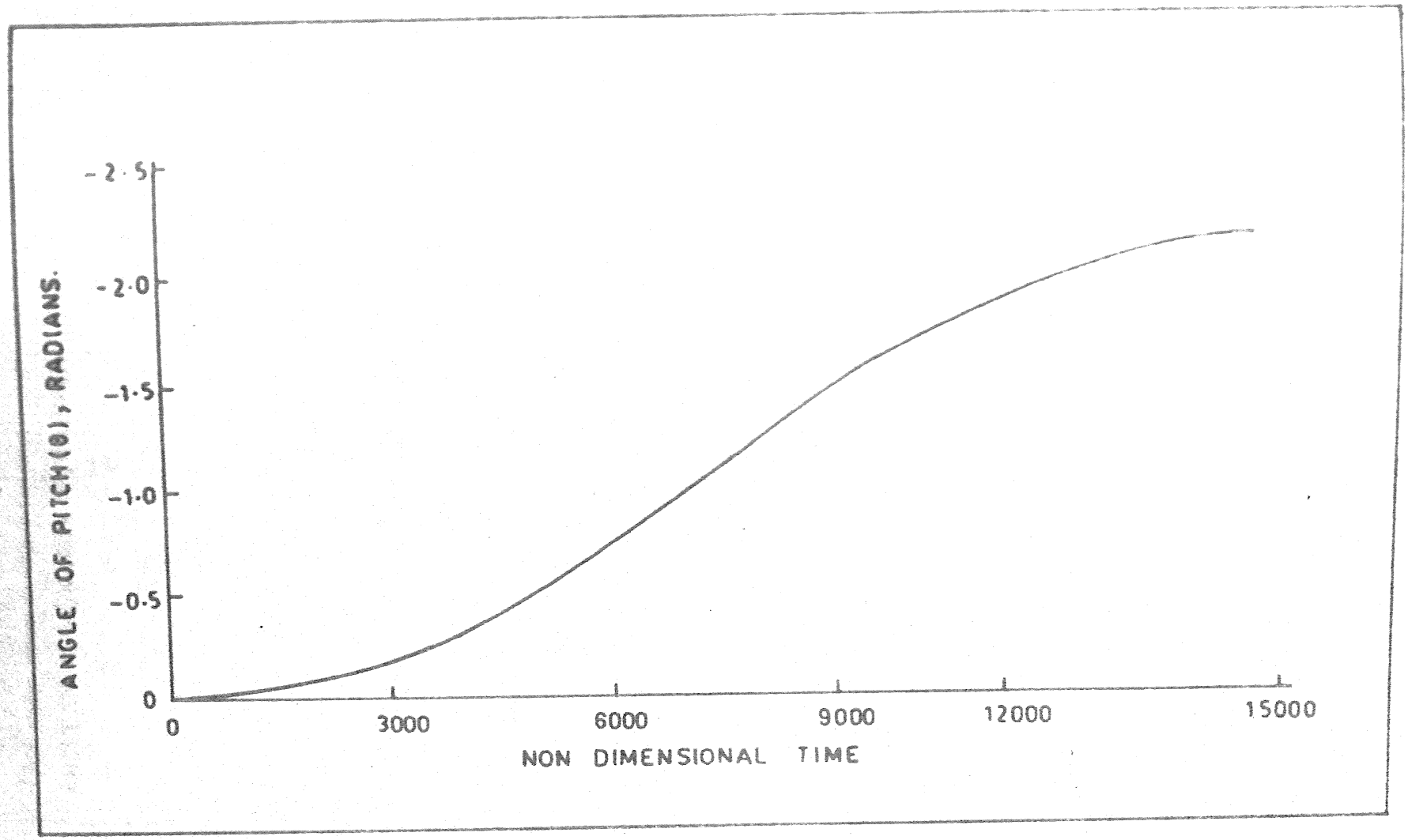

FIG.6.6 VARIATION OF ANGLE OF PITCH WITH NON DIMENSIONAL TIME; θ_o=60 DEG, V_o = 248·1 M/SEC.

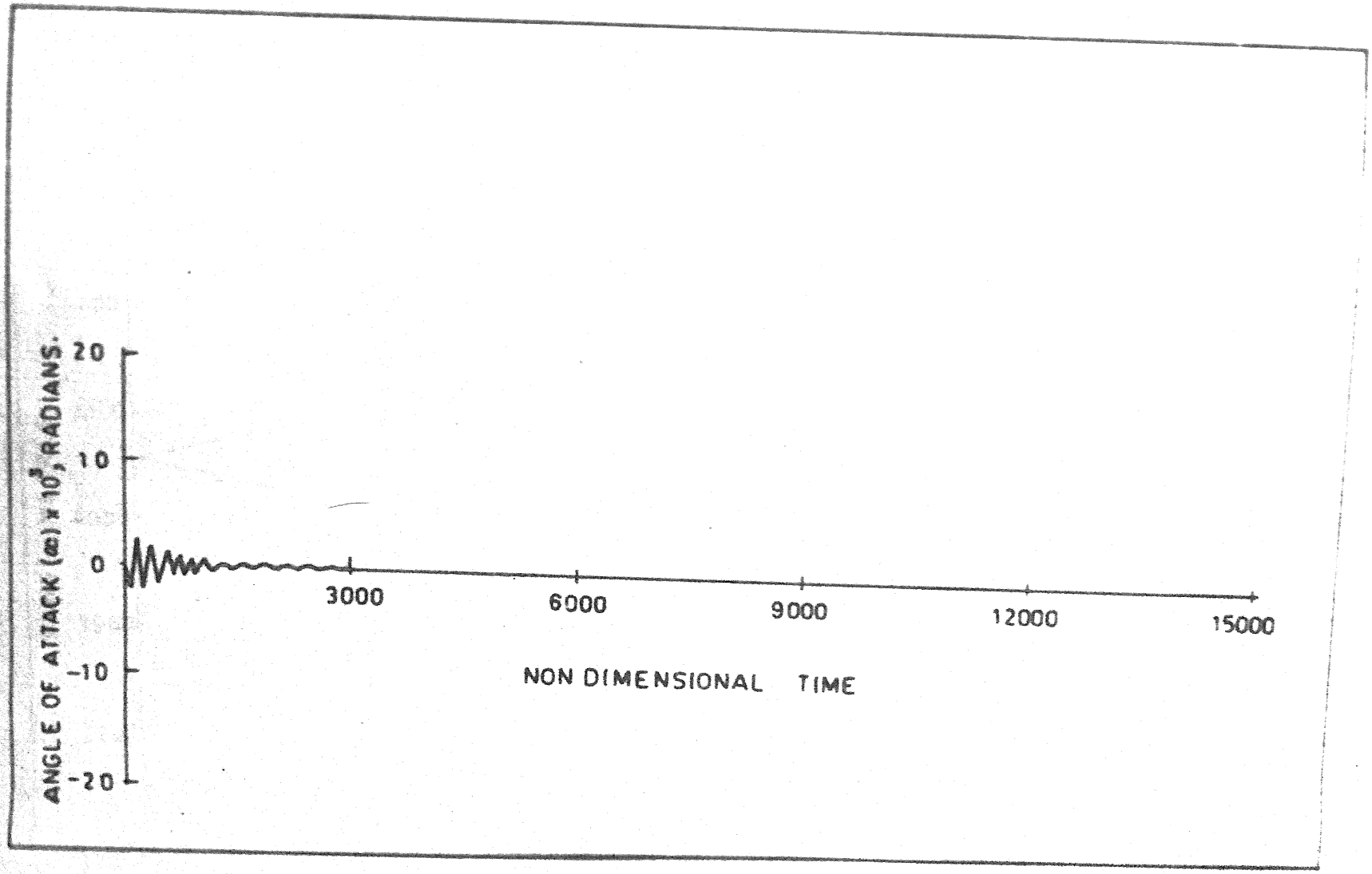

FIG.6.7 VARIATION OF ANGLE OF ATTACK WITH NON DIMENSIONAL TIME;
$\theta_0 = 60$ DEG, $V_0 = 248.1$ M/SEC, ($C_{m_{\dot{\alpha}}} = -1.585$).

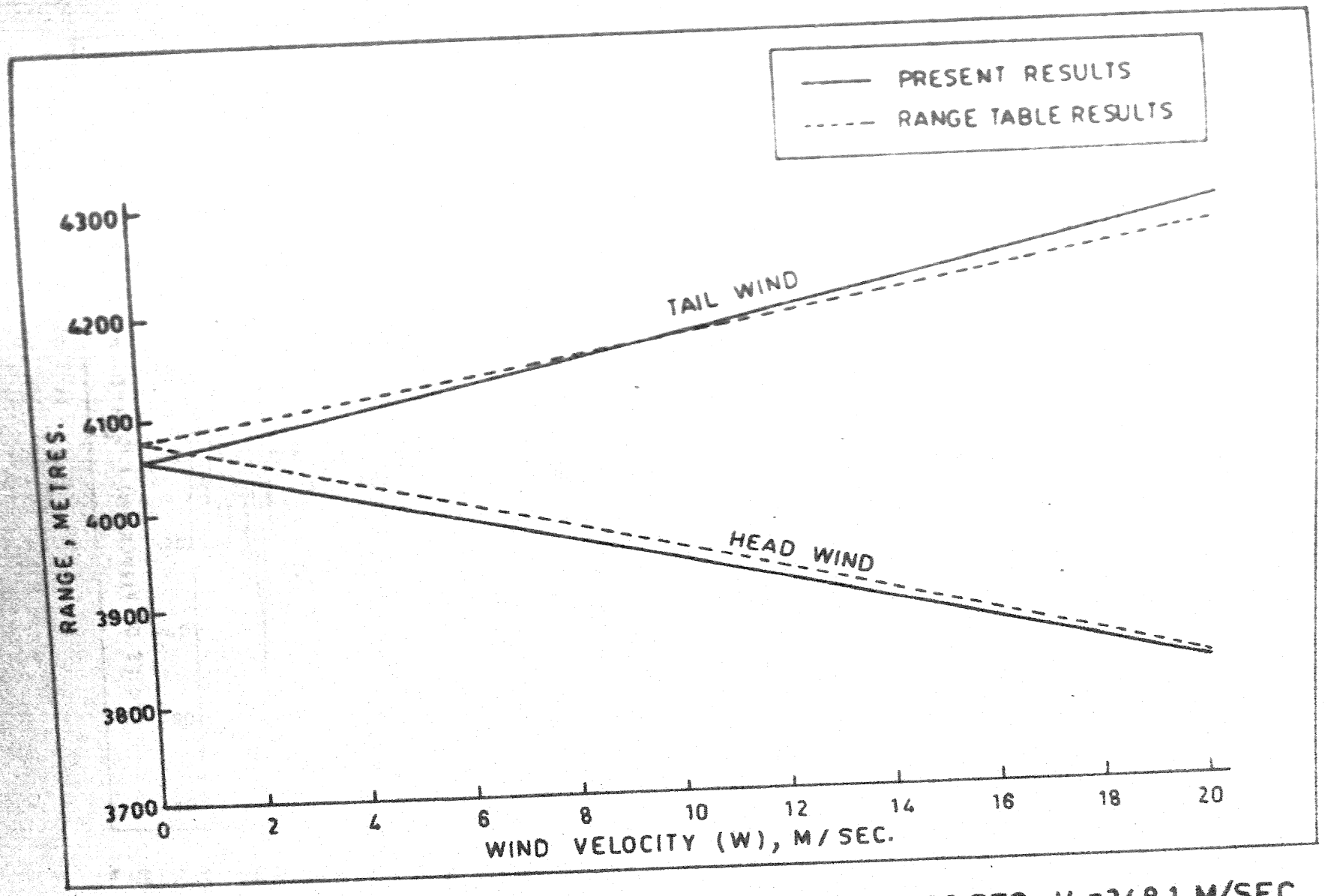

FIG.6.8 EFFECT OF RANGE WIND ON RANGE; $\theta_0 = 60$ DEG, $V_0 = 248.1$ M/SEC.

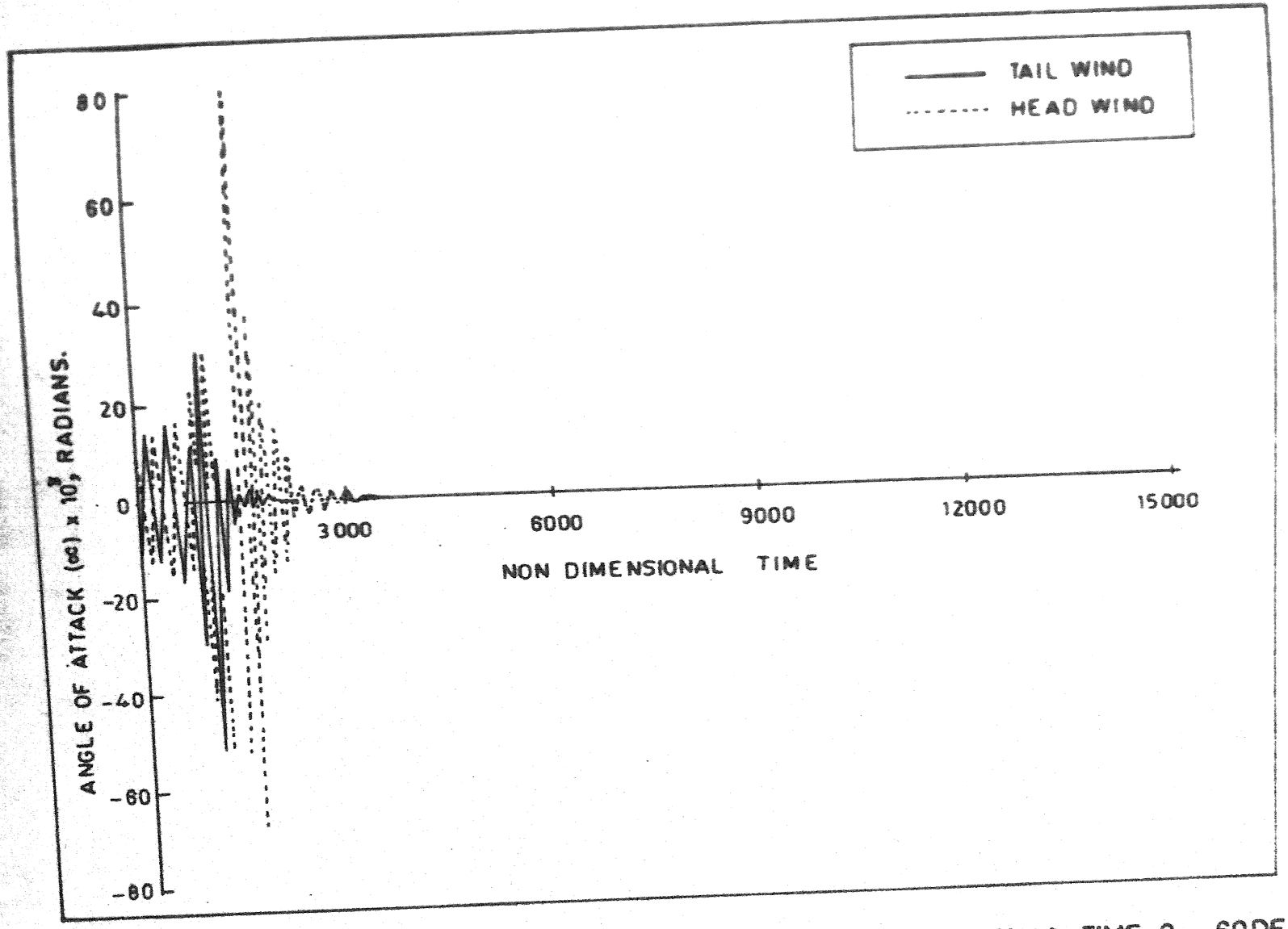

FIG. 6.9 VARIATION OF ANGLE OF ATTACK WITH NON DIMENSIONAL TIME; $\theta_o = 60$ DEG
$V_o = 248.1$ M/SEC, W = 4.0 M/SEC, RANGE WIND.

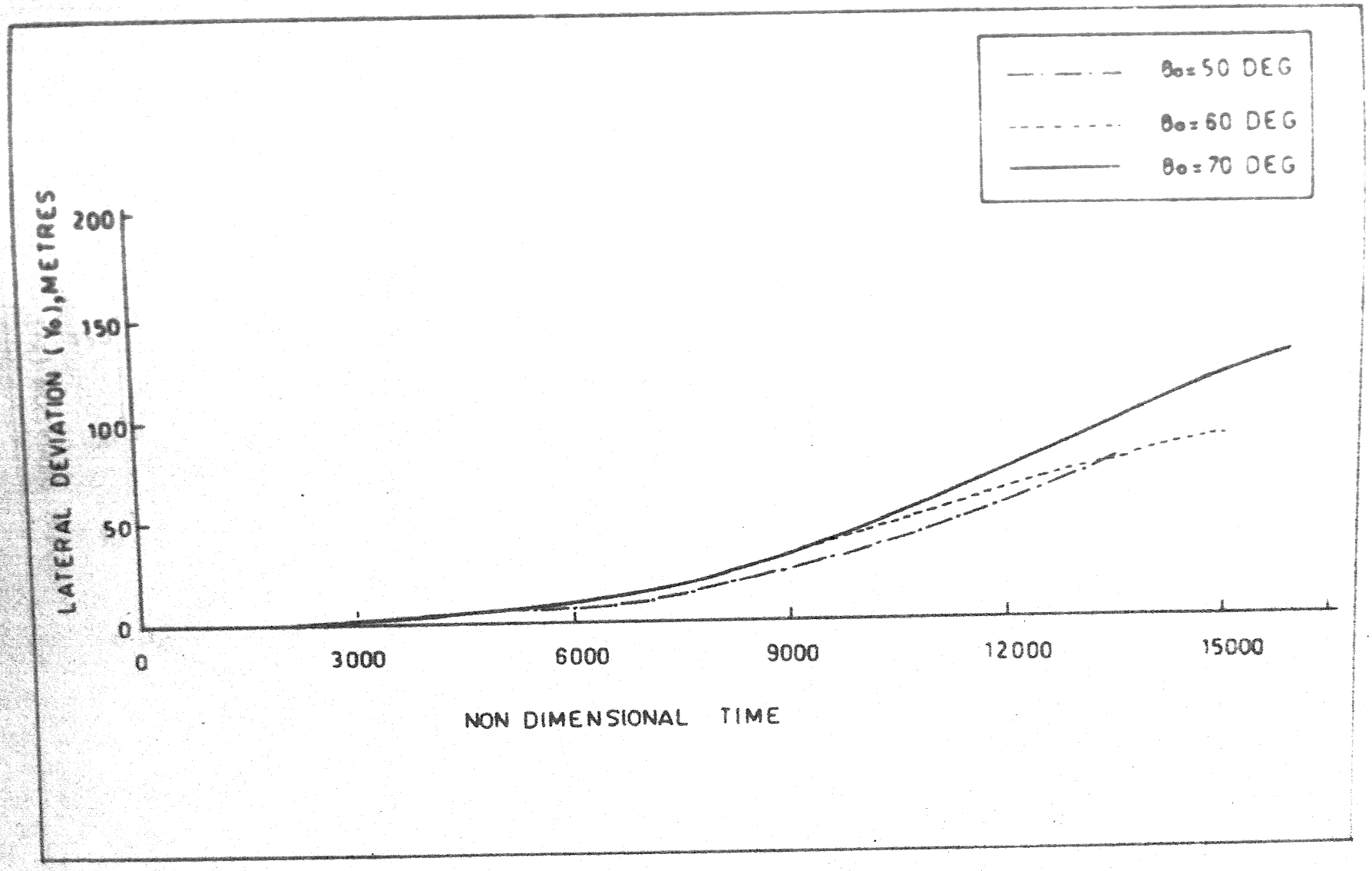

FIG. 6.10 LATERAL DEVIATION VS NON DIMENSIONAL TIME; V_0=248 1 M/SEC, W = 4·0 M/SEC, CROSS WIND.

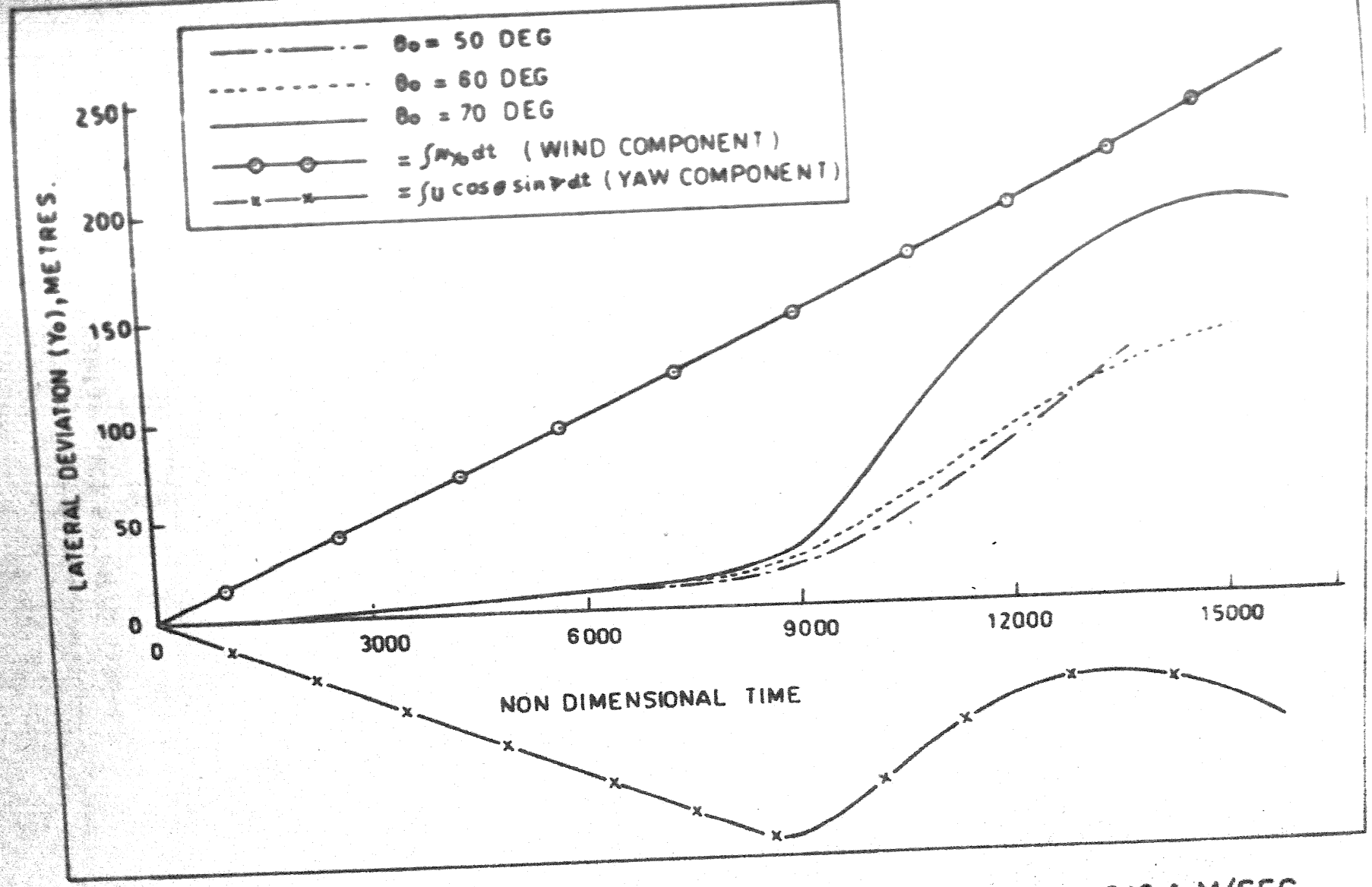

FIG. 6.11 LATERAL DEVIATION VS NON DIMENSIONAL TIME; V_0 = 248.1 M/SEC
W = 6.0 M/SEC, CROSS WIND.

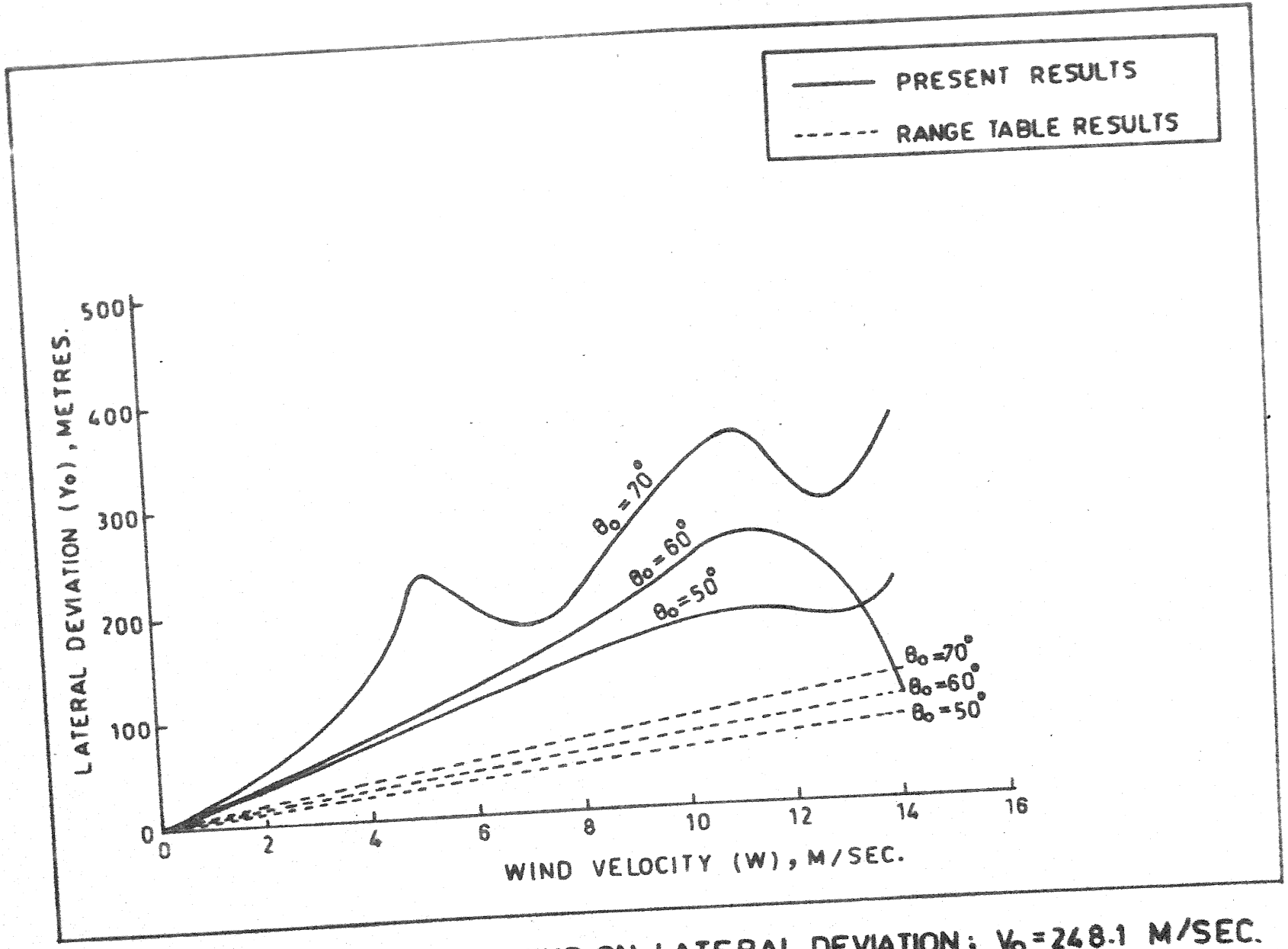

FIG.6.12 EFFECT OF CROSS WIND ON LATERAL DEVIATION; V_o=248.1 M/SEC.

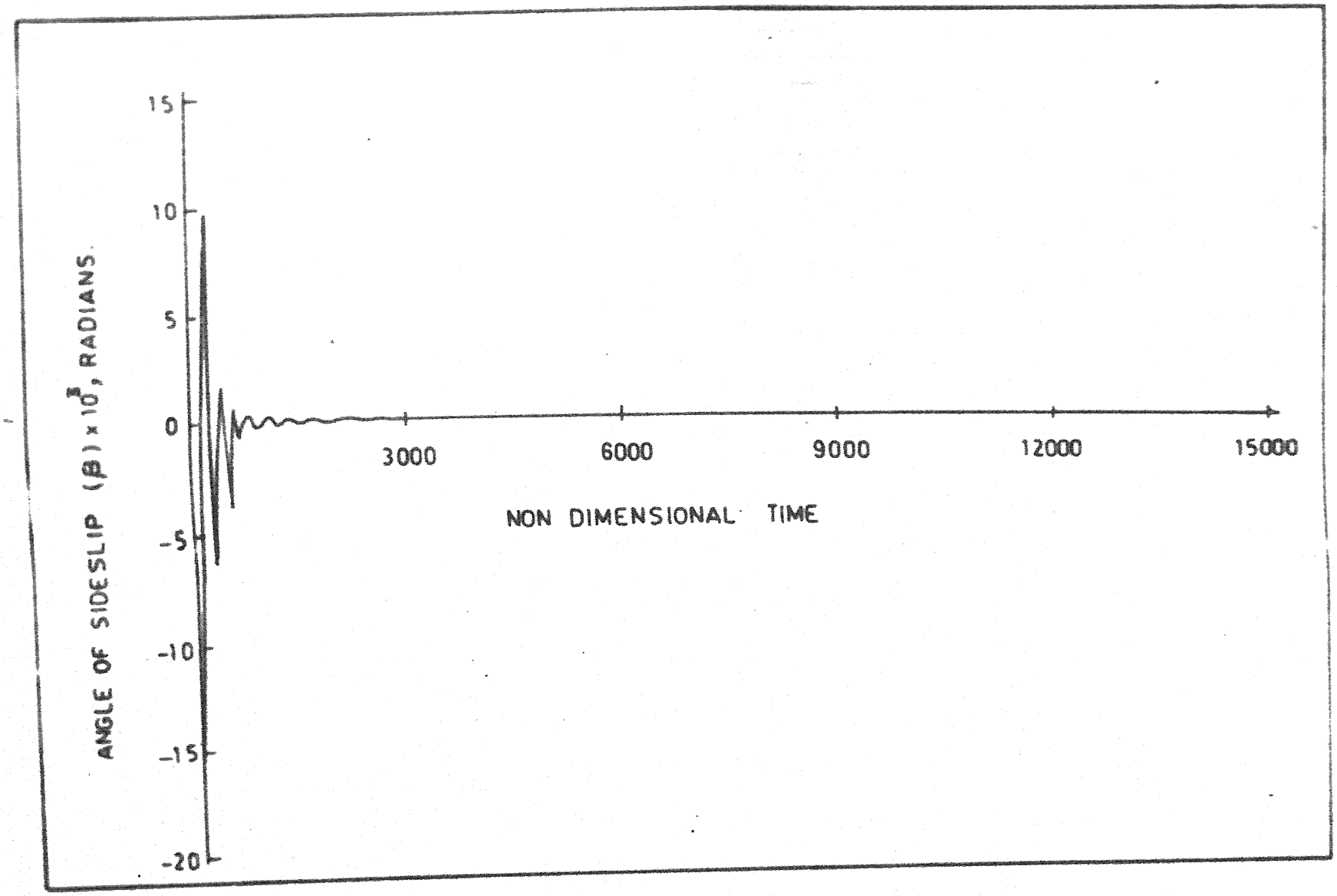

FIG. 6.13 VARIATION OF ANGLE OF SIDE SLIP WITH NON DIMENSIONAL TIME; θ_0=60 DEG, V_0=248.1 M/SEC, W=4.0 M/SEC, CROSS WIND (C_{n_β} = -1.585).

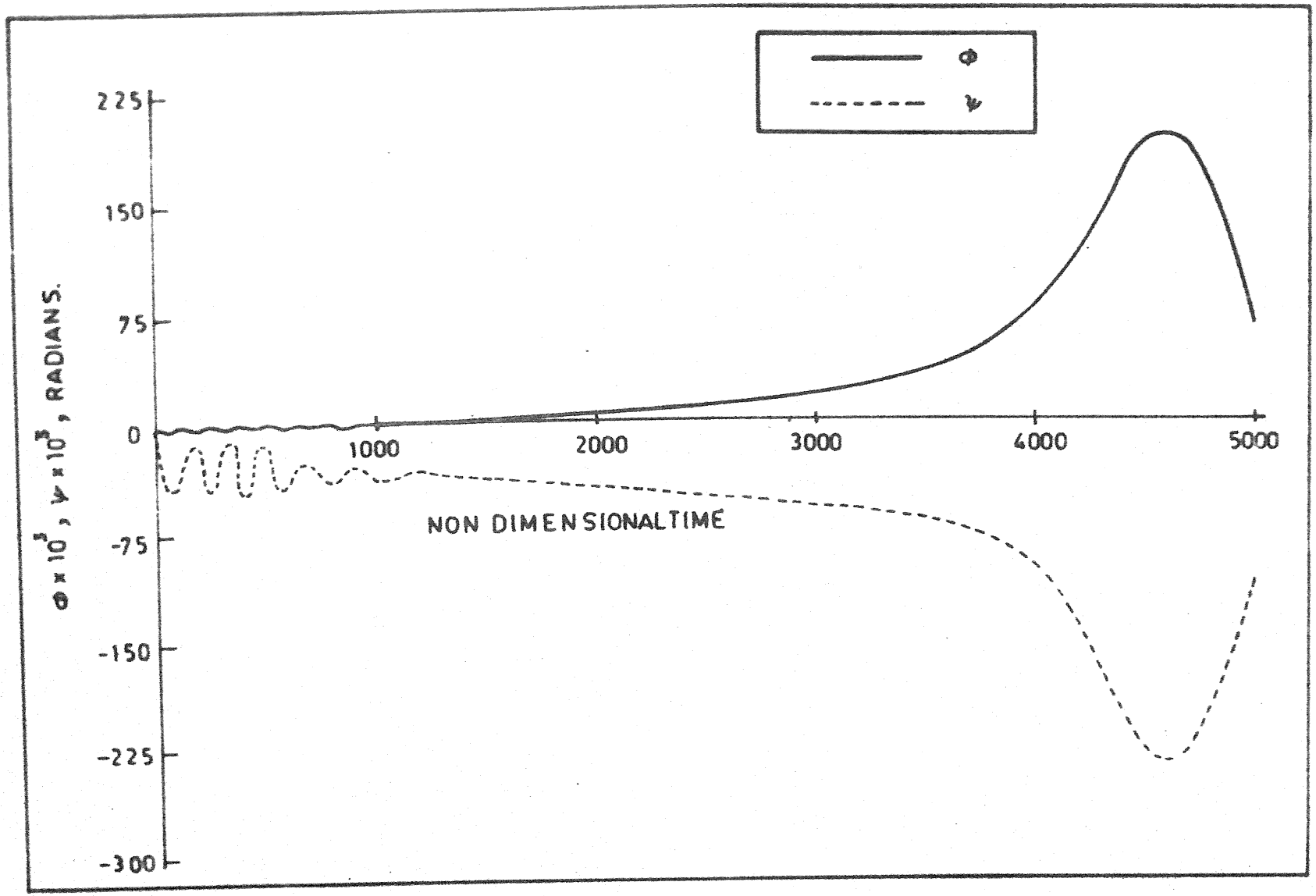

FIG. 6.14 VARIATION OF ANGLES OF ROLL AND YAW WITH NON DIMENSIONAL TIME, θ_0=45 DEG, V_0=153·0 M/SEC, W=4·0 M/SEC, CROSS WIND.

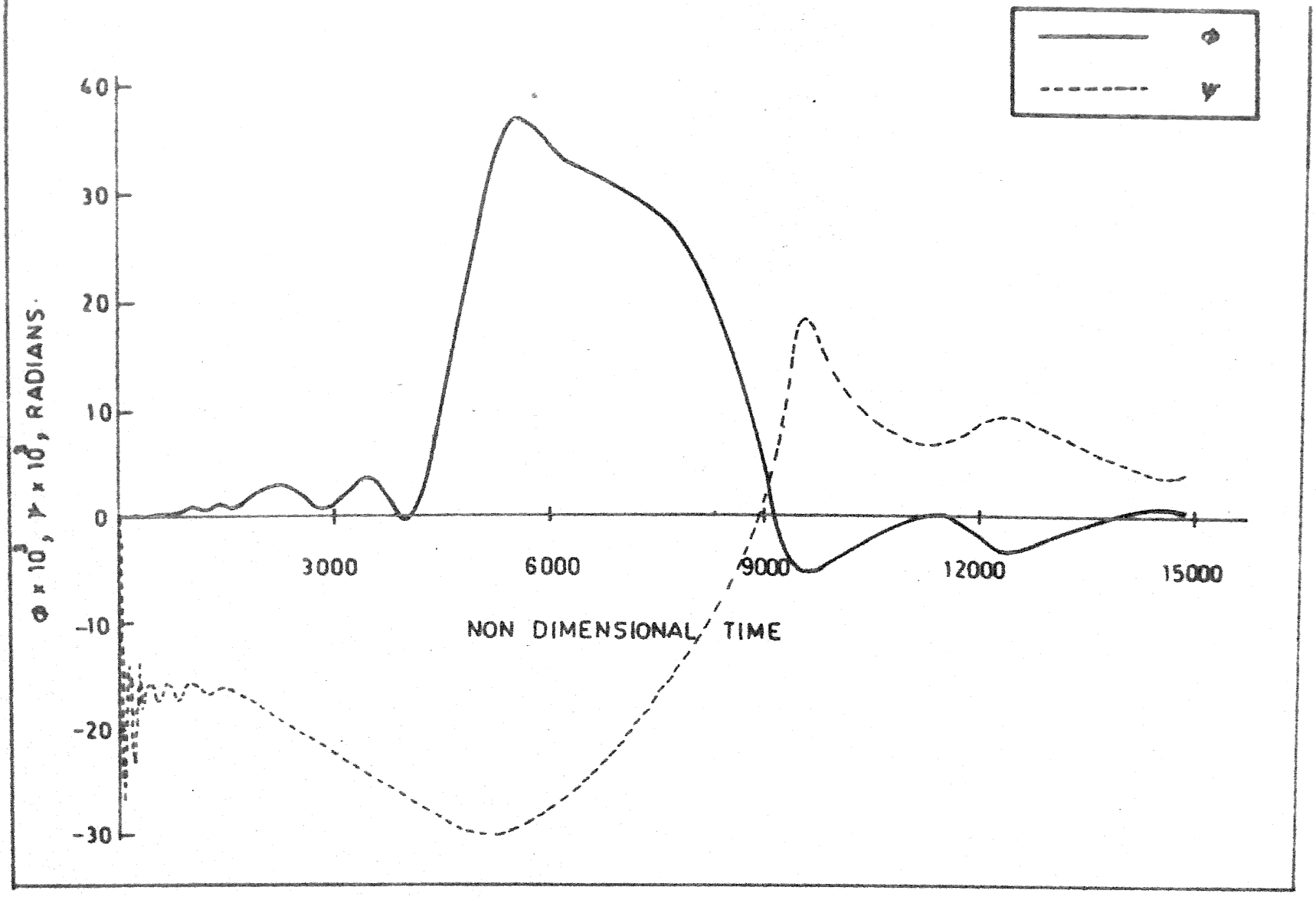

FIG.6.15 VARIATION OF ANGLES OF ROLL AND YAW WITH NON DIMENSIONAL TIME ; θ_0 = 60 DEG, V_0 = 248·1 M/SEC, W = 4·0 M/SEC, CROSS WIND.

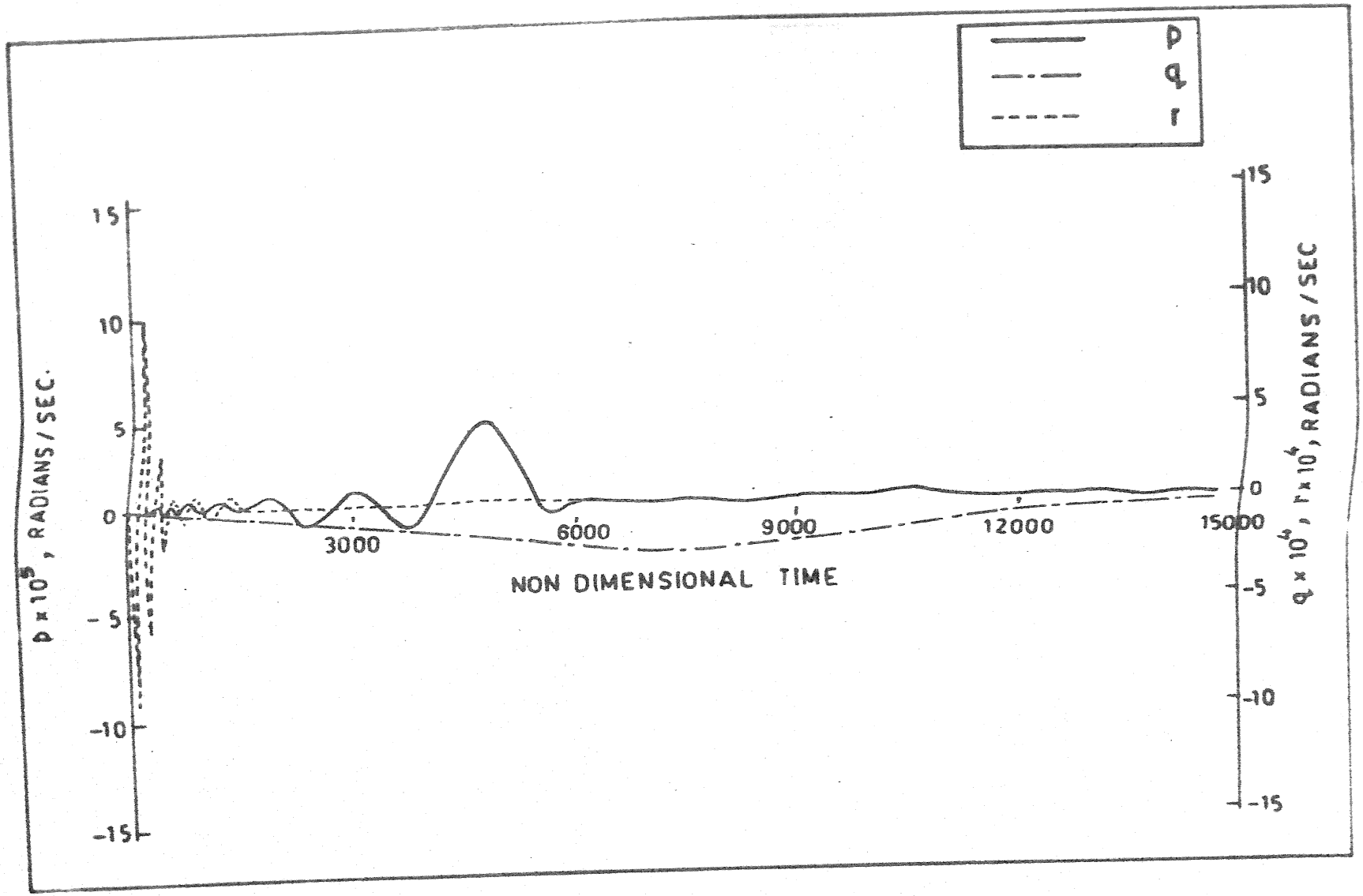

FIG. 6.16 VARIATIONS OF ANGULAR VELOCITY COMPONENTS WITH NON DIMENSIONAL TIME; θ_0=60 DEG, V_0= 248.1 M/SEC , W = 4.0 M/SEC, CROSS WIND.

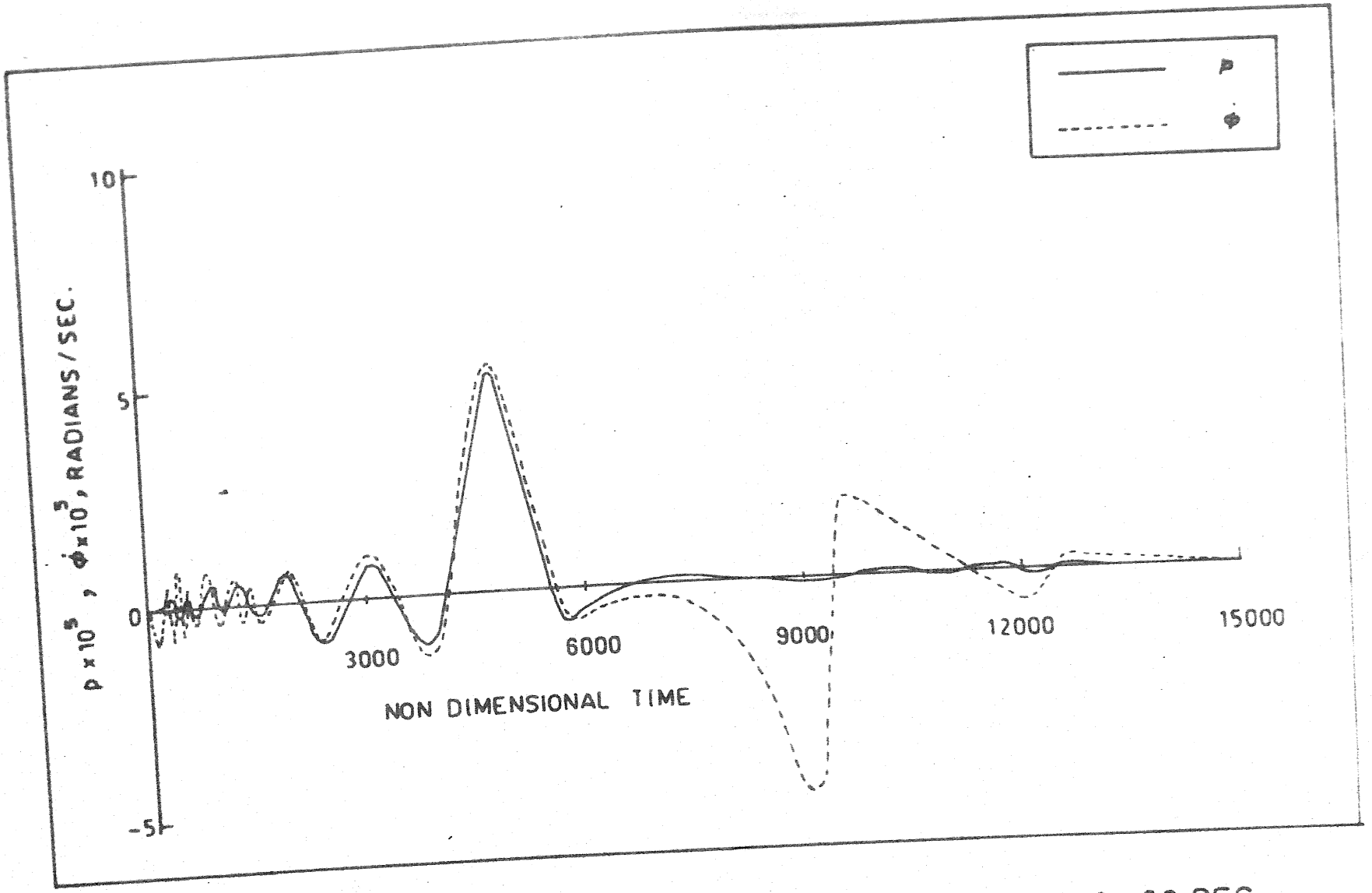

FIG. 6.17 VARIATION OF p AND $\dot{\phi}$ WITH NON DIMENSIONAL TIME; $\theta_o = 60$ DEG
$V_o = 248{\cdot}1$ M/SEC, W=4·0 M/SEC, CROSS WIND.

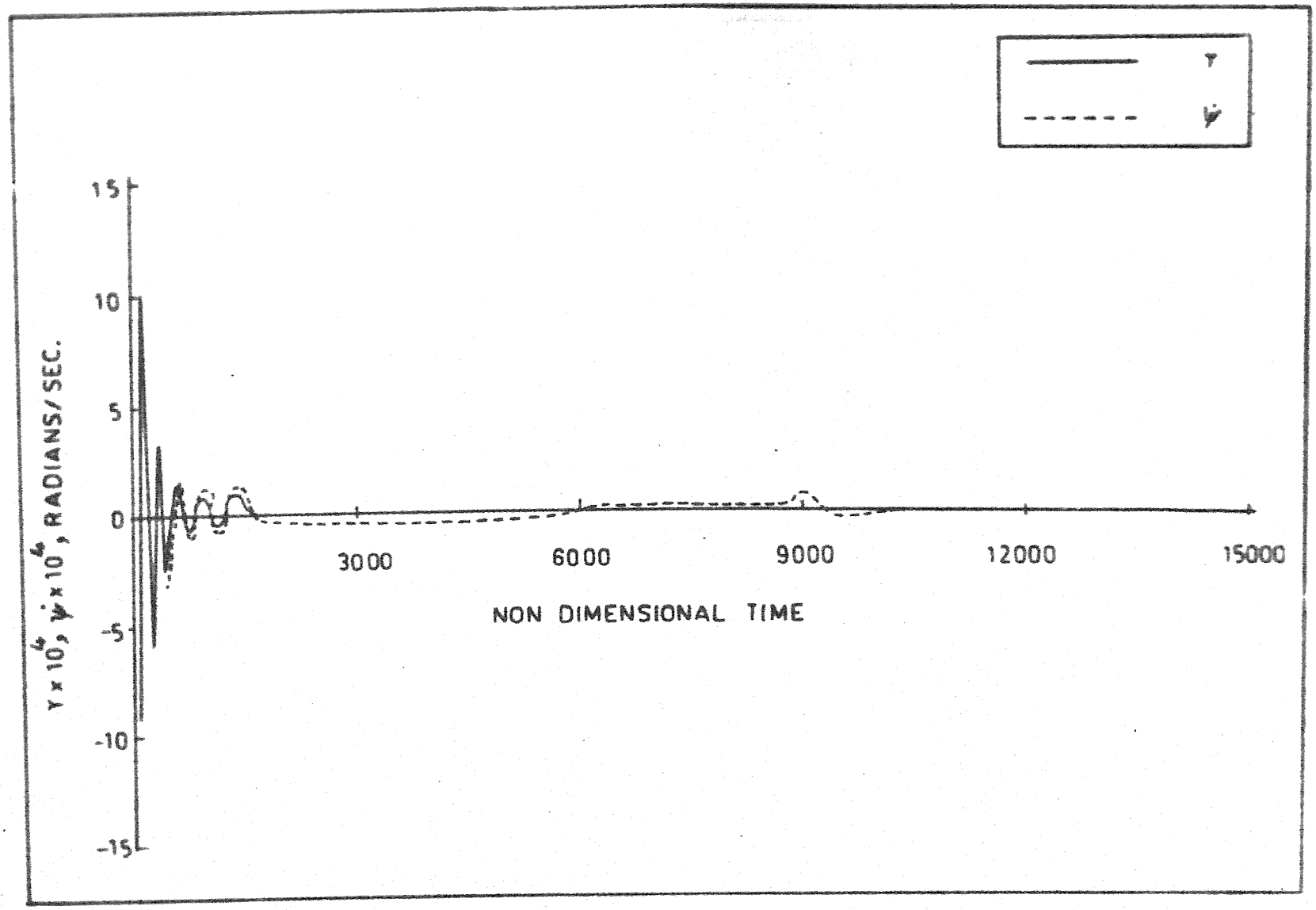

FIG. 6.18 VARIATION OF r AND $\dot{\psi}$ WITH NON DIMENSIONAL TIME; $\theta_0 = 60$ DEG, $V_0 = 248.1$ M/SEC, $W = 4.0$ M/SEC, CROSS WIND.

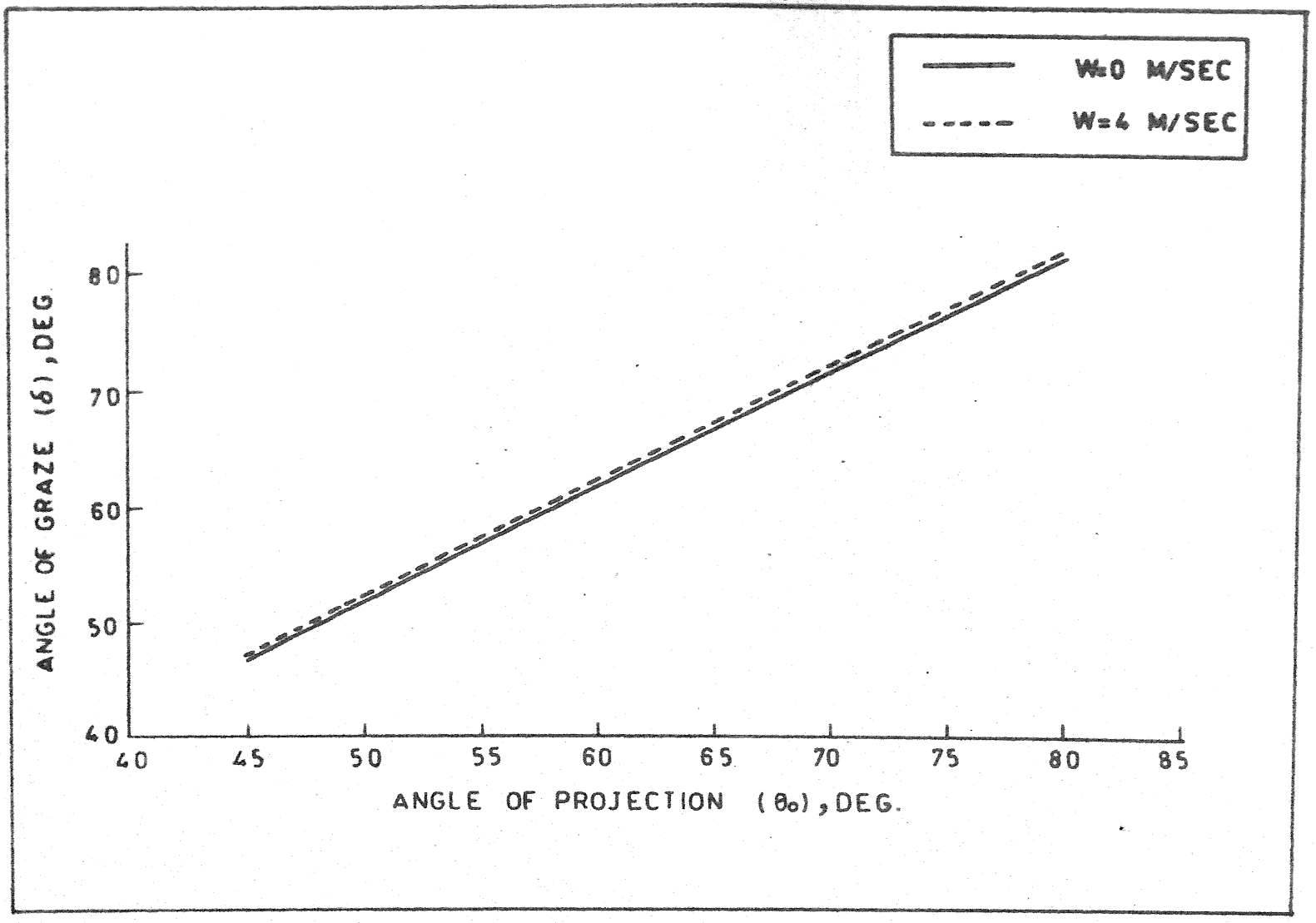

FIG.6-19 ANGLE OF GRAZE VS ANGLE OF PROJECTION V_o=248·1 M/SEC, CROSS WIND.

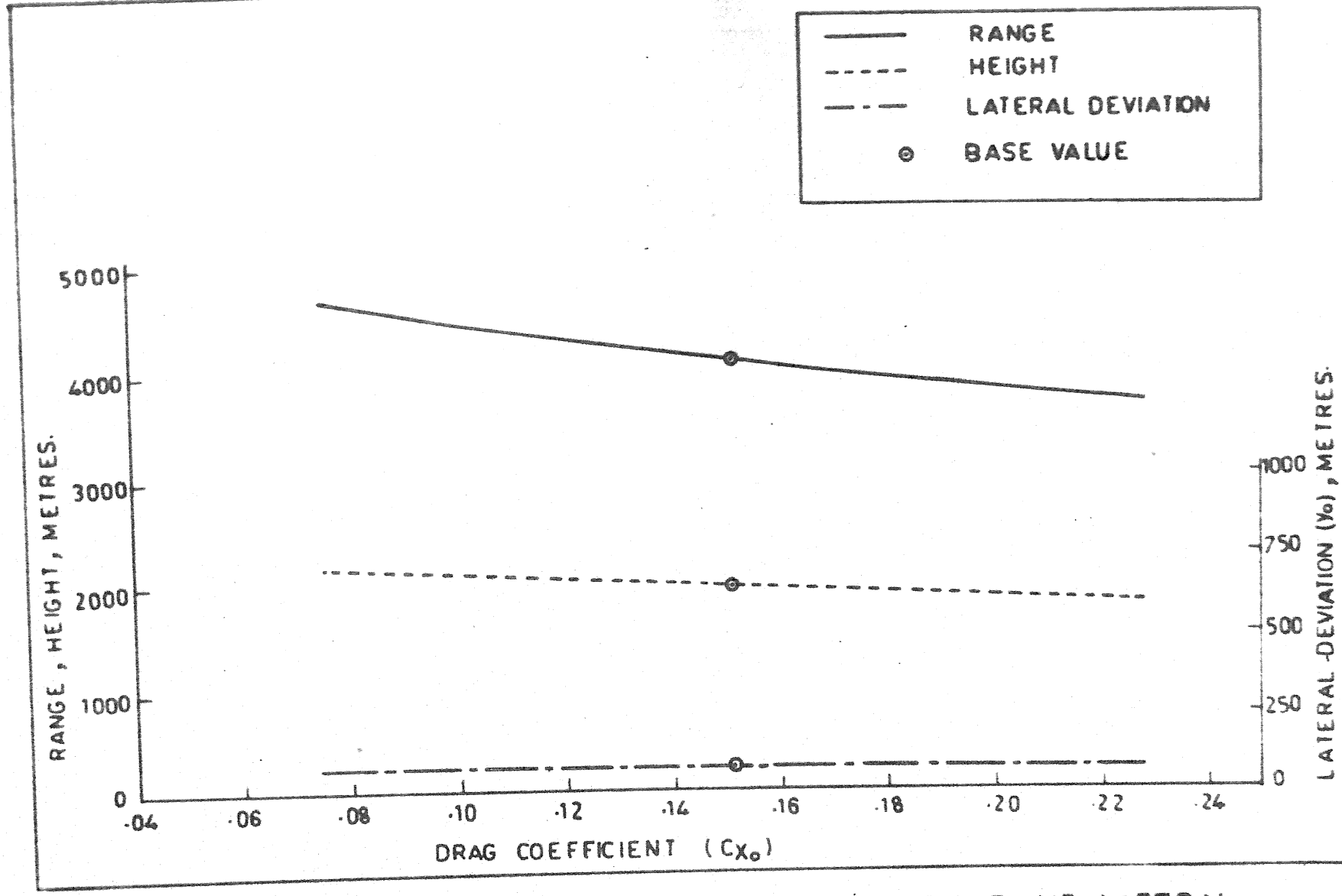

FIG.6-20 EFFECT OF DRAG COEFFICIENT ON RANGE, HEIGHT AND LATERAL DEVIATION; θ_o = 60 DEG , V_o = 248·1 M/SEC, W = 4·0 M/SEC , CROSS WIND.

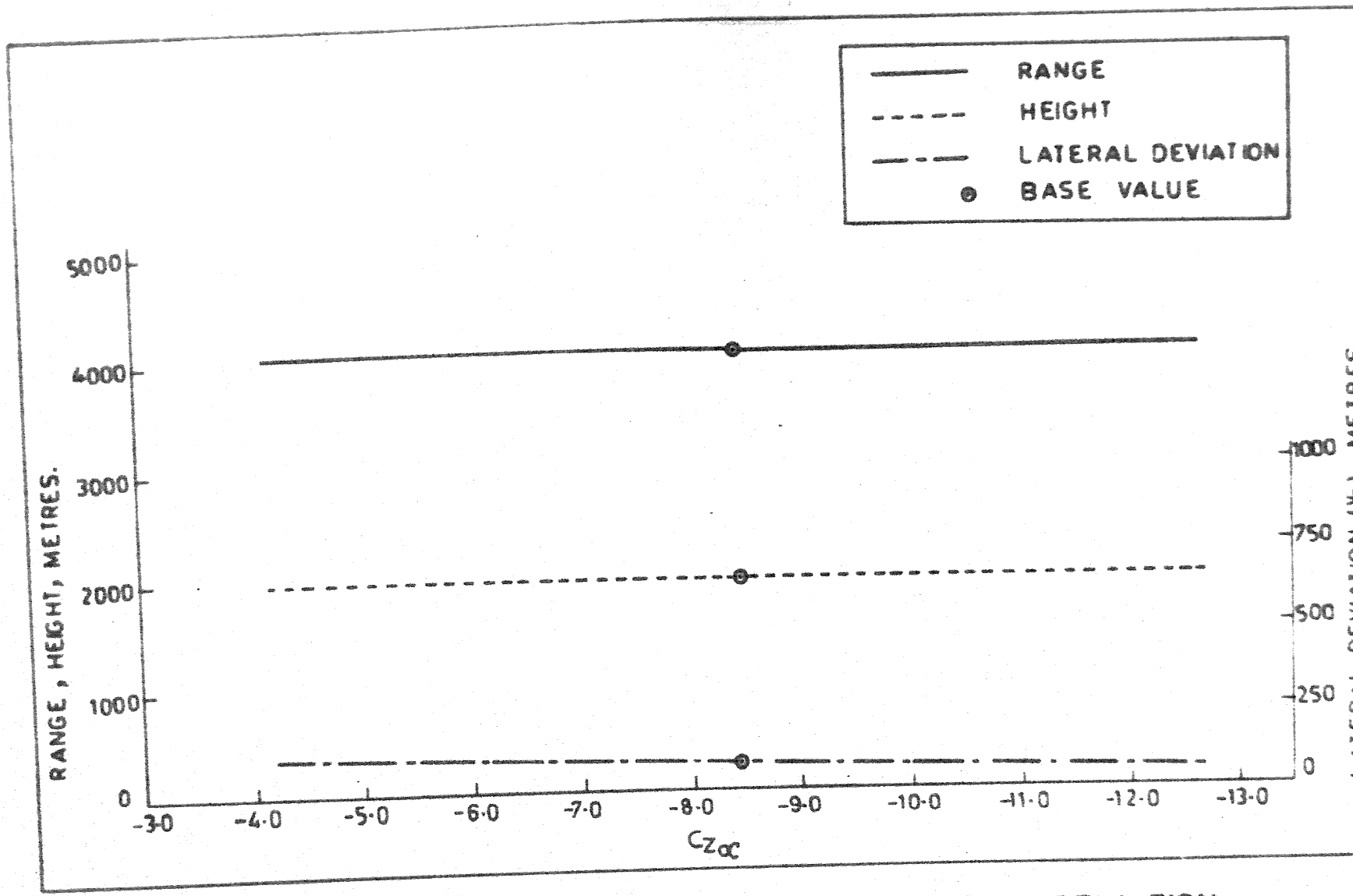

FIG. 6.21 EFFECT OF C_{z_α} ON RANGE, HEIGHT AND LATERAL DEVIATION; θ_o = 60 DEG, V_o = 248·1 M/SEC, W = 4·0 M/SEC, CROSS WIND.

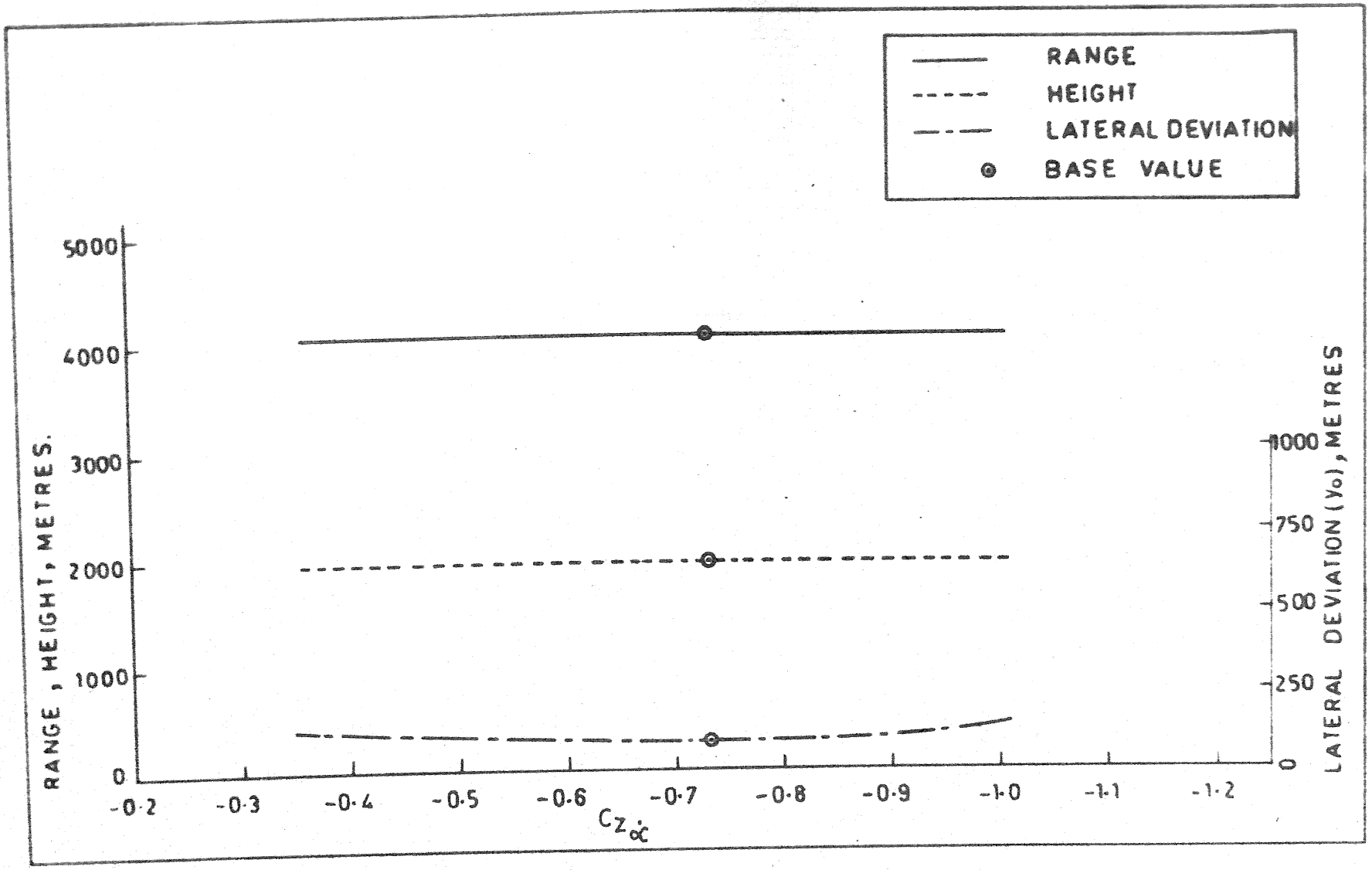

FIG.6.22 EFFECT OF $C_{Z_{\dot{\alpha}}}$ ON RANGE, HEIGHT AND LATERAL DEVIATION; θ_o=60 DEG
V_o = 248·1 M/SEC, W=4·0 M/SEC, CROSS WIND

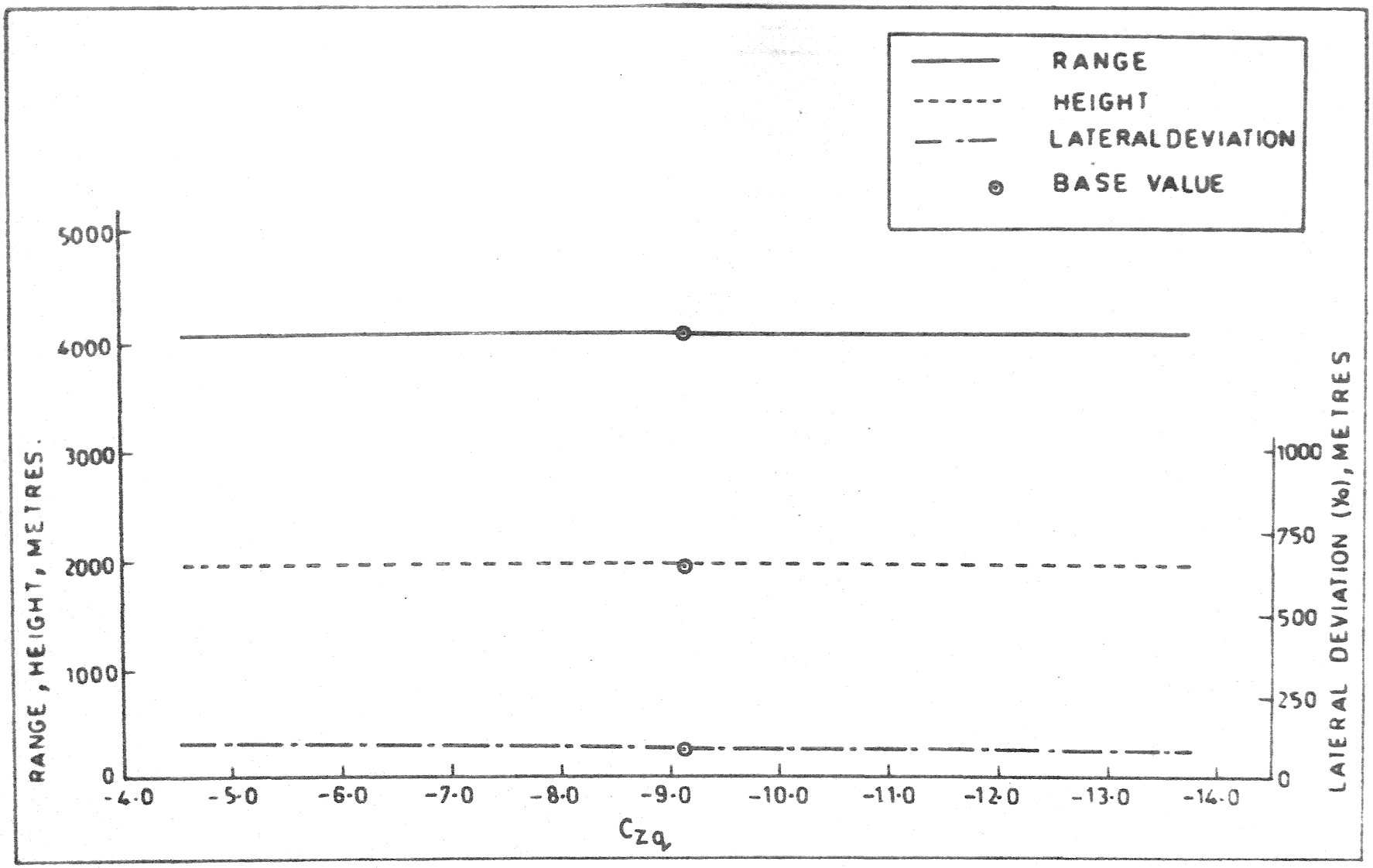

FIG.6.23 EFFECT OF C_{z_q} ON RANGE, HEIGHT AND LATERAL DEVIATION; $\theta_0 = 60$ DEG, $V_0 = 248.1$ M/SEC, W = 4·0 M/SEC, CROSS WIND.

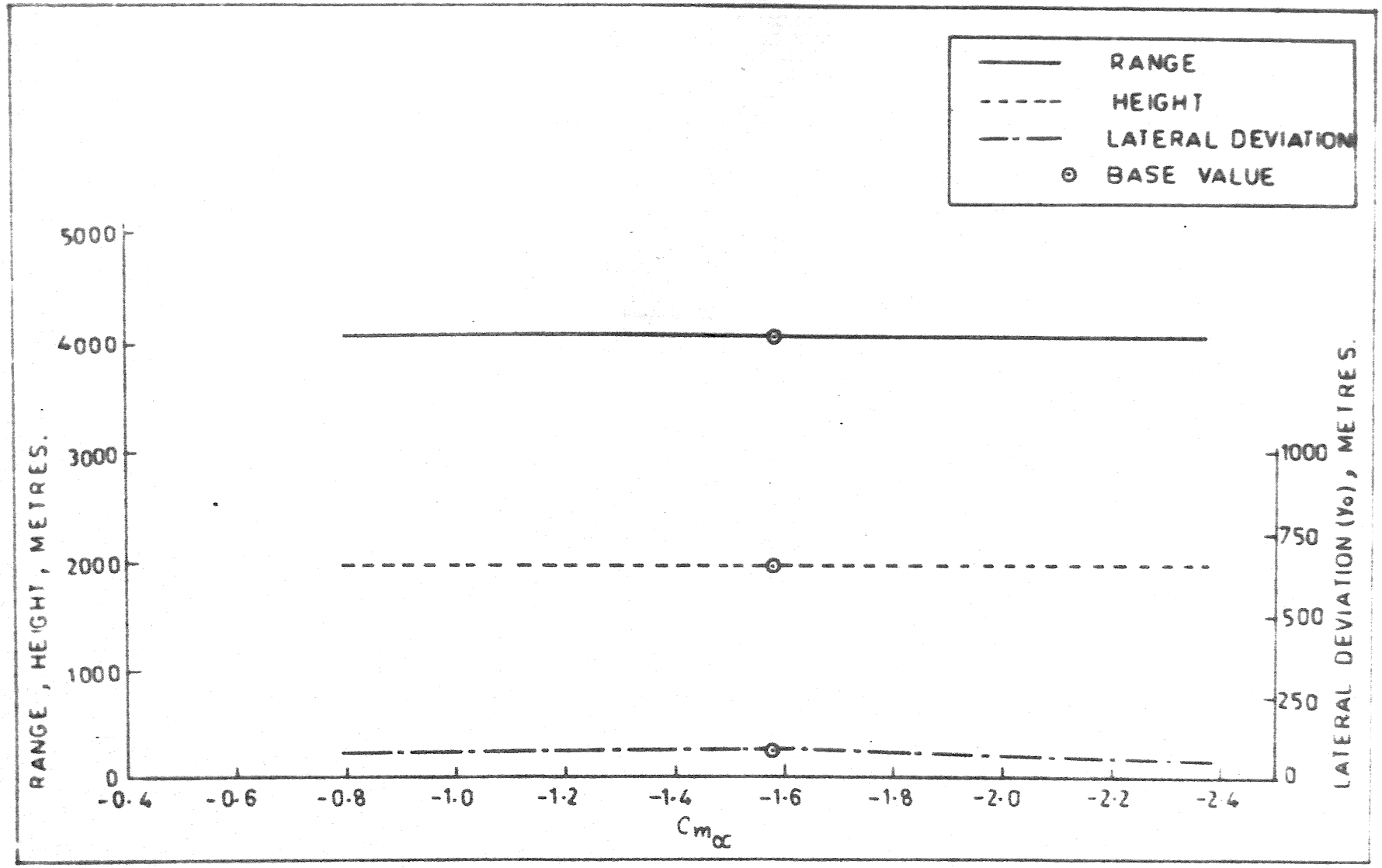

FIG.6.24 EFFECT OF C_{m_α} ON RANGE, HEIGHT AND LATERAL DEVIATION; $\theta_o = 60$ DEG
$V_o = 248.1$ M/SEC, W = 4.0 M/SEC, CROSS WIND.

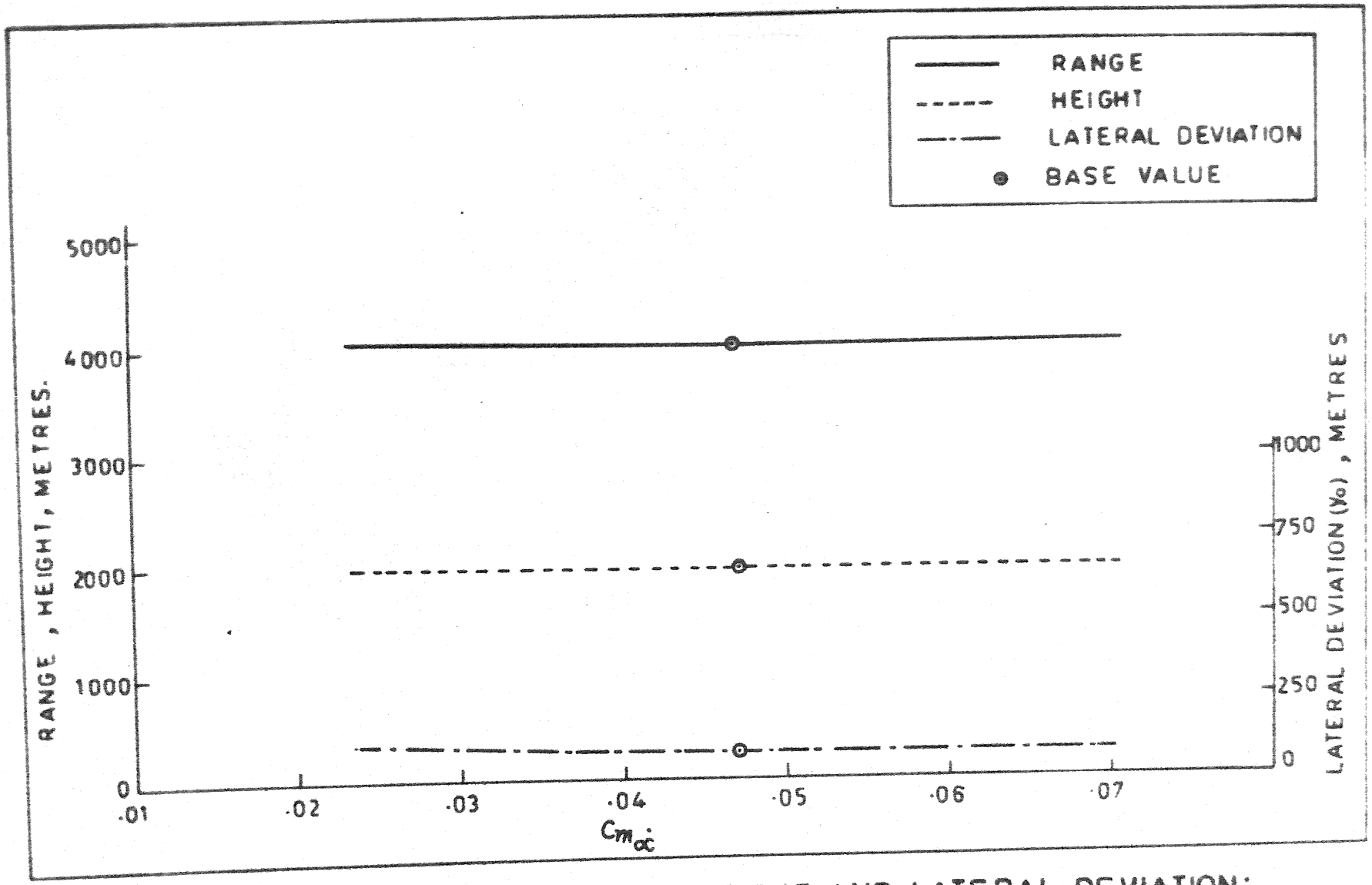

FIG.6.25 EFFECT OF $Cm_{\dot{\alpha}}$ ON RANGE, HEIGHT AND LATERAL DEVIATION; $\theta_o = 60$ DEG, $V_o = 248.1$ M/SEC, W = 4.0 M/SEC, CROSS WIND.

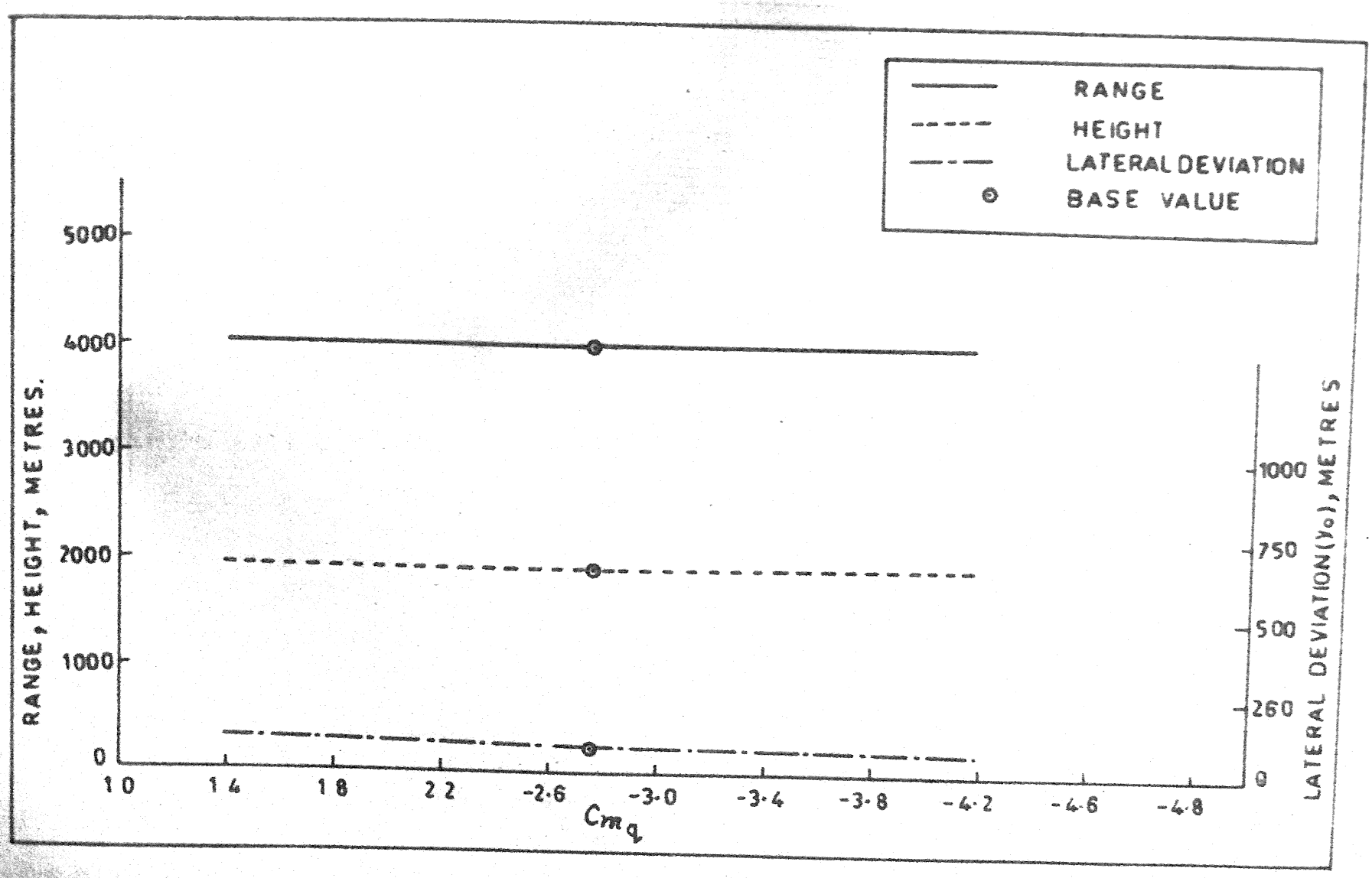

FIG. 6.26 EFFECT OF C_{m_q} ON RANGE, HEIGHT AND LATERAL DEVIATION; θ_0=60 DEG
V_0 = 248·1 M/SEC, W = 4·0 M/SEC, CROSS WIND.

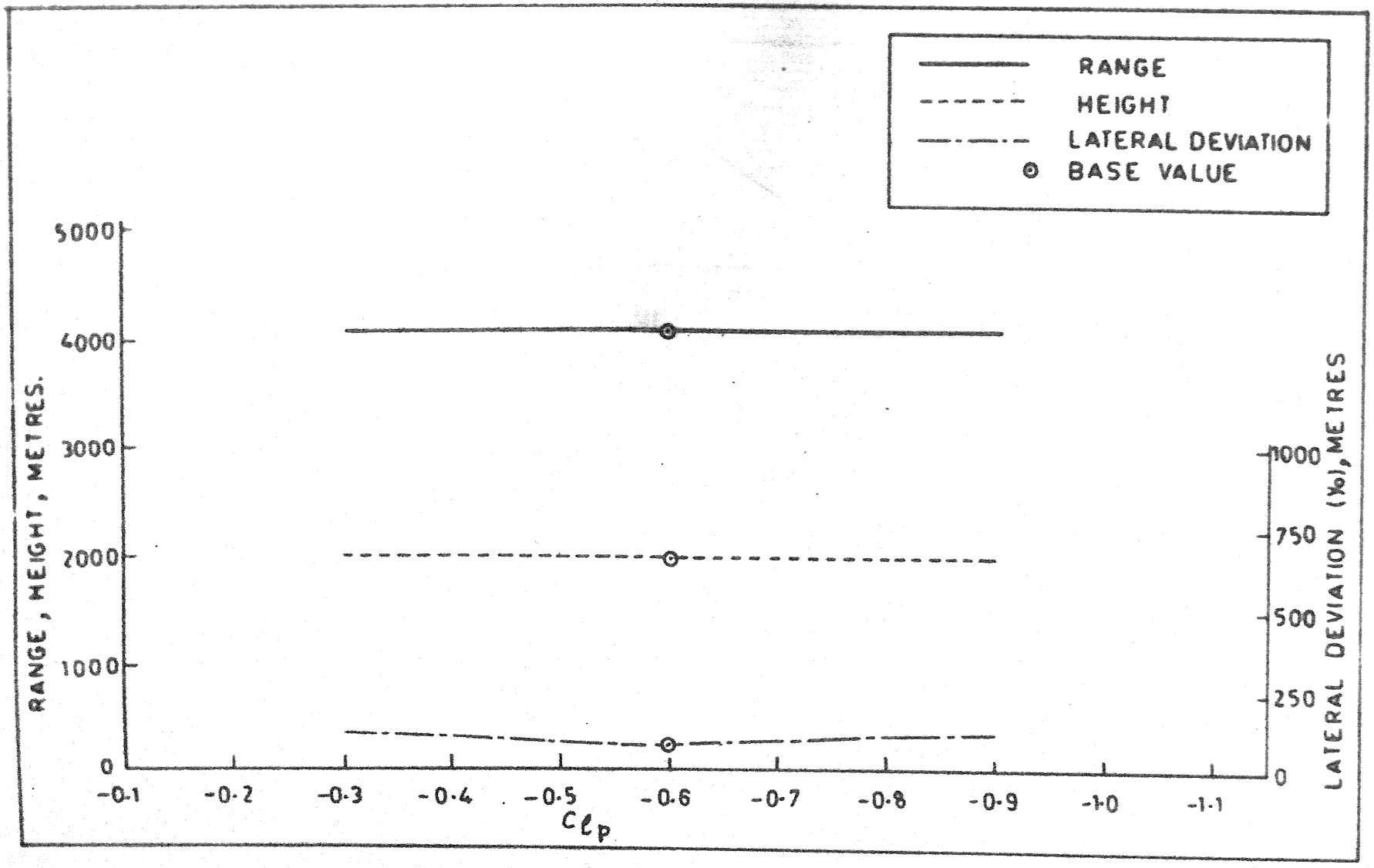

FIG.6.27 EFFECT OF C_{ℓ_p} ON RANGE, HEIGHT AND LATERAL DEVIATION, θ_o =60DEG
V_o =248.1M/SEC, W=4.0M/SEC, CROSS WIND

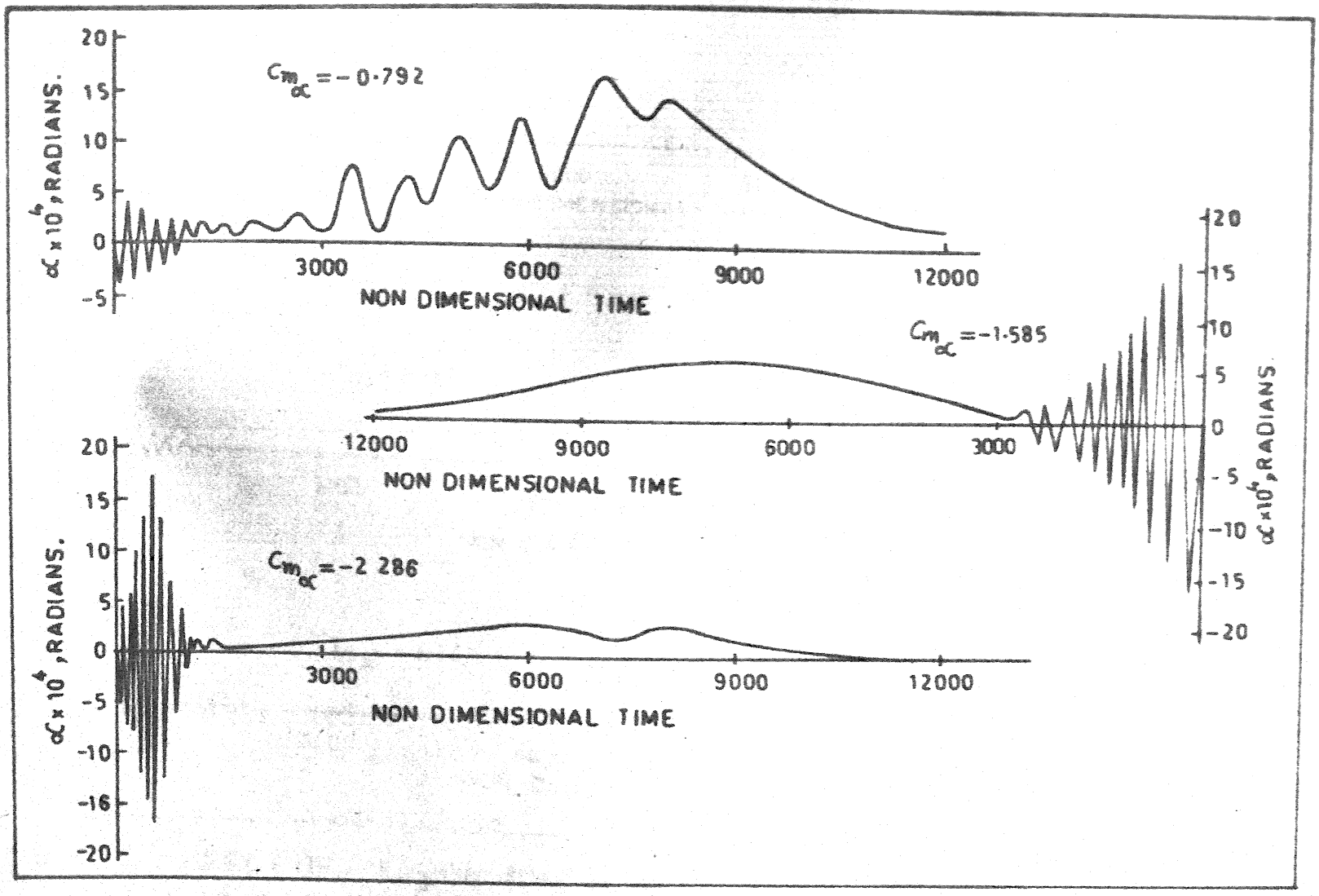

FIG.6.28 EFFECT OF $C_{m_{\alpha\dot{\alpha}}}$ ON TIME HISTORY OF ANGLE OF ATTACK; $\theta_o = 60$DEG
$V_o = 248.1$ M/SEC,

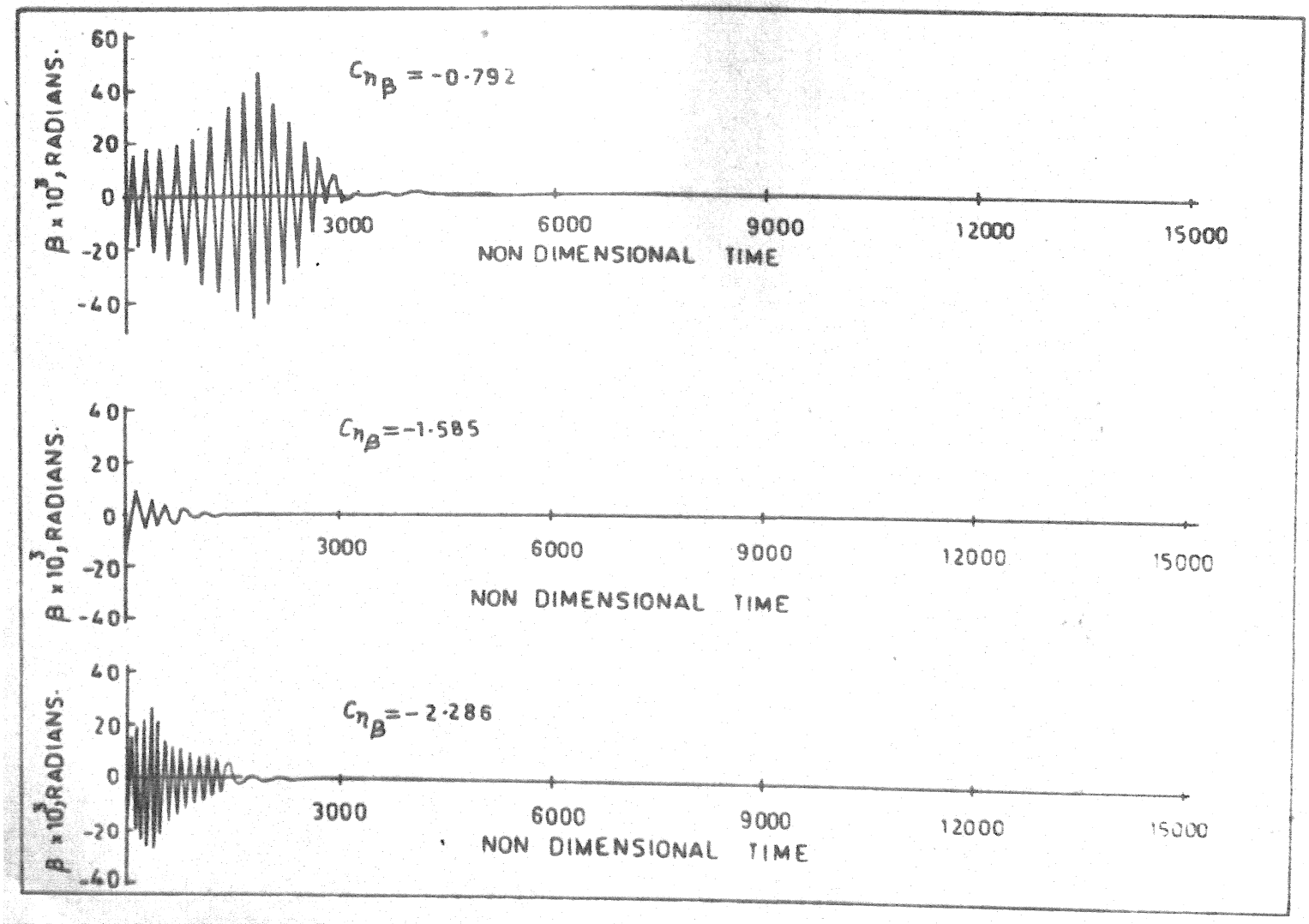

FIG.6·29 EFFECT OF C_{n_β} ON TIME HISTORY OF ANGLE OF SIDESLIP; θ_o = 60 DEG V_o = 248·1 M/SEC, W = 4·0 M/SEC, CROSS WIND.

EE-1984-M-SIN-TRA